ELECTRICAL STRESS MONITORING OF DISTRIBUTION TRANSFORMERS USING SMART GRID TECHNIQUES

Fulufhelo Andrew Netshiongolwe

A research report submitted to the Faculty of Engineering and the Built Environment, University of the Witwatersrand, in fulfilment of the requirements for the degree of Master of Science in Engineering.

Johannesburg, February 2016

Declaration

I declare that this dissertation is my own, unaided work, except where otherwise acknowledged. It is being submitted for the degree of Master of Science in Engineering in the University of the Witwatersrand, Johannesburg. It has not been submitted before for any degree or examination in any other university.

Signed this 12th day of February 2016

Fulufhelo Andrew Netshiongolwe

Abstract

Electrical stresses that distribution transformers rated 16 kVA up to 2 MVA are subjected to can often cause premature transformer failures. In this study, research related to the development of cost effective bushing embedded sensors that can measure the electrical stresses on the MV side of distribution transformers has been conducted. An embedded screen in a specially designed 24 kV bushing was used for both power frequency and transient voltage measurements. Observed results showed that the screen-based bushing capacitive voltage divider offered results that are consistent with those of a commercial capacitive voltage divider for power frequency voltages as low as 1 kV up to 24 kV. Impulse voltage measurements were consistent with those of a wideband resistive divider for voltages lower than 60 kV. Voltages higher than 60 kV revealed non-linear behaviour which increases as the 150 kV BIL rating of a 22 kV transformer is reached. A nonlinear resistor added to ATPdraw simulations was able to compensate for the observed nonlinearity. PD tests conducted on the prototype bushing showed that the designed prototype had surface discharges which are affected by the positioning of the bushing screen. A Rogowski coil embedded in the same bushing was used for the measurement of both power frequency and transient currents. Measured coil parameters used in ATPdraw simulations produced results that were consistent with the output of the Rogowski coils when measuring 8/20 μs current impulses. Numerical integration of the Rogowski coil output voltages was successfully used in the recovery of both power frequency and measured impulse currents. The Rogowski coil sensitivity is affected by both coil dimensions and terminating resistance. The designed prototype bushing opens up opportunities for performing stress monitoring on the MV side of distribution transformers.

For Lutendo, Murangi and Tshedza

Acknowledgements

I would like to thank my supervisor Dr John van Coller for his continuous support, direction and unwavering dedication to technical excellence. I would also like to express my gratitude to the Eskom Power Plant Engineering Institute (EPPEI) for the financial contribution towards my research work My gratitude also goes to the EPPEI HV research team for their continued thought provoking inputs. I am grateful for the assistance received from the team at Electrical Moulded Components. The support and assistance received from the Genmin staff is worth mentioning. I would also like to thank the EPPEI management team for providing an environment conducive for conducting research. Lastly, I would like to thank my family, especially my wife, Lutendo, for her continued support, encouragement and patience.

Contents

List of figures

List of tables

Nomenclature

AC	Alternating Current
ATP	Alternative Transient Program
BNC	Bayonet Neill–Concelman
CT	Current Transformer
CVD	Capacitive Voltage Divider
CVM	Current Voltage Monitor
DC	Direct Current
DGA	Dissolved Gas Analysis
FEMM	Finite Element Method Magnetics
IEC	International Electrotechnical Commission
IEEE	Institute of Electrical and Electronics Engineers
LV	Low Voltage
MV	Medium Voltage
SAIDI	System Average Interruption Duration Index
SAIFI	System Average Interruption Frequency Index
SRAPET	Self-Regulated and Protected Electrification Transformer
SANS	South African National Standard
VT	Voltage Transformer

Chapter 1

1 Introduction

1.1 The smart grid at distribution network level

The change in loads and load profiles increases the types of electrical stresses observed by electricity utilities at distribution level. Distribution network equipment is designed to continue operating in the presence of system and external disturbances whilst severely faulted areas are disconnected by protection equipment. The introduction of the Smart Grid gives utilities the ability to better manage load profiles, monitor and manage electrical stresses and improve electrical equipment availability (Elsworth, 2008). The successful penetration of the Smart Grid at distribution level is complemented by the availability of reliable cost effective monitoring equipment.

The introduction of the Smart Grid concept in South Africa's distribution network is aimed at achieving improved restoration times and improved line and transformer monitoring (Khatri, 2010). Pole mount distribution network transformers rated 16 kVA up to 500 kVA in Eskom have low capital cost. Such transformers are often subjected to a run-to-failure maintenance strategy due to the high costs related to performing diagnostic tests such as dissolved gas analysis (DGA). Increased failures of such transformers in the Eskom Distribution network has resulted in annual replacement costs of over R71 894 000 (Kleinhans, 2011). Studies performed have shown that most of these transformers are subjected to operating conditions that lead to premature failures. Such failures are indicative of the need to develop cost effective monitoring systems that can enable better management of such transformers within the Eskom Distribution network.

Successful implementation of a comprehensive Smart Grid solution contributes to

demand side management. Studies have shown that monitoring loading on supply transformers can enable end users to schedule their loads such that they limit the impact that this has on the aging of transformers and observed peak loads (Masoum et al., 2010). Such advancements require the availability of affordable monitoring technology and robust communication infrastructure.

1.2 Electrical monitoring of distribution networks

Electrical faults can occur during both transient and power frequency operating conditions. The ability to monitor currents and voltages over a wide frequency band can lead to better diagnostics of abnormal operating conditions such as the presence of severe harmonics and lightning transients. Current and voltage monitoring has traditionally been performed using ferromagnetic current transformers (CTs) and voltage transformers (VTs). Coupling such instrument transformers with various relays enables various functionalities to be carried out. These may include carrying out protection activities or various predefined control and operational activities.

IEEE standard C37.235 (2007) shows that ferromagnetic CTs and VTs have limited bandwidth, phase and magnitude errors and exhibit nonlinearities such as saturation. These limitations imply that such VTs and CTs are designed to operate accurately within a predefined range. Electrical monitoring on pole mount transformers is currently performed on the low voltage (LV) side in Eskom (Kleinhans, 2011). Monitoring of currents and voltages in this case has shown that some pole mount transformers rated 16 kVA to 500 kVA were often subjected to severe overloads and load unbalances which lead to premature failure. Other electrical stresses such as harmonics have also lead to premature failure of pole mount transformers (Henderson and Rose, 1994). Monitoring such stresses on the MV side has the potential of identifying additional operating conditions that may lead to premature failure of pole mount transformers.

1.3 Research objectives and contributions

The identification of electrical stresses that lead to premature failures of distribution transformers rated 16 kVA up to 500 kVA is currently being performed on the LV side. Key questions about the possibility and challenges of monitoring such transformers on the MV side remain unanswered. The research was aimed at achieving the following objectives:

- Ferromagnetic CTs can be used on the LV side of distribution transformers. Such CTs however have a limited frequency range. Limited frequency range voltage monitoring can also be performed using ferromagnetic VTs on such transformers. The dimensions of such measuring equipment and their associated cost often increase with the increase in magnitude of the primary electrical signals of interest and the associated level of accuracy. The first objective of the research was that of developing cost effective bushing transducers capable of monitoring current and voltage signals on the MV side of distribution transformers rated 16 kVA up to 2 MVA.

- This research focused on the development of cost effective medium voltage (MV) transformer bushings capable of monitoring power frequency and transient current and voltage signals. The research looked at the use of field control screens in capturing both power frequency and transient voltage signals. Rogowski coils were used for capturing both power frequency and transient current signals.

1.4 Research questions

The following key research questions were considered in the research:

- What levels of monitoring can be achieved considering fault level, frequency response and dynamic range limitations?

The bandwidth of the current and voltage transducers is a function of design. Rogowski coils of different turns and dimension have been investigated as these have different usable bandwidths. The effect of coil parameters on Rogowski coil current measurement has also been considered. Voltage measurements within the BIL rating of interest were studied. Focus was on the design of a 22 kV bushing however the possibility of extending this to other voltage and current ratings is discussed. The effect that the insulation material has on the measurements is discussed.

- What can be achieved with online monitoring, and what are the associated

corrective actions that can be recommended?

Areas that are severely affected by electrical stresses can be identified and thus corrective measures can be implemented. Corrective actions are varied based on the impact that the identified stress has on the transformer. Correct decision making can also be further enhanced by combining findings obtained in this study with the Current Voltage Monitors (CVM) and the Self-Regulated and Protected Electrification Transformer (SRAPET) units already developed in South Africa by Kleinhans (2011) and, Beckers and Beukes (2007) respectively. Further intelligent usage of such units can also lead to effective load management by end users once there is a fully integrated Smart Grid system.

- To whom should the analysed information be addressed and what communication protocol should be considered?

The modernisation of the grid, power constraints and tariff structuring are some of the key issues that distribution centres and end users will have to deal with on ongoing bases. Field measurements can be packaged such that they provide benefits to both distribution centres and end users

.

- Can online monitoring lead to optimum tap selection in distribution transformers?

Effective voltage regulation requires online data. Ensuring the quality of supply to end users can thus be performed with ease by knowing field conditions as provided by the designed bushing.

1.5 Overview

Chapter 2 reviews fault diagnostic methods that are currently used on transformers. The penetration and viability of applying such diagnostic methods on pole mount transformers is considered. The existing limitations in using electrical signals in identifying electrical stresses that impact on transformer failures is addressed.

Chapter 3 looks at the need for modernisation of the distribution grid. The potential benefits derived from modernisation of the distribution grid are presented.

Chapter 4 introduces the use of Rogowski coils and field control screens in monitoring wide band electrical signals. Electrical modelling of the Rogowski coil and field control screen for both transient and power frequency signal is performed.

Chapter 5 presents the experimental setup and observed results related to the measurement of power frequency and transient electrical signals.

Chapter 6 compares simulated and experimental results for both power frequency and impulse voltage measurement.

Chapter 7 revisits the research questions based on the performed studies with emphasis on the findings that were made.

Chapter 8 presents findings related to the construction of a prototype MV bushing capable of monitoring electrical stresses

Chapter 9 provides the overall conclusion to the research

Chapter 2

2 Background

2.1 Transformer fault diagnostics

Transformer oil analysis has been successfully used in determining the inception of faults within liquid immersed transformers. Online DGA and periodic oil laboratory based tests have been used in identifying various fault conditions such as corona, partial discharges, overheating and arcing (Harlow, 2004). This is based on identifying the concentration of gasses that get released when a fault occurs within a transformer. Coupling DGA results with artificial intelligence methods is currently widely used in attempts to increase the accuracy levels of transformer fault diagnostics. (Mehta et al., 2013) showed that 92% fault classification accuracy could be achieved using trained support vector machines whilst Annapoorani and Umamaheswari (2012) successfully implemented artificial neural networks in determining the health condition of transformers. Implementation of DGA comes at a cost and thus only gets implemented on either critical transformers or large power transformers.

DGA laboratory analysis and the use of online oil condition monitoring is not economically viable for the many MV/LV transformers which are found in the distribution network. Due to the low capital cost of distribution transformers, minimal condition monitoring is implemented. Colour coded thermal stickers that require field inspection are currently used for overload monitoring on Eskom distribution transformers rated up to 2 MVA (Meyer and Carter-Brown, 2010). A delayed response to overload conditions often leads to premature aging of transformers. Transformers rated up to 2 MVA are in the majority, thus premature failure increases operational costs associated with downtime and replacement. The unavailability of online monitoring systems on such transformers increases the risk of premature transformer failures.

2.2 Electrical stresses and their effects on the distribution transformers

Electrical stresses observed within the distribution network occur due to faults occurring internally within the network and due to external factors such as lightning. Electrical stresses that may cause damage to distribution transformers are discussed below:

2.2.1 Harmonics

The need to save energy has resulted in an increase in the use of nonlinear loads such as Compact Fluorescent Lamps (CFL), electronic light ballasts and inverter-fed air conditioners. Other nonlinear loads that are more prevalent within the distribution network include battery chargers, computers, uninterruptable power supplies, adjustable speed drives, television sets and refrigerators. Nonlinear loads within the distribution system generate harmonics which may lead to premature failure of transformers. The current total harmonic distortion (THD) introduced by these components can be calculated as follows:

$$I_{THD} = \frac{\sqrt{\sum_{k=2}^{h} I_k^2}}{I_1} \text{ x } 100\% \qquad (2.1)$$

-where:

I_{THD} is the current total harmonic distortion [%]

I_1 is the fundamental current component [A]

I_k is the harmonic current component [A]

Harmonic currents cause harmonic voltages that increase the core loss. Eddy current losses are the most affected by harmonic currents as these are proportional to the square of the harmonic current magnitude and the square of the harmonic frequency. The presence of current harmonics often results in excessive losses and irregular heating, which may lead to premature transformer insulation failure. IEEE C57.12.00-1993 recommends that the total current harmonic distortion must be limited to 5% of the nominal load current. Excessive presence of harmonics often results in the need for derating of the loading capacity of a transformer. Sharengi et al. (2012) showed that the

loading capacity of a transformer had to be reduced by 35% percent when supplying CFLs as compared to linear loads such as incandescent lamps.

The penetration of CFLs in South Africa is on the rise and domestic loads are no longer purely linear as more non-linear equipment is used by households. The availability of a system that can monitor harmonics online can lead to the identification of transformers that are at risk of premature failure.

2.2.2 Overloading

Distribution transformers are subjected to different loading cycles at different environmental temperatures. Oil is often used to remove the heat generated by the transformer windings and the core. The cooling efficiency is often enhanced by the use of air-cooled radiators for transformers with ratings up to 500 kVA. The amount of heat generated is a function of the winding losses and the core losses. An increase in the load current results in an increase in the winding losses whilst an increase in the applied voltage results in an increase in the core losses which are proportional to the applied voltage squared (Harlow, 2004).

Overloading transformers causes (NL Meyer, 2010):

- Damage to tap changers and bushings as these are not designed to operate beyond certain current limits (typically 150% of the rated current)
- Paper degradation when the maximum winding temperature (i.e. hot spot temperature) exceeds 90^0C. Transformer life is halved for every 6^0C the hot spot temperature exceeds 98^0C.

Overloading of distribution transformers due to unplanned additional loads and changes in consumer patterns often occurs without the knowledge of distribution service providers. Other factors such as energy theft further increase the loading of distribution transformers.

2.2.3 Current and voltage transients

Distribution equipment is selected and co-ordinated such that it can either endure certain current and voltage stresses or be isolated by protection equipment. Pole mount transformer protection in Eskom Distribution is achieved through fuses and surge

arrestors. Fuses are rated such that they operate under short circuit conditions so as to isolate faulty transformers. Surge arrestors offer protection against high voltage transients which may be induced by lightning or switching.

Failure of a surge arrestor may lead to transformer failure and the unnecessary disconnection of a large number of customers. Annual lightning-induced transformer failures for the 2013/2014 financial year were reported as being 77.9 % out of 638 failed transformers within the Free State Operating Unit as shown in Table 2.1. The types of surges that such transformers experience are currently unmonitored. Failed surge arrestors often remain undiscovered and thus transformers are left exposed to high voltage transients. Due to the lack of online monitoring, distinction between transformer failures caused by prolonged overloading and surges remains blurry and thus development of wideband online monitoring systems is important. In this study transients in the form of impulse voltages and currents as defined in Appendix A and C respectively are studied.

Table 2.1: Financial year 2013/2014 transformer equipment failures in the Free State Operating Unit (Van Schalkwyk, Van Coller, 2013)

Average failures per year	*Total*	*Due to lightning*	*% Due to lightning*
MV fuses	7895	6160	78 %
MV\LV Pole Mounted Transformers	638	497	77.9 %
MV surge arrestors(10kA)	2312	2312	100 %

2.3 Electrical stress monitoring

The lack of monitoring on Eskom distribution transformers rated up to 2 MVA has resulted in the recent introduction of LV Current Voltage Monitors (CVM) by Kleinhans (2012). The use of such monitors which also log transformer operating temperature has shown that distribution transformers are often subjected to system faults, severe overloads and unbalances. Coupling such a system with GPRS communication has afforded distribution network operators with the ability to plan efficiently and implement corrective actions in a timely manner. Benefits observed from the system also include the ability to identify areas where illegal connections have been made.

The need to overcome low voltages occurring due to extension of long MV lines for further electrification of rural areas has led to the design of the Self-Regulated and Protected Electrification Transformer (SRAPET) (Beckers and Beukes, 2007). SRAPET combats the effect of increased load growth and provides overload protection. SRAPET monitors online voltages, currents (on the LV side) and temperature. This information is then used in estimating internal operating conditions of the transformer. Based on the analysed information, an effective tap position is selected to ensure that the voltage on the LV side remains within acceptable limits. SRAPET provides the benefit of reducing excessive aging and minimising downtime of distribution transformers. Although both SRAPET and CVM are different in their application, the additional information added by these technologies in the distribution networks optimizes transformers availability and thus contributes to the asset optimization attribute of the Smart Grid.

Electrical stresses such as harmonics and transients are currently not detected by the CVM units. Currently available monitoring units within Eskom do not monitor any electrical stresses observed on the MV side of such transformers. The lack of monitoring on the MV side can be attributed to the practicality of installing CTs and VTs that can perform such monitoring and the cost associated with implementing them. The impact that electrical stresses monitoring on the MV side would have opens up research opportunities related to the development of cost effective practical sensors that can be installed on such transformers. Figure 2.1 below shows a typical electrical stress monitoring system. CVMs are already structured in the form below; however these field transducers only capture LV signals and temperature readings. In this study, focus is on introducing wideband MV transducers capable of monitoring operating conditions on the MV side.

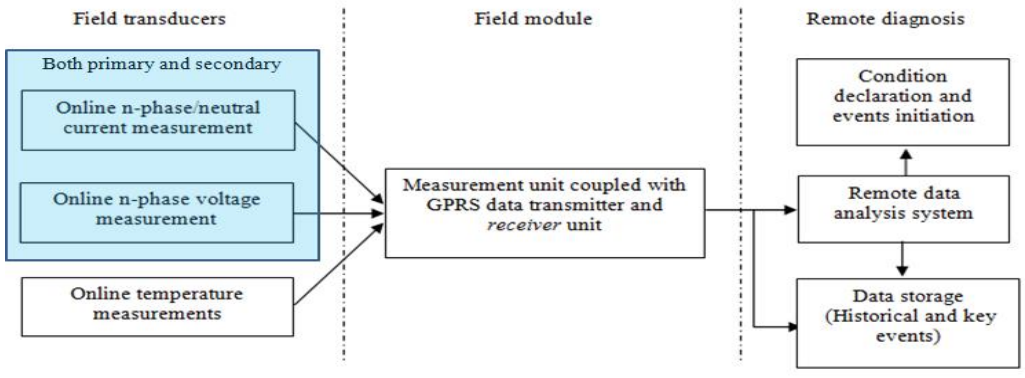

Figure 2.1: Typical electrical stress monitoring system applicable to pole mount transformer

2.4 Conclusion

The cost and practicality associated with the use of DGA remains the preferred diagnostics tool for larger transformers. Alternatives to DGA have had to be developed to curb premature failure of distribution transformers. The development of LV monitoring at distribution level has helped in identifying some of the electrical stresses that lead to premature failure of distribution transformers. Other stresses such as harmonics and electrical transients have also been shown to be factors that also lead to premature failure but remain unmonitored at distribution level. Transformers operating with failed surge arrestors are exposed to transient overvoltage conditions that may lead to premature failure. The development of cost effective MV side sensors capable of monitoring a wide variety electrical stresses is important.

Chapter 3

3 Modernisation of the distribution network (The Smart Grid)

Changes in loads and supply sources at distribution level are often not accompanied by corresponding changes in electrical infrastructure. The introduction of the Smart Grid concept provides viable options for modernising the distribution grid. Aging distribution networks often accommodate increased burdens from non-linear loads and varying energy penetration from distributed sources. Advancements in monitoring with the aim of identifying electrical stresses and implementing effective load management are key features that future grids must be equipped with. Online monitoring gives distribution Operating Units the ability to continue using aged infrastructure whilst identifying electrical stresses and applying control measures against potential threats that may lead to premature equipment failure. Key benefits that Eskom intends to achieve at distribution level with the introduction of the Smart Grid in South Africa include (Khatri, 2010):

- Circuit breaker and hot spot monitoring
- Overhead line and transformer monitoring
- Improved restoration times
- Performance improvement: SAIDI and SAIFI
- Energy management, demand response, energy theft, temper detection, usage management (appliances)

3.1 Performance improvement: SAIDI and SAIFI

Evaluation of online stresses provides network operators with an opportunity of identify areas that may require upgrades. Addition of cost effective sensors at strategic points in the network also has the added benefit of allowing network operators to identify areas

that may require strengthening. Systematic upgrades can thus be done within the network with minimal capital expenditure by prioritising areas that are at risk of failure. Price escalations can thus be limited as capital expenditure is directed at areas that have been prioritised. Implementation of prioritised upgrades has the added benefit of reducing the System Average Interruption Frequency Index (SAIFI) as areas that are most likely to fail are identified before they actually fail.

The planning of spares inventories is aided by identifying equipment that is severely stressed within the network. Advanced monitoring also reduces downtime as areas that are faulted can be quickly identified. Equipment for repairs can be identified prior to site visits based on the types of failures observed, thus reducing the System Average Interruption Duration Index (SAIDI). The monitoring system can also provide information with regards to historical data and performance once corrective actions have been implemented. This also has the added benefit of improving customer relations as the perceived level of service would have improved. Other added benefits include improved restoration times to critical areas within the network as faulted areas are identified quickly.

3.2 Line monitoring

Monitoring of currents and voltages contributes towards line condition monitoring. Failures of lines can thus be identified in a timely manner. Studies have shown where partial discharges on overhead lines aided in identifying areas where lines were sagging excessively (Hashmi et al, 2007). Identification of overloaded lines can be easily done and corrective actions can be implemented. Modernisation of the distribution grid that includes line monitoring thus improves equipment and human safety.

3.3 Asset management

Studies have shown that scheduled charging, also referred to as Smart Charging, of Plug-in Electric Vehicles (PEV) based on monitoring supply transformer operating limits and temperature often results in the reduction of transformer aging (Hilshey et al , 2013). Future penetration of electric vehicles is inevitable in the South African market. Management of the increased loading of transformers remains critical when considering future distribution grid conditions. Implementation of a monitoring system that schedules

charging based on transformer loading requires online monitoring of the distribution transformers and a communication infrastructure between end users and their supply transformers.

3.4 Theft management

Nontechnical losses that include high levels of theft of equipment and electricity, including illegal connections, affect network and service performance, thus increasing Eskom's operating costs (Eskom, 2013). Nontechnical losses are not unique to South Africa, with annual losses being reported to be as high as $4.5 billion in India, $1.6 billion in the USA and about $100 million in Canada (Depuru et al.,2012). Energy theft has an adverse effect on the tariffs paid by end users. Energy theft lowers the revenue available to distribution Operating Units, which in turn has an adverse effect on funds available for expansion projects and maintenance of existing assets (Smith, 2004). Online monitoring assists in identifying areas affected by energy theft, which can allow utilities to disconnect such areas or prosecute those responsible. Currently developed systems for monitoring energy theft require availability of online data.

3.5 Load management

Recent problems within Eskom have led to load shedding throughout South Africa. Load shedding mitigation steps taken initially involve requesting customers to reduce the load as informed by the media. If the load remains high then load shedding is implemented so as to prevent a nationwide blackout. Online monitoring provides Operating Units with information regarding areas that comply with the request to reduce load. This opens up opportunities to educate customers in areas that are not compliant and thus contributes towards load management. Studies have shown that the introduction of the Smart Grid can lead to a reduction in peak loads thus reducing the costs related to the generation of electricity (Ghosh and Schrader, 2012).

3.6 Distributed generation and renewable energy sources

The penetration of renewable energy sources at distribution level is projected to rise in the future South African energy mix (DoE, 2013). Sources such as solar and wind depend

on environmental condition and thus provide variable electrical energy to the distribution networks which increases electrical stresses on equipment. The penetration of rooftop solar energy has resulted in the need to improve online monitoring so as to account for the rapid changes in supply and load (Alam et al, 2013). The presence of Independent Power Producers (IPPs) at distribution level also warrants online monitoring.

3.7 Cost to benefit overview

Modernisation of the South African distribution grid will come at a cost; however long term benefits outweigh potential failures if nothing is done. The availability of affordable transducers will allow the adoption of modernisation strategies. Current Voltage Monitors (CVMs) provide online LV side currents and voltages and top oil temperature measurements that are then communicated to distribution network operators. Transformers which experience severe stresses such as overloading and unbalances have been successfully identified. This has led to a reduction in the number of transformers that fail prematurely.

Monitoring of other stresses such as harmonics and transients has the potential of further reducing premature failure of distribution transformers. The introduction of MV side monitoring is critical as most IPPs access the distribution networks at MV level. Changes introduced by variation of electrical energy supply can thus be monitored if affordable monitoring technology is available. Challenges brought about by distributed generation can thus be continuously monitored to allow optimised integration with existing centralised generation sources. Information obtained from monitoring can thus be used for protection, control and fault diagnosis.

3.8 Conclusion

The challenges associated with rolling blackouts experienced in South Africa are some of the key reasons why electrical monitoring has become critical. The ability to communicate with end users and alter behaviour with regards to energy usage has been highlighted as a key factor that can result in the reduction of peak load. The ability to monitor whether power has been restored as per the scheduled rolling blackout schedule is one of the main areas that can further improve consumer relations. The financial burden currently experienced within Eskom also highlights the need to ensure effective revenue

collection and the need to identify areas where energy theft is being experienced. The limited funds availability also implies that assets in the field are required to operate for their designed life. Thus monitoring of electrical stresses is critical in achieving the maximum service life of assets such as transformers.

The penetration of renewable sources also introduces electrical stresses that have to be monitored within the distribution networks. An increase in the percentage share of renewable energy sources also implies that there may be areas that may require network strengthening and identification of such areas requires an increased level of monitoring. The future penetration of electric vehicles has also been identified as one of the loads that may require scheduling so as to avoid premature aging of key distribution assets such as distribution transformers. Increased levels of reliability and availability of future distribution networks, needs increased levels of monitoring Continuous monitoring at distribution level offers opportunities to improve planning and maintainability of the network. Monitoring also leads to opportunities for improving turnaround time for repairs within the network. Such monitoring also offers opportunities to interact with consumers such that consumer energy consumption patterns may be altered such that there is a delayed need for large capital expenditure to meet peak load demand. Modernisation of the distribution grid remains crucial in meeting the ever changing consumer patterns and expected service levels of the modern day consumer. The availability of cost effective sensors and associated communication infrastructure are features that can enable improved service delivery by utilities.

Chapter 4

4 Current and voltage monitoring

4.1 Introduction

Wideband current and voltage monitoring is unachievable with conventional CTs and VTs due to their frequency bandwidth limitations. These limitations have resulted in the development of non-conventional current and voltage transducers such as Hall Effect current transducers (Hartmann et al., 2009). Embedding wideband current and voltage sensors into bushings such as those in Figure 4.1 has the capability of providing online operational data that can enhance the management of utility equipment. The research presented focusses on Rogowski current transducers and capacitive voltage dividers for measuring both power frequency and transient currents and voltages on the MV side of distribution transformers.

Figure 4.1: Combined current and voltage sensing bushing and a variety of non-sensing bushing (Netshiongolwe, et al)

4.2 Rogowski coil current monitoring

4.2.1 Operating principle

Rogowski coil is a current measuring device that usually takes the form of a winding with a non-magnetic core. Rogowski current transducers such as the one depicted in Figure 4.2 have been shown to have the following superior features by Ray and Hewson (2000), Javora et.al (2009) and the IEEE standard C37.235 (2007):

- High bandwidth (suitable for transients)
- Large primary current measurement range
- Non-intrusive in the primary circuit
- Modular in size
- Linear

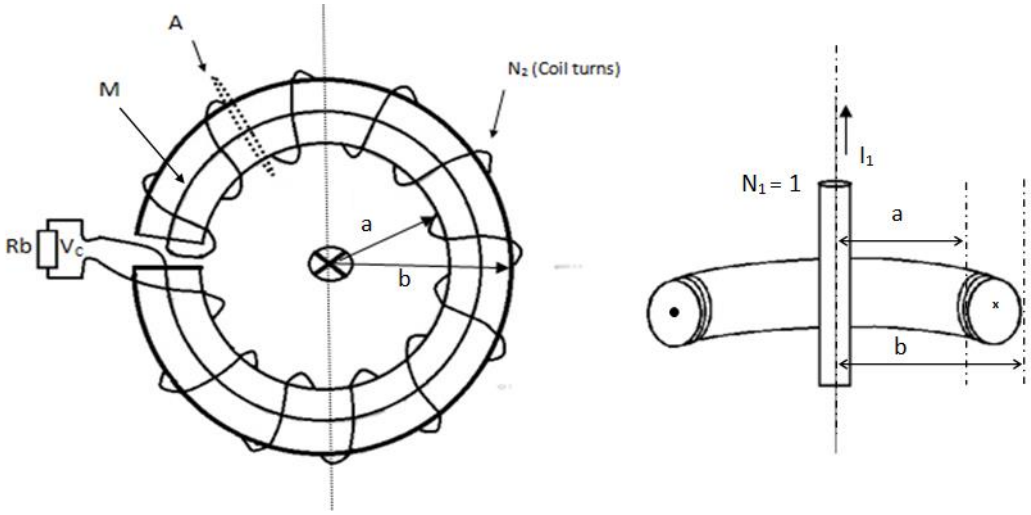

Figure 4.2: Toroidal Rogowski coil sensor with circular cross-sectional area

Rogowski coil operation is based on Ampere's Law, wherein the coil senses the magnetic field in the space around a current carrying conductor, based on the following expression (Ward et. al, 1993):

$$H = \frac{i}{2\pi R} \tag{4.1}$$

-where:

i is the primary current [A]

H is the magnetic field strength at radius R [A/m]

R is the radius at which the magnetic field strength is calculated [m]

The flux linking the entire coil given by (Ward, 1993, Phillips et al., 1996):

$$\varphi = NBA = N\mu_0 HA = N\frac{\mu_0 i}{2\pi R}A = \mu_0 \frac{N}{2\pi R}Ai \tag{4.2}$$

-where:

φ is the total flux linkage [webers]

$\mu_0 = 4\pi \times 10^{-7}$[H/m], Permeability of air

N is the number of turns

A is the coil cross sectional area [m^2]

B is the flux density [webers/m^2]

The voltage induced in the Rogowski coil is then given by Faraday's Law (Ward et al, 1993, Phillips et al., 1996):

$$v = -\frac{d\varphi}{dt} = -\mu_0 \frac{N}{2\pi R} A \frac{di}{dt} = -M\frac{di}{dt} \tag{4.3}$$

-where:

v is the coil output voltage [V]

M is the mutual inductance [H]

The primary current is obtained by integrating the coil voltage. Petting and Siersema (1983) implemented integrating circuits capable of measuring currents with frequencies below 100 kHz, whilst Ray and Davis (1999) developed methods of measuring currents beyond 100 kHz. The parameters of the coils in both cases did not change whilst measuring power frequency and transient currents. A combination of the coil parameters and the parameters of the circuit performing the integration influenced the overall bandwidth of the Rogowski coils. Swanson (2006), Schon and Schuppel (2007) replaced the integration using electronic circuits with numeric integration. In this study numerical integration was performed using Matlab.

4.2.2 Rogowski coil electrical modelling

Distributed parameter modelling of Rogowski coils was done by Ray and Davis (1999). Kojovic (2005) recently used a lumped parameter model and the ATPdraw saturable transformer modified to give a linear magnetization branch as illustrated in Figure 4.3.

The physical dimensions of a Rogowski coil affect the overall performance with regards to current sensitivity and bandwidth.

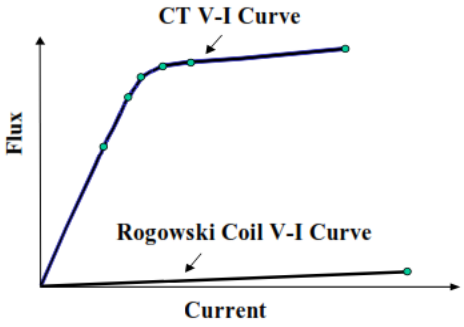

Figure 4.3: Rogowski coil flux-current characteristics (Kojovic, 2005)

4.2.3 Calculated Rogowski coil parameters

In this study toroidal Rogowski coils with a circular cross sectional area were evaluated. Two Rogowski coils, with properties shown on Table 4.1, were designed and their performance under transient and power frequency conditions was compared. Each of the Rogowski coils was screened to avoid electrostatic interference (Swanson, 2006, Ray, 2004). Table 4.2 below shows the calculated coil parameters based on the designed Rogowski coils. The coil self-inductance and mutual inductance based on physical parameters can be calculated as follows, with reference to Figure 4.4 (Hlavacek et al., 2008):

$$L_2 = \frac{\mu_0 {N_2}^2}{2}\left(a + b - 2\sqrt{ab}\right) \tag{4.4}$$

$$M_{12} = \frac{\mu_0 N_2}{2}\left(a + b - 2\sqrt{ab}\right) \tag{4.5}$$

-where:

L_2 is the coil self-inductance [mH]

M_{12} is the coil mutual inductance between the coil and the primary conductor (current carrying conductor) [H]

N_2 is the number of turns

a is the toroid coil inner diameter [mm]

b is the toroid coil outer diameter [mm]

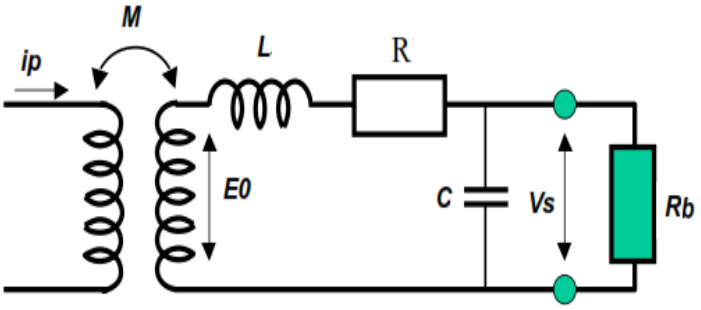

Figure 4.4: Model of a Rogowski coil

Thus, using Equation 4.4, the self-inductance numerical expression for Coil 1(418 turns) which has parameters shown in Table 4.1 is the given by:

$$L_2 = \frac{4\pi\times10^{-7}\mathrm{H}m^{-1}\times418^2}{2}\times\left(0.035+0.0425-2\times\sqrt{0.035\times0.0425}\right)m\ = 0.096\ \mu H$$

The corresponding self-inductance numerical expression for Coil 2 (875 turns) with the parameters in Table 4.1 then becomes:

$$L_2 = \frac{4\pi\times10^{-7}\mathrm{H}m^{-1}\times875^2}{2}\times\left(0.0335+0.0557-2\times\sqrt{0.0335+0.0557}\right)m\ = 1.75\ \mu H$$

From Equation 4.5 the numerical expression for mutual inductance M_{12} for Coil 1 is given by:

$$M_{12} = \frac{4\pi\times10^{-7}\mathrm{H}m^{-1}\times418}{2}\times\left(0.035+0.0425-2\times\sqrt{0.035\times0.0425}\right)m\ = 0.040\ mH$$

The numerical expression for mutual inductance M_{12} of the Coil 2 is given by:

$$M_{12} = \frac{4\pi\times10^{-7}\mathrm{H}m^{-1}\times875}{2}\times\left(0.0335+0.0557-2\times\sqrt{0.0335+0.0557}\right)m\ = 1.5\ mH$$

Kojovic (2005) however suggests that the mutual inductance is given by:

$$M = \mu_0\frac{N_2}{L}A \qquad (4.6)$$

-where:

L is the coil length[m]

A is the toroidal core area[m^2]

N_2 is the number of turns

M is the coil mutual inductance[μH]

Based Equation 4.6 and Table 4.1 the 418 turns Coil 1 mutual inductance:

$$M = 4\pi \times 10^{-7}\mathrm{H}m^{-1} \times \left(\frac{418}{9.2m}\right) \times \pi\left(\frac{0.0425 - 0.035}{2}\right)^2 m^2 = 45\ pH$$

From Equation 4.6 the 875 turns Coil 2 mutual inductance is given by:

$$M = 4\pi \times 10^{-7}\mathrm{H}m^{-1} \times \left(\frac{875}{60.5m}\right) \times \pi\left(\frac{0.0557 - 0.0335}{2}\right)^2 m^2 = 38.5\ pH$$

The corresponding calculated turn-to-turn wire stray capacitance (C_{ct}) is given by:

$$C_{ct} = \frac{\pi\varepsilon_0 L}{(N_2 - 1)\left(\log\left[\frac{\frac{L}{N_2}}{b-a}\right] + \sqrt{\left[\frac{\frac{L}{N_2}}{b-a}\right]^2 - 1}\right)} \tag{4.7}$$

-where:

C_{ct} is the turn-to-turn wire stray capacitance [F]

ε_0 is the permittivity of free space[F/m]

L is the coil length [m]

a is the toroid coil inner diameter [mm]

b is the toroid coil outer diameter [mm]

For the 418 turns coil the turn-to-turn capacitance C_{ct} is given by:

$$C_{ct} = \frac{\pi \times 8.85\text{x}10^{-12}\frac{\mathrm{F}}{\mathrm{m}} \times 9.2m}{(418-1) \times \left(log\left[\frac{\frac{9.2m}{418}}{(0.0425-0.035)\mathrm{m}}\right] + \sqrt{\left[\frac{\frac{9.2m}{418}}{(0.0425-0.035)\mathrm{m}}\right]^2 - 1}\right)}$$

$= 0.19\ pF$

For the 875 turns coil the turn-to-turn capacitance C_{ct} is given by:

$$C_{ct} = \frac{\pi \times 8.85\text{x}10^{-12}\,\frac{\text{F}}{\text{m}} \times 65\text{ m}}{(865-1) \times \left(log\left[\frac{\frac{65\text{m}}{865}}{(0.0575-0.0335)\text{m}}\right] + \sqrt{\left[\frac{\frac{65\text{m}}{865}}{(0.0575-0.0335)\text{m}}\right]^2 - 1} \right)}$$

$= 0.6\ pF$

C_{ct} is however often ignored as it is much smaller than the turn to return wire capacitance as given by:

$$C_c = \frac{4\pi^2 \varepsilon_0 (2a+2b)}{log\left[\frac{2a+2b}{2b-2a}\right]} \tag{4.8}$$

-where:

C_c is the turn to return wire stray capacitance [F]

The turn to return wire capacitance for the 418 turns coil is then given by:

$$C_{ct} = \frac{4 \times \pi^2 \times 8.85\text{x}10^{-12}\,\frac{\text{F}}{\text{m}} \times (2\text{ x }0.0425 + \ 2\text{ x }0.035)m}{log\left[\frac{(2\text{ x }0.0425 + \ 2\text{ x }0.035)}{(2\text{ x }0.0425 - \ 2\text{ x }0.035)}\right]}$$

$= 53.394$ pF

Whilst the return wire capacitance for the 875 turns coil is given by:

$$C_{ct} = \frac{4 \times \pi^2 \times 8.85\text{x}10^{-12}\,\frac{\text{F}}{\text{m}} \times (2\text{ x }0.0575 + \ 2\text{ x }0.0335)m}{log\left[\frac{(2\text{ x }0.0575 + \ 2\text{ x }0.0335)}{(2\text{ x }0.0575 - \ 2\text{ x }0.0335)}\right]}$$

$= 110$ pF

Table 4.1: Designed Rogowski coil properties

Parameter	*Parameter description*	*Coil 1*	*Coil 2*
$d_w[mm]$	Wire diameter	0.455	0.375
$R[\Omega]$	Wire resistance	1.33	18.66
a[mm]	Toroid inner radius	35	33.5
b[mm]	Toroid outer diameter	42.5	57.5
L[m]	Coil length	9.2	65
A[mm^2]	Coil area	38.48	452.39
N_2	Number of coil turns	418	875
ε_0[F/m]	Permittivity of free space	$8.85x10^{-12}$	$8.85x10^{-12}$

Table 4.2: Calculated coil parameters

Parameter	*Coil 1*	*Coil 2*
$L_2[\,mH]$	0.04	1.5
$M_{12}[\mu H]$	0,096	1.75
$C_{ct}[pF]$	0.190	0.604
$C_c[pF]$	53.394	110

4.2.4 Measured coil parameters

Studies have shown a difference between simulations based on calculated and measured coil parameters, with most authors opting for measured parameters in wideband applications (Hashmi et al., 2007, Shafiq et al., 2014). Hashmi et al. (2007) used coil parameters measured at 1 kHz to determine the parameters of a Rogowski coil used for partial discharge measurement. Shafiq et al. (2014) developed a parameter identification method that involved measuring impulse waveforms with a Rogowski coil. A Fast Fourier Transform (FFT) was used to find the resonant frequencies for different configurations and the resonant frequencies are used to determine the relationship between the inductances and capacitances of the coil.

In this study, an LCR meter, function generator, oscilloscope and tank circuit were used to determine the coil parameters. An Isotech LCR 821 meter at a frequency of 1 kHz was used to determine the coil inductance. The measured inductance was also verified using an LCR 612 meter also set to a frequency of 1 kHz. The measured inductance, L_m, shown in Table 4.3 below was then used to determine the coil stray capacitance. A resistor in

series with a coil that was parallel to a known capacitor (C_T) was used to determine the coil capacitance.

The voltage across the coil reaches a peak at the point of resonance where the relationship between the total circuit capacitance and the inductance is given by:

$$F_r = \frac{1}{\sqrt{L_T(C_m + C_p + C_T)}} \tag{4.9}$$

-where:

F_r is the tank circuit resonance frequency[Hz]

L_m is the coil inductance[H]

C_m is the coil stray capacitance[F]

C_p is the probe capacitance[F]

C_T is the known capacitor[F]

Based on Equation 4.9 and the known capacitor C_{T1} with a measured tank resonant frequency F_{r1}, Equation 4.9 can be rearranged such that:

$$F_{r1}{}^2 L_m(C_s + C_m + C_{T1}) = 1 \tag{4.10}$$

For known capacitance C_{T1} and measured tank resonant frequency F_{r2} the above equation becomes:

$$F_{r2}{}^2 L_m(C_s + C_m + C_{T2}) = 1 \tag{4.11}$$

Taking a ratio of Equations 3.10 and 3.11 results in the following expression:

$$\left(C_p + C_m + C_{T1}\right) = \frac{F_{r1}{}^2}{F_{r2}{}^2}\left(C_p + C_m + C_{T2}\right)$$

From the above expression the coil stray capacitance and probe capacitance are given by:

$$C_m + C_p = \frac{C_{T2}\left(\frac{F_{r1}{}^2}{F_{r2}{}^2}\right) - C_{T1}}{1 - \frac{F_{r1}{}^2}{F_{r2}{}^2}} \tag{4.12}$$

Shafiq et al. (2014) suggested taking other measurements with the tank circuit components unchanged; however in this case two probes are used in order to determine the probe capacitance. The above expression is then modified such that:

$$C_m + 2C_p = \frac{C_{T2}\left(\frac{F_{r21}^{\,2}}{F_{r22}^{\,2}}\right) - C_{T1}}{1 - \frac{F_{r21}^{\,2}}{F_{r22}^{\,2}}} \tag{4.13}$$

-where:

F_{r21} and F_{r22} are the new resonance frequencies resulting from the additional probe capacitance

The probe capacitance is calculated by subtracting Equation 4.13 from Equation 4.12. Once the probe capacitance is calculated, the coil capacitance is then evaluated using Equation 4.12. Table 4.3 gives all the corresponding measured parameters of the designed Rogowski coils. The accuracy of both measured and calculated parameters is evaluated by comparing simulated and measured results in the next section.

Table 4.3: Measured coil parameters

Parameter	*Coil 1*	*Coil 2*
Coil turns	418	875
C_{T1} [pF]	12	12
C_{T2}[pF]	56.25	56.25
F_{11} [MHz]	3.9	1.27
F_{12} [MHz]	3.1	1.07
F_{21} [MHz]	3.7	1.02
F_{22} [MHz]	3.0	0.88
C_p[pF]	17.9	19
C_m[pF]	46	84
L_m[mH]	0.029	0.88
M[μH]	0,069	1
C_m[pF]	44	84

4.2.5 Rogowski coil bandwidth and terminating resistance impact

Rogowski coils with the previously measured parameters were terminated with 1% 179 Ω and 2 kΩ resistances. The Rogowski coil transfer function, $H(s)$, for the equivalent circuit of Figure 4.4 is given by :

$$H(s) = \frac{s.M}{s^2LC + s.\left(RC + \frac{L}{R}\right) + \left(\frac{R}{Rb} + 1\right)} \qquad (4.14)$$

-where:

$H(s)$ is the coil transfer function

L is either the calculated or the measured coil inductance [mH]

M is the coil mutual inductance based on either measured or calculated parameters, in [μH]

C is either the calculated or the measured coil capacitance [pF]

R is the coil resistance [Ω]

Rb is the coil terminating resistance [Ω]

Plots of the transfer function based on both measured and calculated parameters are given in Figures 4.5 to 4.8 below. The observed waveform show that the coil parameters of the 418 turn Rogowski coil shown in Figures 4.7 and 4.8 have larger bandwidth when compared to the 875 turn Rogowski coil. This is consistent with studies that have shown that an increase in the number of turns reduces the observed bandwidth because of the self-inductance.

Further analysis of the plots also shows that the bandwidth of the coils can be increased by increasing the size of the terminating impedance. A comparison between calculated and measured behaviour shows that the bandwidth resulting from measured parameters is less than that of the calculated parameters. Figures 4.5 to 4.8 exclude the influence of the mutual inductance, however Tables 4.2 and 4.3 how that the 875 turn Rogowski coil has a much larger mutual inductance (as expected) which increases its output voltage to primary current ratio.

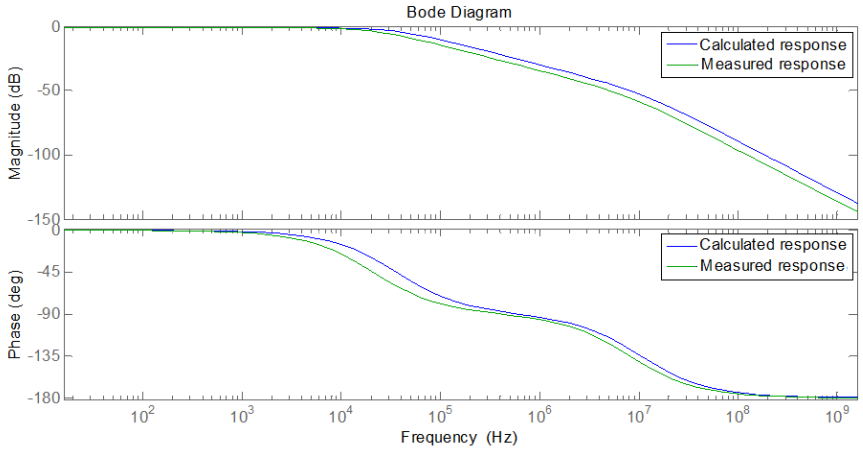

Figure 4.5: Transfer function for the 875 turn Rogowski coil terminated with a 2 **kΩ** resistor

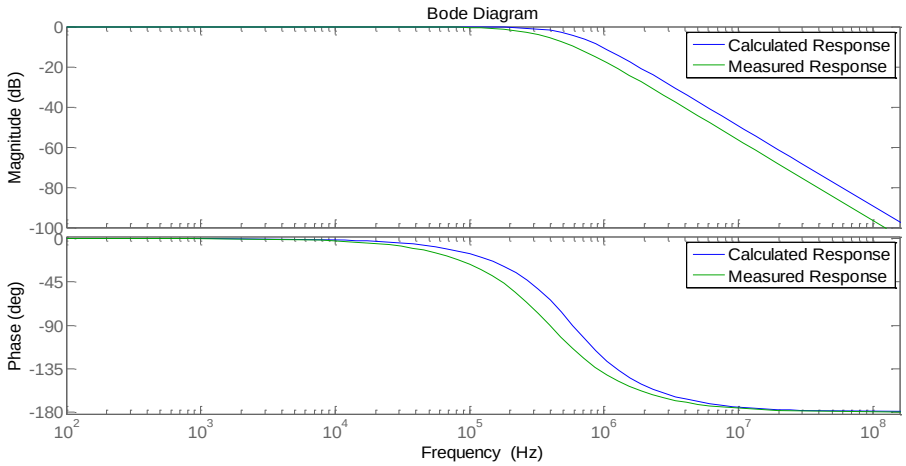

Figure 4.6: Frequency response of the 875 turn Rogowski coil terminated with a 2 kΩ resistor

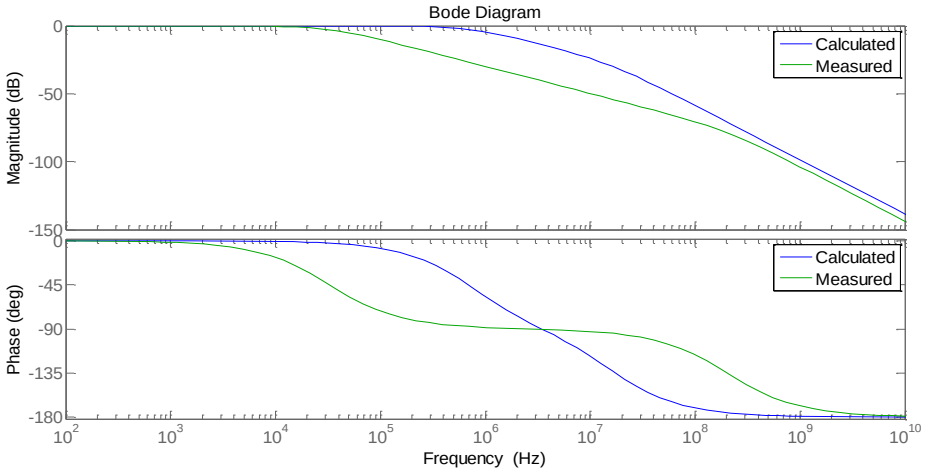

Figure 4.7: Transfer function for the 418 turn Rogowski coil terminated with a **179 Ω** resistor

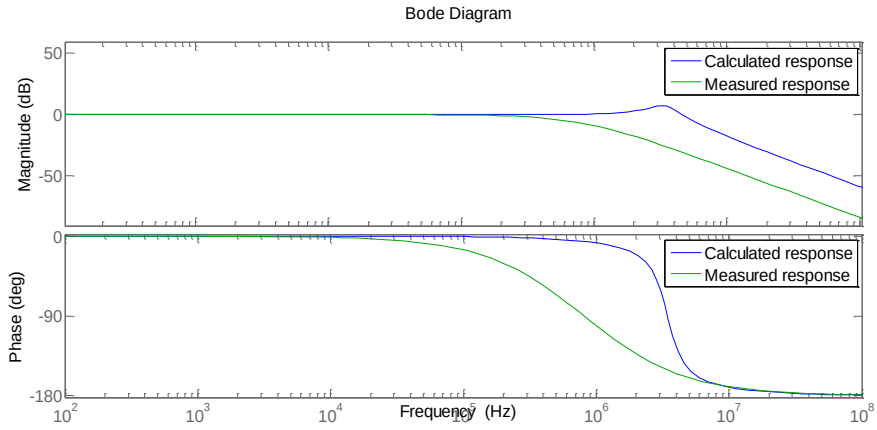

Figure 4.8: Transfer function for the 418 turn Rogowski coil terminated with a **2 kΩ** resistor

4.3 Capacitive Voltage Divider

4.3.1 Operating principle

Recent developments have resulted in the use of capacitive voltage dividers in medium voltage switchgear and overhead lines as shown by Javora et al. (2009) and Behzadi et al. (2007) respectively. Solid insulation bushings used on transformers can either be ceramic, cycloaliphatic epoxy resin or silicone enclosed epoxy resin. Silicone enclosed epoxy resin bushings will be considered for this study. Solid insulation bushings often contain an embedded screen used for field control in the area where the bushing passes the earthed transformer tank (Ryan, 2001). The presence of such a screen sets up capacitance between the conductor and the screen. The magnitude of such a capacitance is a function of the dimension of the screen relative to the MV conductor and the dielectric properties of the insulation that separates them.

4.3.2 Capacitive voltage divider modelling

A 24kV screened epoxy bushing was used for this research. The electrical properties of the insulation between the screen and the MV conductor can be represented as a resistor in parallel with a capacitor as shown in Figure 4.9. The insulation capacitance between the conductor and the screen is given by Kuffel et al. (2000) with reference to Figure 4.9 and Table 4.4 parameters:

$$C_1 = \frac{2\pi\varepsilon_0\varepsilon_r' h}{\ln\frac{b}{a}} \tag{4.16}$$

-where:

C_1 is bushing internal capacitance [F/m]

ε_0 is permittivity of free space [F/m]

ε_r' is relative permeability(Re - Real)

a is the conductor radius [m]

b is the screen radius [m]

h is the screen height [m]

The corresponding insulation resistance at angular frequency w is given by:

$$R_1 = \frac{h \ln \frac{b}{a}}{4\pi^2 f \varepsilon_0 \varepsilon_r''} \tag{4.17}$$

-where:

R_1 is bushing internal resistance [Ω/m]

f is the conductor radius [m]

ε_0 is permittivity of free space [F/m]

ε_r'' is Relative permeability (I_m-Imaginary)

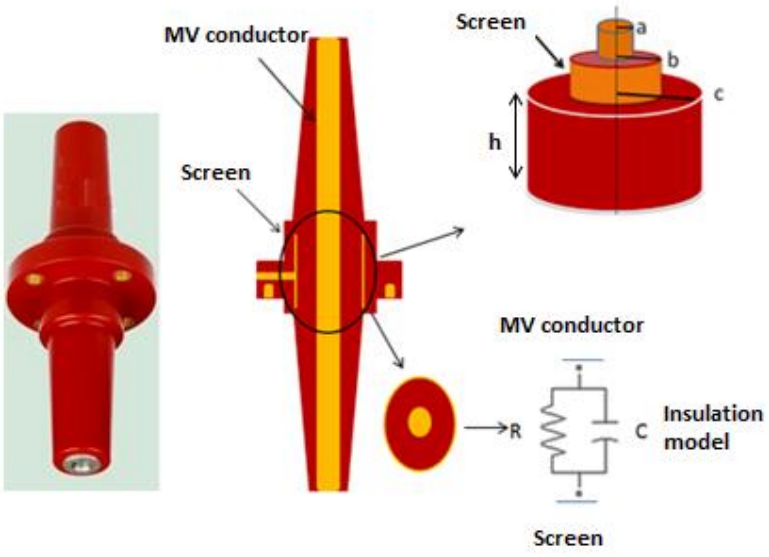

Figure 4.9: Cross-sectional view of a screened 24 kV epoxy resin bushing with emphasis on the position of the screen relative to the MV conductor

Table 4.4: Epoxy resin 24 kV bushing parameters

Parameter	*Parameter description*	*Value*
ε_0	Free space permittivity	8.854E-12 F/m
ε_r'	Relative permeability(R_e)	3.8
ε_r''	Relative permeability (I_m)	0.038
tan delta	Epoxy resin tan delta	0.01
a	Conductor radius	0.012 m
b	Screen radius	0.03 m
h	Screen height	0.06 m
f	Frequency in Hz	_____

The capacitance of the bushing is sensitive to variations in the screen dimensions and overall screen positioning relative to the MV conductor. Slight variation of the screen dimensions may occur during the hot curing of the epoxy insulation during assembly. Table 4.5 below shows a comparison between calculated capacitance and measured capacitance using an LCR 821 meter. The calculated capacitance is slightly less than the measured capacitance. Variation of the capacitance screen radius from 0.03m to 0.027m matches the capacitance value, which could have resulted during curing of the screen. In this study the measured capacitance value is used in simulations that compare measurements of both power frequency and transient voltages.

Table 4.5: Bushing insulation capacitance

Parameter	*Radius*	*Calculated*	*Measured*
C_1[pF]	0.03 m	13.8 Pf	22 pF
C_1[pF]	0.027 m	22 pF	22 Pf

Connecting a fixed capacitor, C_2, between ground and screen results in the resistor-capacitor (RC) divider shown in Figure 4.10. The insulation resistance is high at power frequencies and thus the MV voltage V_{in} can be related to the screen voltage V_{out} by the equation:

$$V_{out} = \frac{C_1}{C_1 + C_2} V_{in} \tag{4.18}$$

-where:

V_{in} is the MV conductor phase-earth voltage [V]

C_1 is the insulation capacitance [F]

C_2 is the fixed external capacitance [F]

V_{out} is the screen output voltage [V]

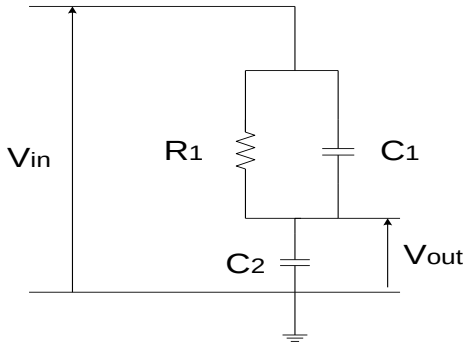

Figure 4.10 Equivalent circuit of the RC

4.4 Conclusion

Rogowski coils offer wideband current monitoring that is not affected by saturation effects as compared to conventional ferromagnetic CTs. The transfer function (gain) of the Rogowski coil is determined by the coil parameters. A comparison between calculated and measured parameters of the 875 and 418 turn Rogowski coils shows that calculated parameters suggest a larger bandwidth as compared to the measured parameters. Parameters were measured using coil resonance point identification. The 418 turn Rogowski coil has a larger bandwidth than the 875 turn Rogowski coil.

A screened bushing provides a viable solution for MV voltage monitoring. The insertion of a capacitance between ground and screen sets up a capacitive voltage divider capable of wideband voltage measurements. The insulation resistance however affects the overall performance of the divider as will be shown in the next section.

Chapter 5

5 Experimental setup and corresponding circuit simulations

5.1 Power frequency current measurement

5.1.1 Experimental setup

The performance of the 418 and 875 turn Rogowski coils was evaluated under power frequency conditions by varying the 50 Hz primary currents from 1 A to 1600 A. Figure 5.1 shows the experimental setup. The two Rogowski coils were placed around the 24 kV bushing that had the 50 Hz current passing through it.

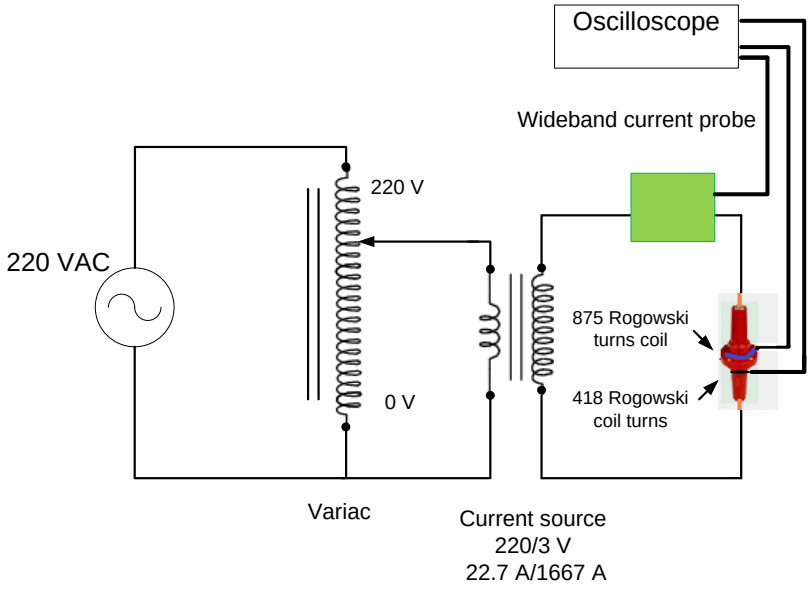

Figure 5.1: Power frequency current measurement using Rogowski coils and a wideband current probe. (Netshiongolwe et al., 2015)

A wideband current probe was placed around the current carrying conductor in close proximity to the bushing for comparison purposes. The outputs of the Rogowski coils and the wideband current probe were connected to a RIGOL 1064B oscilloscope using 10:2 voltage probes. Current adjustment was achieved by using a variac that varied the input voltage of a current source from 1V up to 220 V which in turn varied the output current from 1A up to 1600 A. The output of the wideband current probe was a 50 Hz voltage signal that was in phase with the primary current with a scaling factor of 100 A:1 V. The Rogowski coil output voltages were 90 degrees out of phase with the primary current (as expected). Each of the measured Rogowski coil output voltages were processed using numerical integration and compared with simulated currents.

5.1.2 Rogowski coil simulation

The Rogowski coil simulations were performed using ATPdraw. The parameters in section 4.2 were used in the simulations using the circuit shown in Figure 5.2 below. The 10/1 voltage probe connected to the coil terminating resistor R_b was included in the model. The oscilloscope was modelled with an input resistance of 1 $M\Omega$. The ATPdraw saturated transformer model discussed in section 4.2.2 above was used with the corresponding mutual inductances identified during the parameter identification stage. The ATPdraw AC current source with magnitude, phase and frequency comparable to the lab supply was used to simulate the current passing through the bushing. The ATPdraw user-defined voltage source was used to reproduce the lab measured Rogowski coil output voltage which is referred to as the measured reference signal in Figure 5.2.

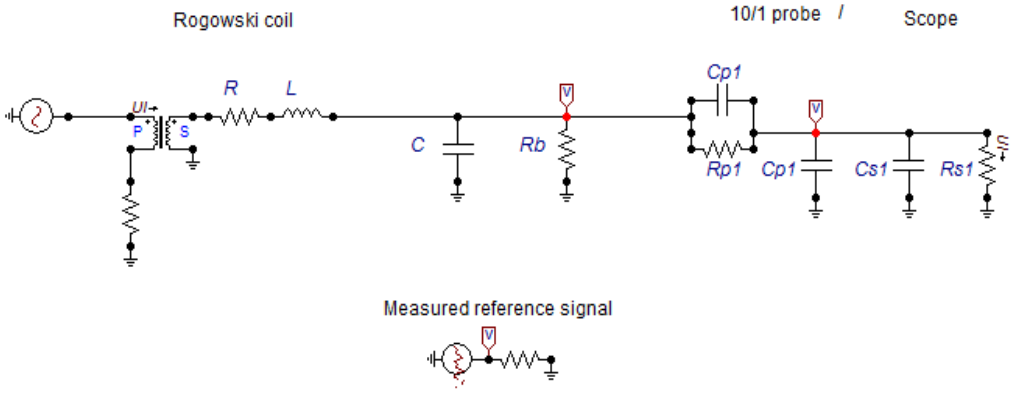

Figure 5.2: Model used for power frequency current simulations

5.2 Impulse Current Measurements

5.2.1 Experimental setup

8/20 µs current impulses of various amplitudes were generated using the current impulse generator shown in Figure 5.3 below. The input voltage was varied with a variac which varied the output of a 220/22000 V transformer. The output of the transformer was rectified and then used to charge up a bank of capacitors. The capacitors were then discharged through a wave shaping circuit that consisted of a resistor and inductor connected in series with the bushing surrounded by both the 418 and 875 turn Rogowski coils as shown in Figure 5.3. A wideband current probe was placed around the current carrying conductor in close proximity to the bushing. Once the pulse had been captured excess charge was removed from the capacitor through the dump resistor. Each of the measured signals was sent through to the scope with an input resistance of 1 $M\Omega$ in parallel with an18 pF capacitance.

5.2.2 Rogowski coil simulations

The ATPdraw user-defined current source was used to reproduce the impulse currents generated by the impulse generator in Figure 5.3 below.

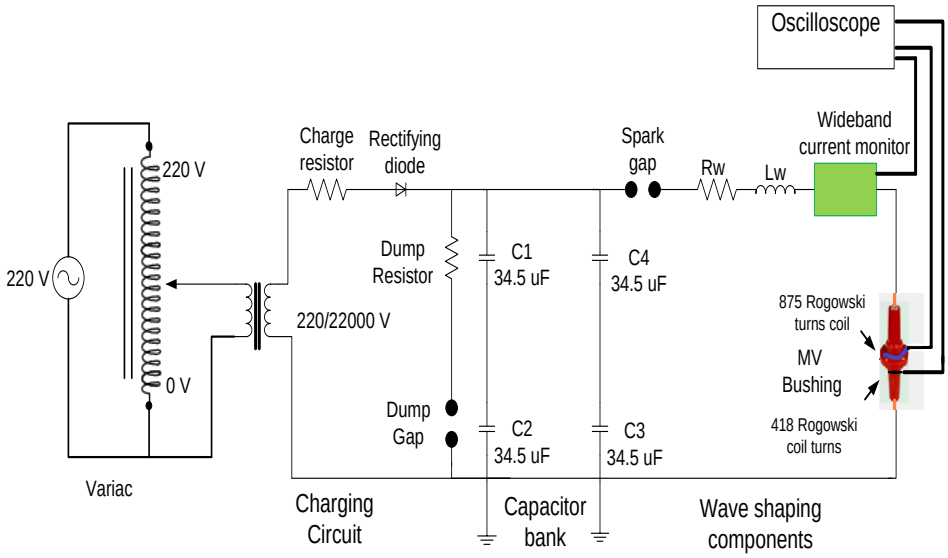

Figure 5.3: Impulse current measurement using Rogowski coils and a wideband current probe

The simulated circuit is shown in Figure 5.4. The reproduced current impulses were the input signal to the model of the Rogowski coil. Another ATPdraw user-defined voltage

source was used to reproduce the laboratory measured Rogowski coil output voltage which is referred to as the measured reference signal in Figure 5.4. The 10:1 voltage probe was modelled as well as the 1 MΩ input resistance of the oscilloscope.

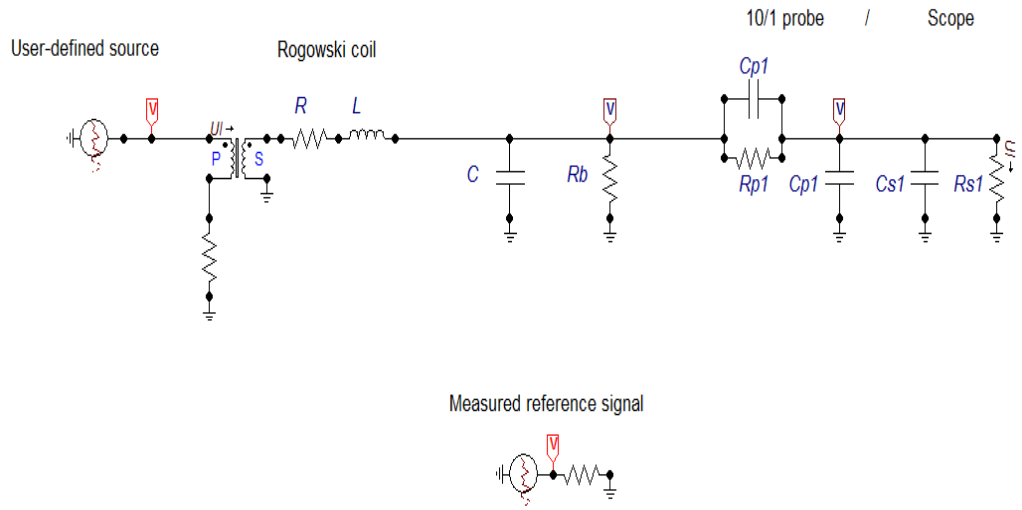

Figure 5.4: Model used for impulse current simulations

5.3 Power Frequency Voltage Measurements

5.3.1 Experimental setup

A variac was used to vary the output of a 220/60000 V transformer as shown in Figure 5.5 below. The output of the transformer was connected to the 24 kV bushing load. A laboratory 1000/1 capacitive voltage probe was used to measure the line voltage for comparison purposes. The 24 kV bushing screen was connected to a capacitor to create a capacitive voltage divider. The input voltage was varied such the transformer output voltage varied from 1 kV up to 24 kV. The outputs of both the commercial capacitive voltage divider and the bushing capacitive voltage divider (CVD) were both connected to a Rigol 1046B oscilloscope.

5.3.2 Model used for bushing capacitive voltage divider simulations

The ATPdraw AC voltage source was used to generate the output of the step-up transformer in Figure 5.5 below. The amplitude of the simulated AC voltage source was varied from 1 kV up to 24 kV whilst the corresponding bushing CVD output was measured and compared to the output of the laboratory capacitor divider. The ATPdraw

user-defined voltage source was used to reproduce the waveform produced by the laboratory supply transformer for input to the models of the laboratory capacitor voltage divider and the bushing capacitive voltage divider.

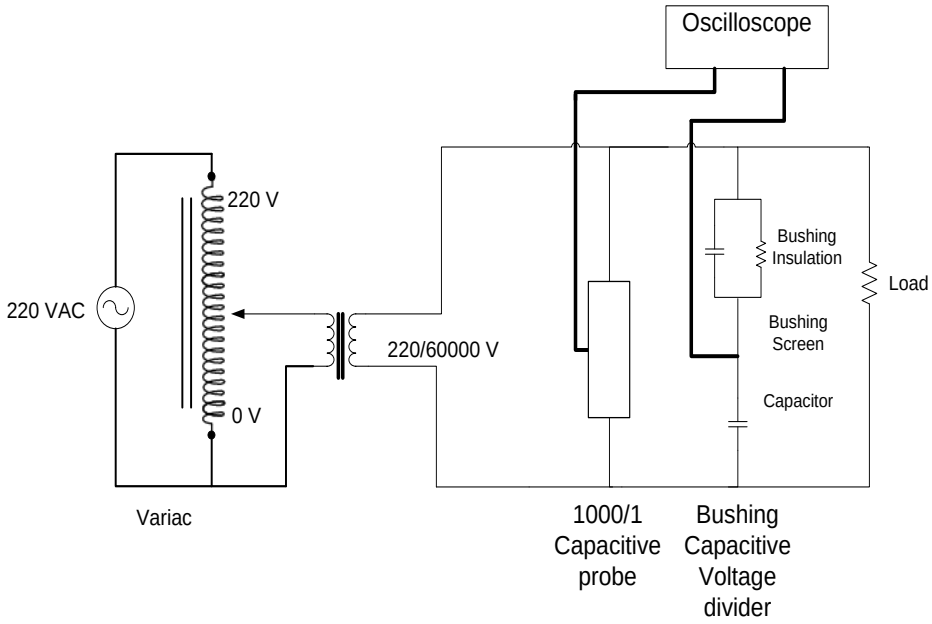

Figure 5.5: Power frequency voltage measurement using the bushing capacitor voltage divider (CVD) and a laboratory capacitive voltage divider.

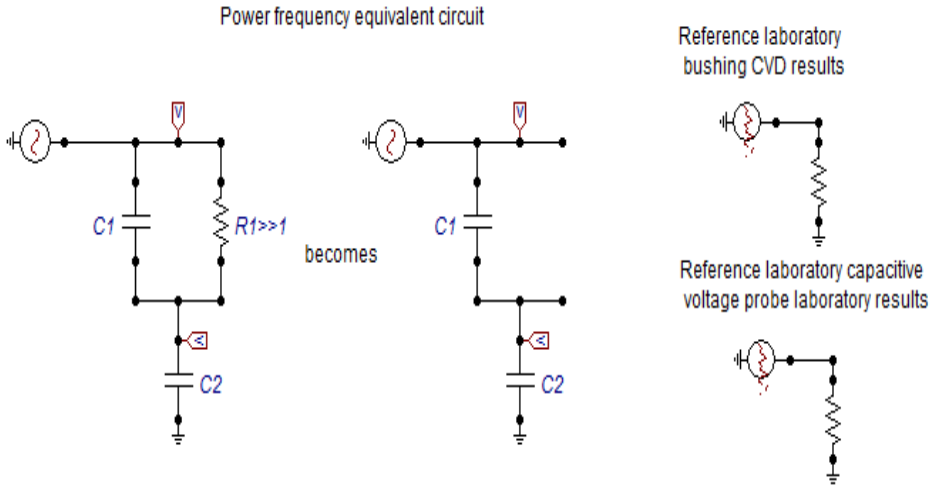

Figure 5.6: Models used for power frequency voltage simulations

5.4 Impulse Voltage Measurements

5.4.1 Experimental setup

A 4 stage Marx impulse generator shown in Figure 5.7 was used to generate 1.2/50 μs voltage impulses that were applied to a 24 kV bushing. The impulse voltages were measured using the bushing screen connected to a fixed external capacitor and a wideband resistive voltage divider. Each of the measured signals was sent to a Rigol 1046 oscilloscope. The peak of the voltage impulse was increased from 30 kV up to the BIL of the bushing.

The components used in generating the impulse voltage are listed in Appendix A. The definition of the 1.2/50 μs full wave impulse voltage and the corresponding correction factors are also given in Appendix A.

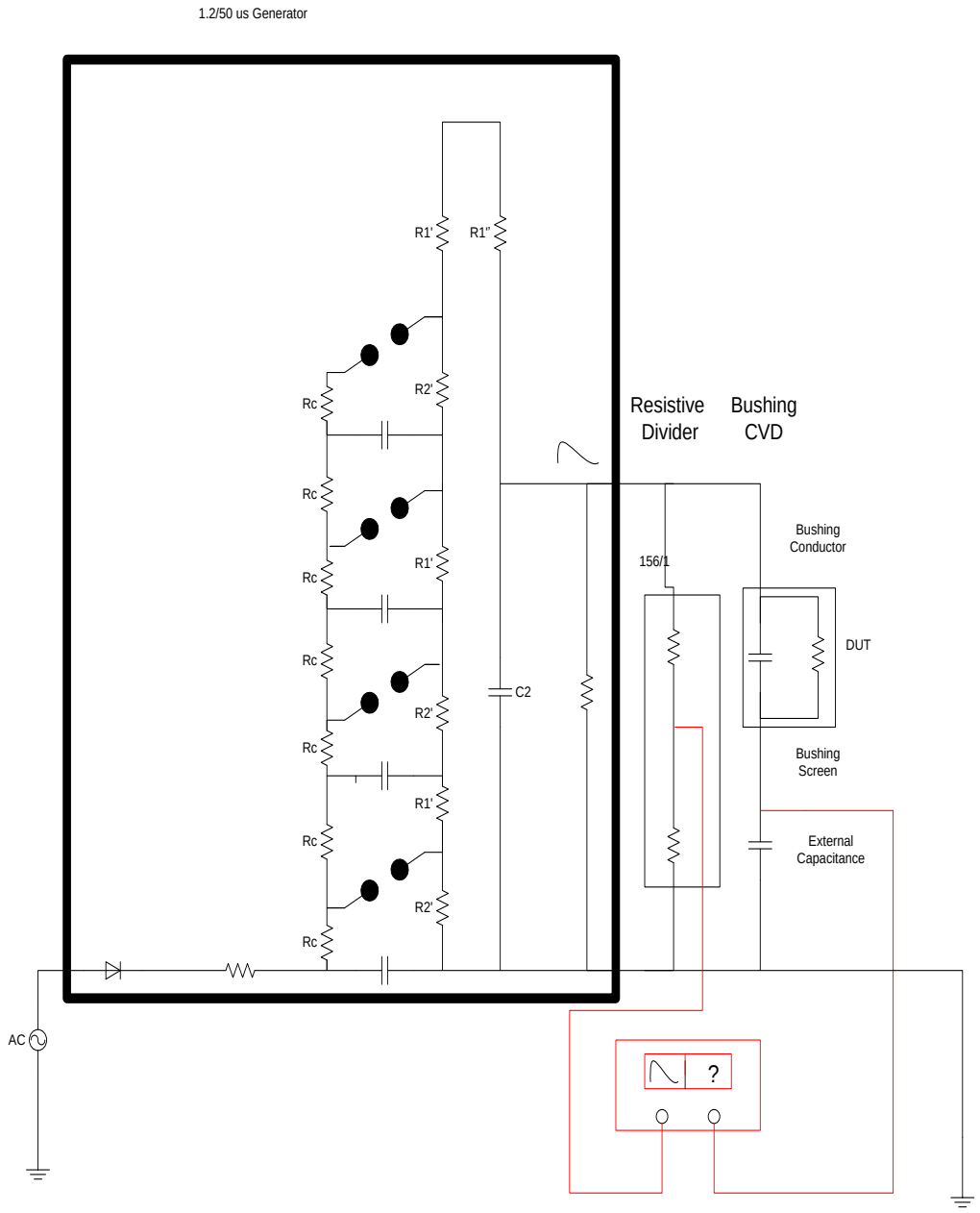

Figure 5.7: Impulse voltage measurement using the bushing capacitive voltage divider and a laboratory resistive divider

5.4.2 Models used in the bushing capacitive voltage divider simulations

The voltage impulses measured by the wideband resistive divider were reproduced using the ATPdraw user-defined voltage source which is used as input to the model of the bushing capacitive voltage divider. The use of the captured waveform allows simplification of the circuit in Figure 5.8. This also enables comparison of the simulated

output and the lab measured results. The bushing parameters used in this study were based on the parameters that were defined in Table 4.5 above.

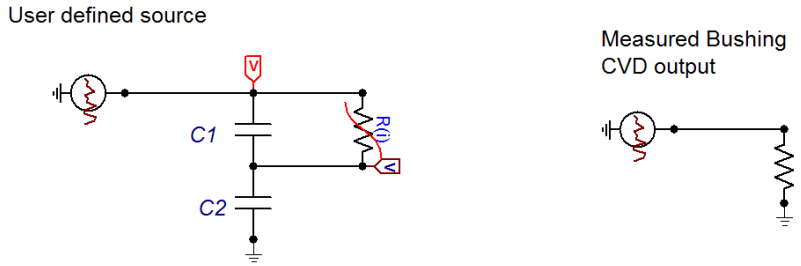

Figure 5.8: Models used for Impulse voltage simulations

5.5 Conclusion

The 875 and 418 turn Rogowski coils were subjected to varying 50 Hz and impulse currents so as to compare their performance with a precision current probe. Both calculated and measured coil parameters were used in simulations that compared measured results to simulated results. The ATPdraw user-defined current source was used to reproduce measured impulses such that they could be used in the simulations.

The performance of the bushing screen was determined by comparing with a laboratory capacitor voltage divider. The bushing capacitive voltage divider was subjected to 50Hz and impulse voltages to compare performance with laboratory capacitor and resistor voltage dividers. The results of the comparisons and the results of the simulations are presented and discussed in the next chapter.

Chapter 6

6 Results from measurements and simulations

6.1 Power frequency current measurement

In Figures 6.1 and 6.2 waveforms of primary current and output voltage are shown for the 875 turn and the 418 turn Rogowski coils. The waveforms show that the 875 turn coil gives a larger output voltage as expected. Both Rogowski coil output voltages were 90^0 out of phase with the primary current as expected from the theory. Numerical integration of the Rogowski output voltage in Figure 6.1, using Matlab, recovered the primary current as shown in Figure 6.3. The observed percentage noise on the output voltage with the 418 turn coil decreased with an increase in the amplitude of the measured current as expected and as shown in Figure 6.4 below. These findings further emphases the impact of the dimensions of the coil with regards to overall sensitivity of the Rogowski coil. Numerical integration of the output voltage of the 875 turn Rogowski coil allowed the recovery of the primary current passing through the bushing as shown in Figure 6.5.

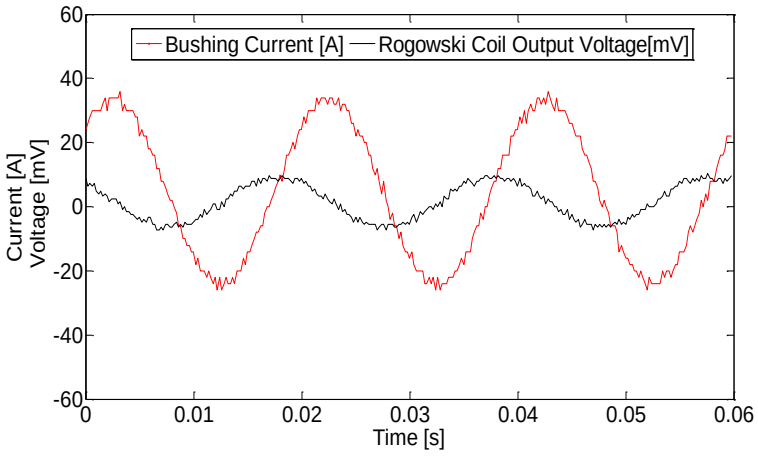

Figure 6.1: Power frequency current measurement with 875 turn Rogowski coil

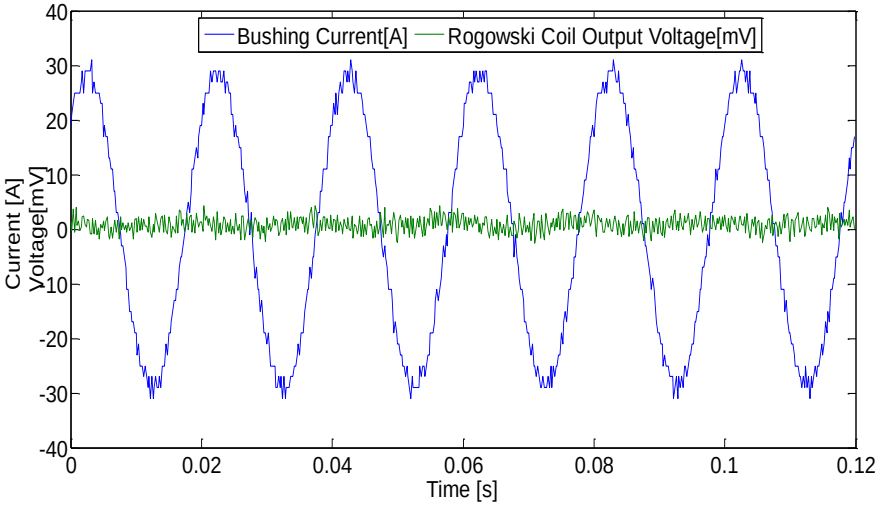

Figure 6.2: Power frequency current measurement with the 418 turn Rogowski coil

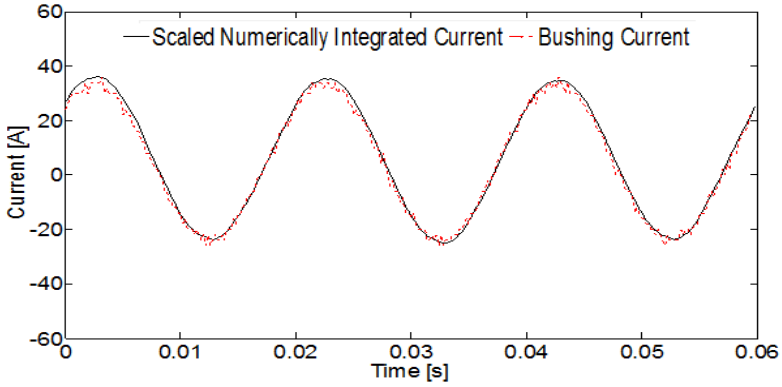

Figure 6.3: Numerically integrated output voltage for the 875 turn Rogowski coil

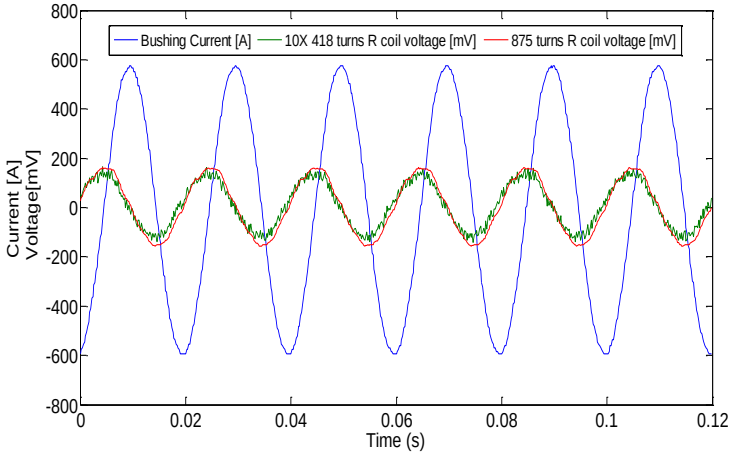

Figure 6.4: Power frequency current measurement with 875 turn Rogowski coil and the 418 turn Rogowski coil.

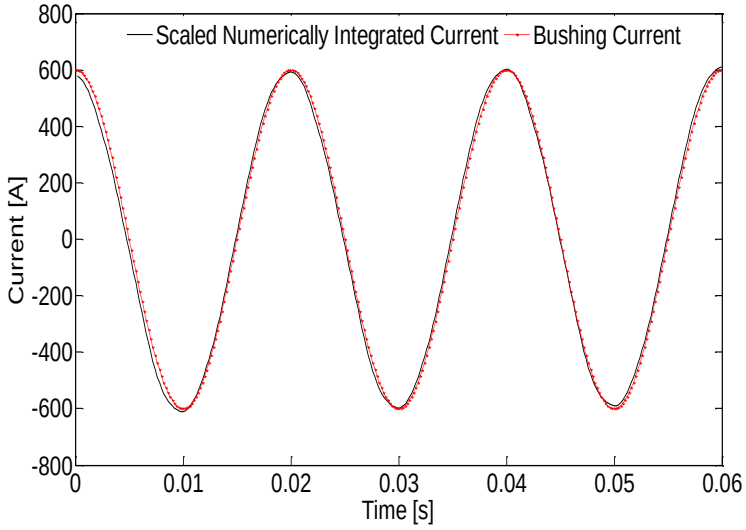

Figure 6.5: Numerically integrated output voltage for the 875 turn Rogowski coil

A comparison between measured and simulated results is shown in Figures 6.6 and Figures 6.7 below. The results show that the use of calculated parameters yielded an overestimation of the outputs of both the 418 and 875 turn Rogowski coils. Further analysis also showed that the use of measured parameters yielded results that are consistent with the lab measured results. Measured parameters with the mutual inductance suggested by Kojovic in equation 4.6 results in simulated results with slight variation in amplitude to the measured impulse.

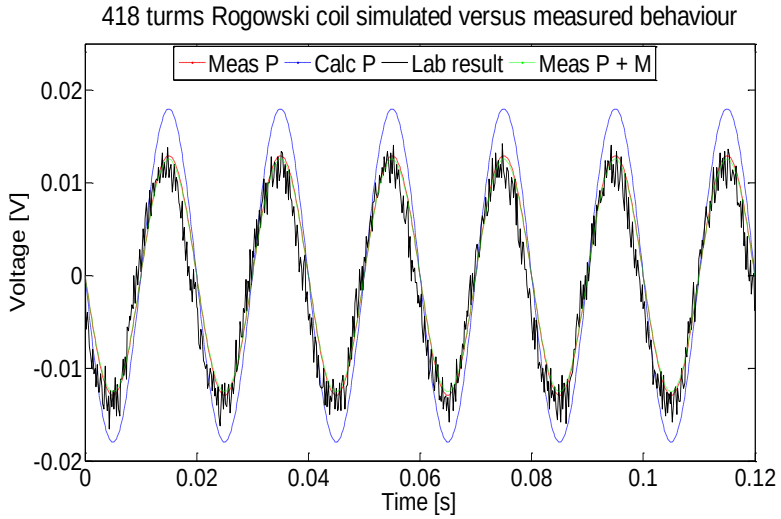

Figure 6.6: Comparison of simulations and measurements with 584A primary current (418 turn Rogowski coil) (Meas P = Measured parameters, Calc P = Calculated parameters, Meas P + M are the measured parameters with modified mutual inductance)

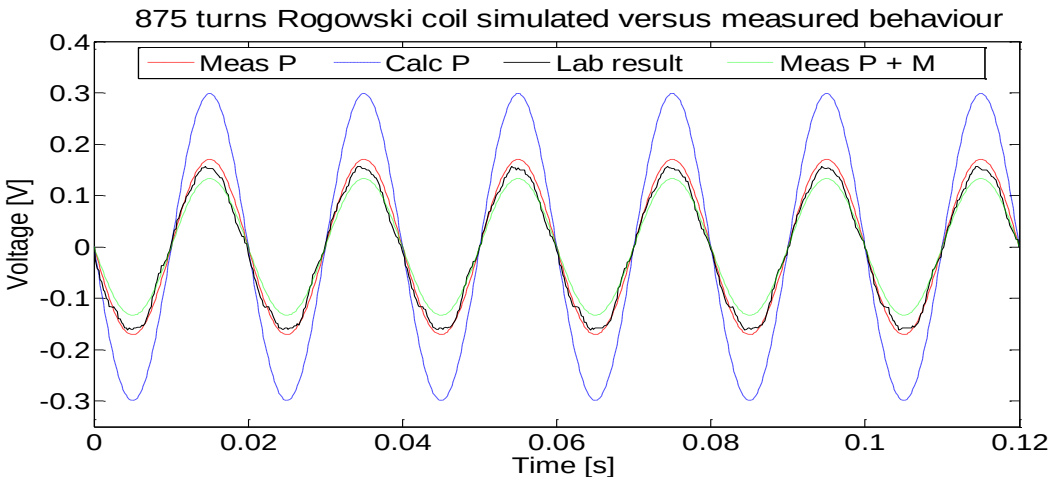

Figure 6.7: Comparison of simulations and measured waveforms for 584A primary current (875 turn Rogowski coil) (Meas P = Measured parameters, Calc P = Calculated parameters, Meas P + M are the measured parameters with modified mutual inductance)

6.2 Impulse current measurements

The measurement of a 6 kA 8/20 µs current impulse shown in Figure 6.8 was performed using both the 418 and the 875 turns Rogowski coils. A comparison between simulated results and lab measured results shows that the use of calculated parameters yielded results that overestimated the Rogowski coil output voltage as shown in Figures 6.9 and 6.10. The use of measured parameters for the 875 turn Rogowski coil provided an overestimation of the measured waveform. Measured parameters provided results that were consistent with the measured waveform for the 418 turn Rogowski coil. Results obtained from combining the measured parameters with the modified mutual inductance given by Kojovic provided results that were consistent with the measured output voltage for both the 875 and the 418 turn Rogowski coils. Using measured parameters of the 418 turn Rogowski coil provided waveforms consistent with the observed waveforms. Numerical integration of the 875 turn Rogowski coil output voltage gave results shown in Figure 6.11.

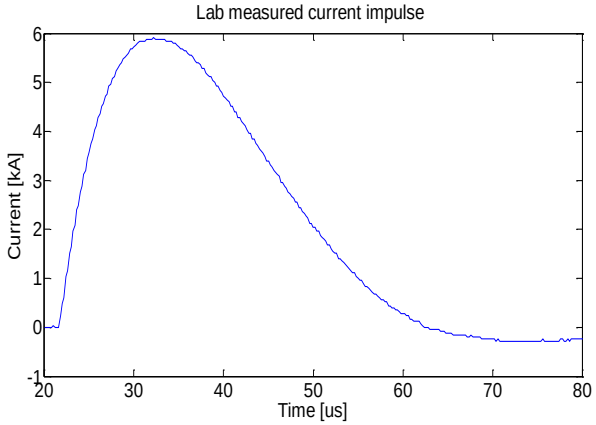

Figure 6.8: 6.6 kA 8/20 $\boldsymbol{\mu s}$ current impulse passed through the transformer bushing

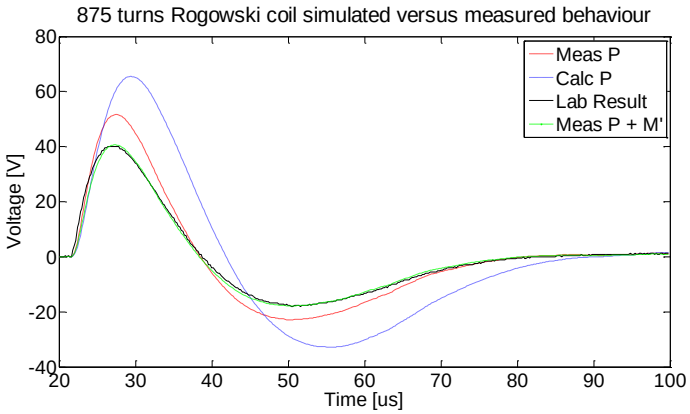

Figure 6.9: Comparison of measurements and simulations (Meas P = Measured parameters, Calc P = Calculated parameters, Meas P + M are the measured parameters with modified mutual inductance)

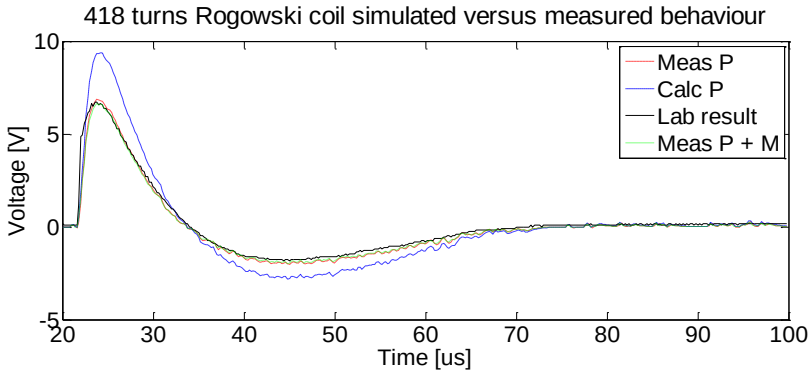

Figure 6.10: Comparison between simulated and measured 418 turn Rogowski coil output voltage

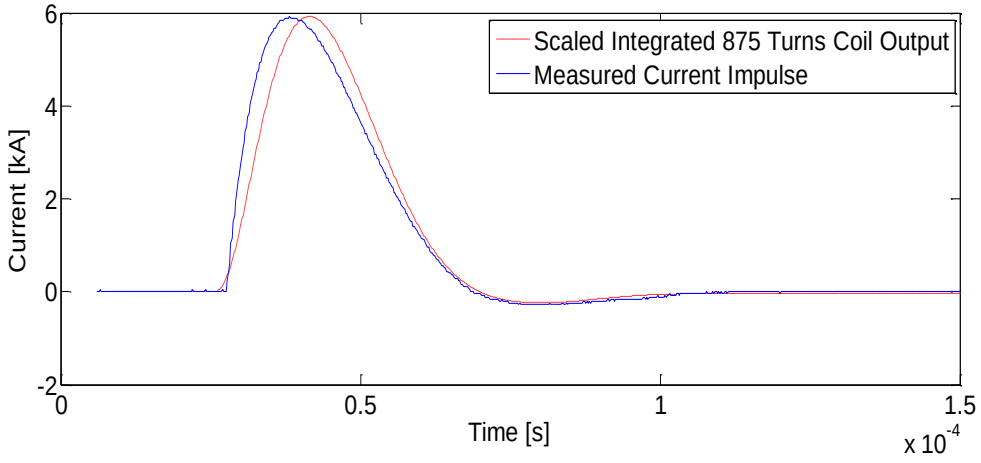

Figure 6.11: Integrated Rogowski coil output voltage

6.3 Power frequency voltage measurement

Figure 6.12 compares the measurement error obtained after repeated measurements were taken. The output from the bushing CVD was compared using a 1000/1 resistive divider instead of the capacitive divider. Observations showed that the bushing CVD had errors above 5% when measuring voltages at 1 kV. The use of a polynomial approximation in one range of measurements was used to develop a polynomial expression used to reconstruct other measured voltages as depicted in Figure 6.13 below. The corresponding results are shown in Figure 6.13 below and indicate an improvement in the reconstruction of the 1 kV measurements. Based on the polynomial measurements, all other measurements above 1 kV have errors within 5%.

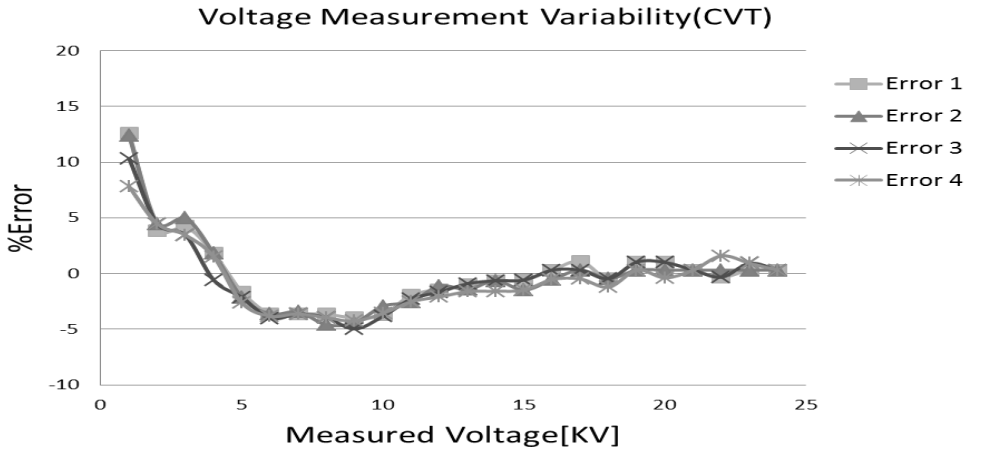

Figure 6.12: Error when comparing output of laboratory 1000/1 resistive divider and the bushing CVD output

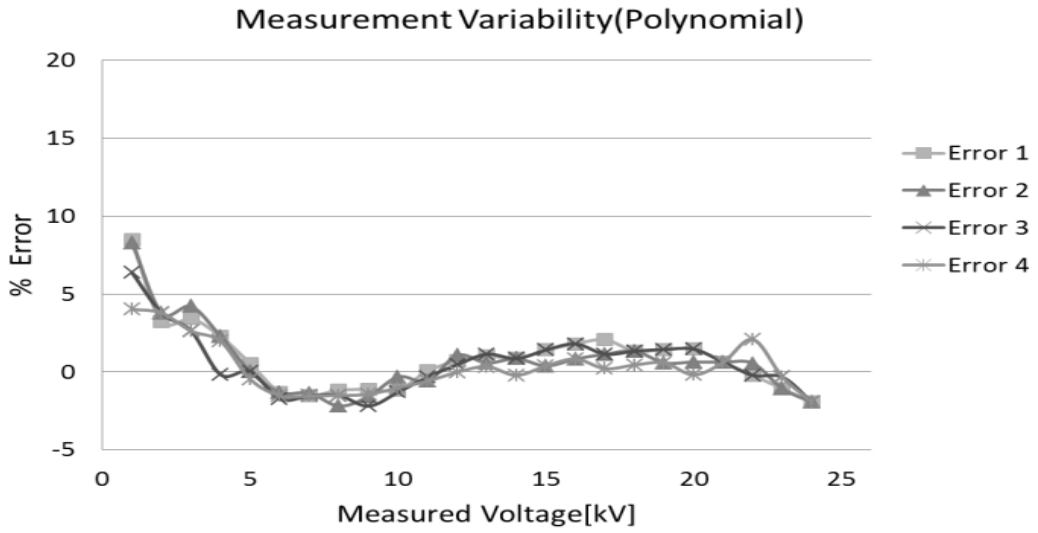

Figure 6.13: Error when comparing out of 1000/1 resistive divider and a polynomial calculation of the bushing CVD output

The bushing capacitive voltage divider offered results that were consistent with that of the laboratory capacitive voltage divider. The designed bushing CVD has a division ratio of 2115:1, as shown in Figures 6.14, 6.15 and 6.16 respectively.

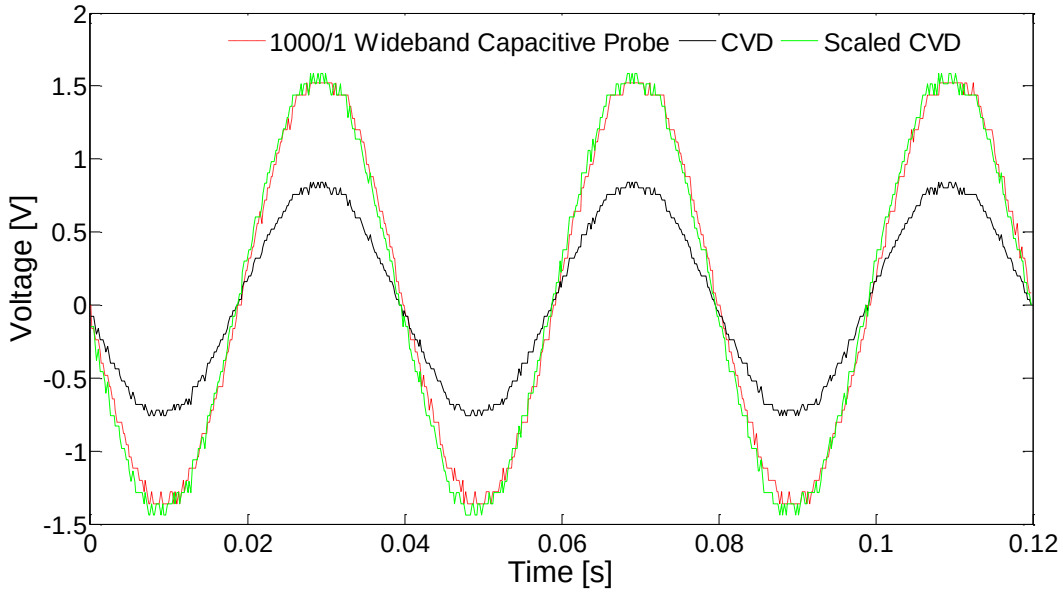

Figure 6.14: 50 Hz voltage measurement (primary voltage of 1.4 V)

Analysis of the measured waveforms shows that the division ratio remained constant up to 27 kV (more than the maximum 50 Hz voltage the 22 kV is likely to be exposed to in the network). A series of power frequency measurements taken using the bushing screen showed that power frequncy measurements can be achieved at a low cost by simply using a bushing embedded voltage screen. The magnitude of the CVD output voltage can be adjusted by changing that external capacitance presented in Equation 2.

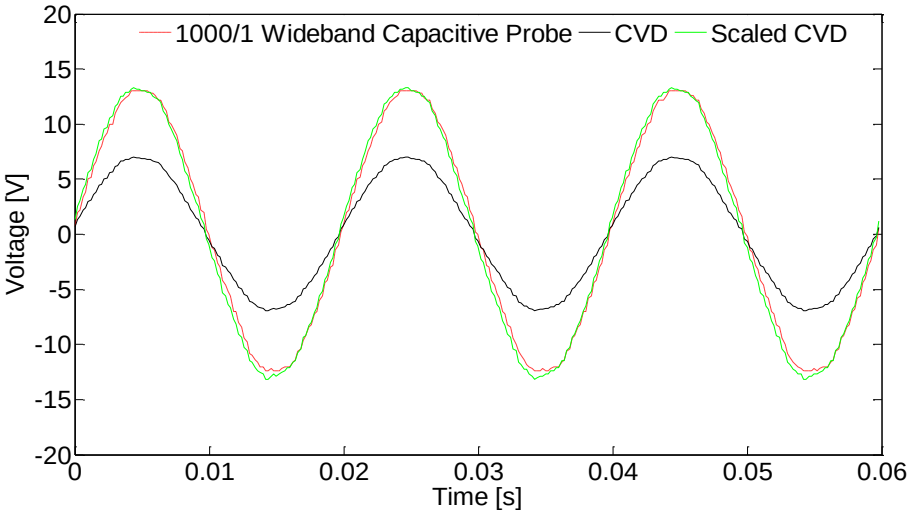

Figure 6.15: 50 Hz voltage measurement (primary voltage of 13 kV)

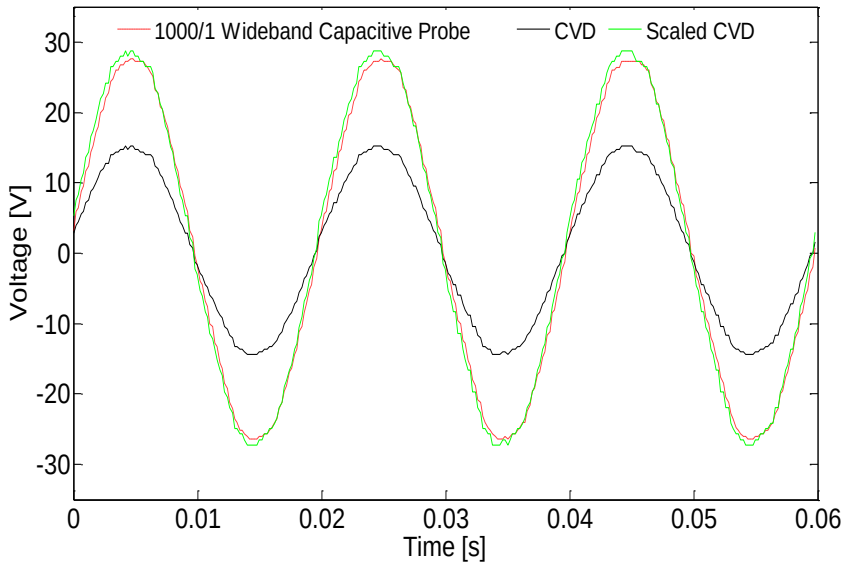

Figure 6.16: 50 Hz voltage measurement (primary voltage of 27 kV)

6.4 Impulse voltage measurement

The bushing CVD gave results similar to a laboratory resistive divider when measuring 50 kV 1.2/50 µs voltage impulses as shown in Figure 6.17and 6.18. The division ratio was the same as when measuring power frequency voltages. An increase in the magnitude of the applied voltage resulted in non-linearity as shown in Figures 6.19 and 6.20. Such variations are related to the presence of the non-linear resistor included in the simulations performed in chapter 5.

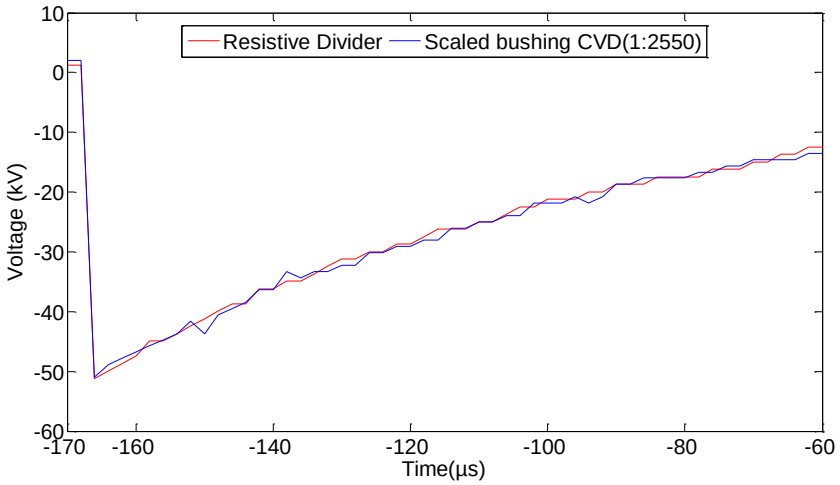

Figure 1.17: Impulse voltage with an external capacitance of 47 nF

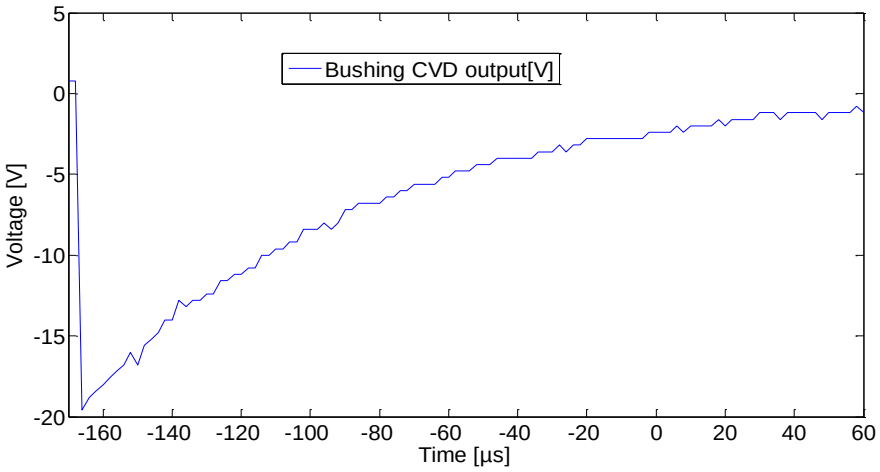

Figure 6.18: Bushing CVD output for the 50 kV 1.2/50 µs impulse voltage in Figure 6.15

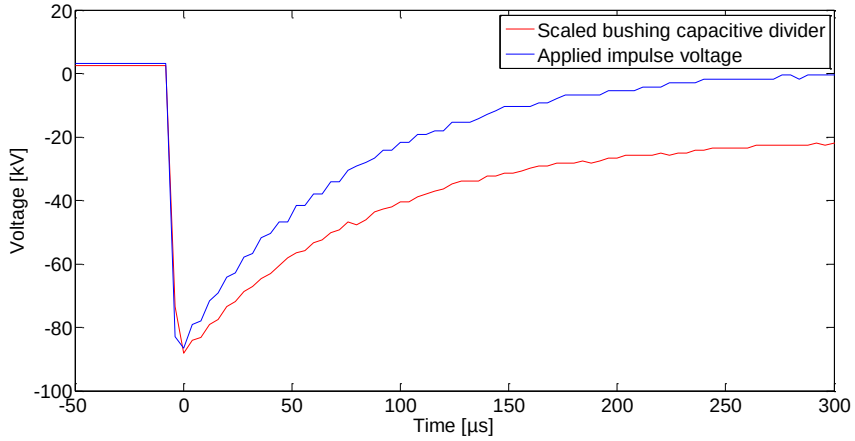

Figure 6.19: 90 kV peak voltage impulse

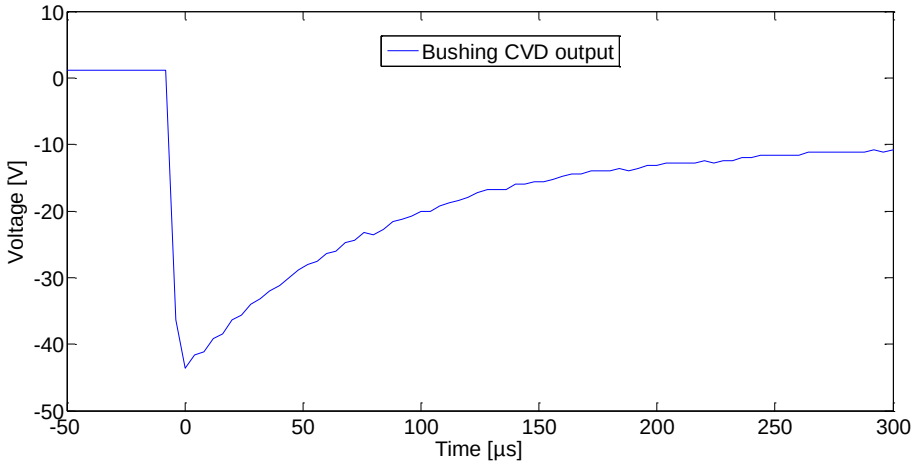

Figure 6.20: Bushing CVD output for the 90 kV 1.2/50 µs impulse voltage in Figure 6.19

Chapter 8 provides simulations that address compensation for the observed non-linearity using a user defined non-linear resistor.

6.5 Conclusion

Studies showed that the Rogowski coils could be used to measure both power frequency and impulse currents. The 875 turn Rogowski coil was better able to measure low amplitude currents (as expected). Both the 875 turn Rogowski coil and the 418 turn Rogowski coil were able to measure larger currents. Impulse current measurements with both the 875 turn Rogowski coil and the 418 turn Rogowski coil were consistent with the simulated currents. The best coil with regards to monitoring both power frequency and impulse current was observed to be the 875 turn Rogowski coil. The measured power frequency voltages using the bushing screen were consistent with the simulated bushing voltages. The bushing capacitor voltage divider low range impulse voltage outputs were observed to be consistent with the calculated ratio that is dependent on the measured bushing capacitance and the external capacitance. Measurements of high range impulses showed that the bushing CVD output has non-linearity that results in incorrect reconstruction of the bushing voltage. This was addressed by implementing a user-defined non-linear resistor to compensated for the non-linearity that were observed.

Chapter 7

7 Addressed research questions revisited

- What levels of monitoring can be achieved considering fault level, frequency response and dynamic range limitations?

The literature review performed showed that current and voltage monitoring on the LV side of distribution transformers yielded results that identified limited electrical stresses that contribute to premature transformer failure. Other stresses such as those observed on the MV side of distribution transformers also offer insight towards better management of distribution transformers. A comparison between the designed 875 and 418 turns coil has shown that Rogowski coils offer viable options for monitoring currents on both the LV and MV side. The low range sensitivity of the 875 turns coils shows that this is a viable option for monitoring low range electrical stresses. In this study, the use of a 179 Ω coil terminating resistor limited the bandwidth of the 875 turns to 88 kHz whilst an increase in the coil terminating resistance also resulted in an increase in the coil bandwidth. Monitoring of 8/20 μs impulse also showed the designed coils are capable of monitoring transient currents as low as 1 kA. The transient and power frequency behaviour of the coils was reproduced with simulations that yielded results that are consistent with the measured parameters of the coils.

The use of the bushing screen offered a viable option of measuring varying 50Hz voltages above 1 kV. The screen arrangement relative to the bushing conductor offered insulation based electrical parameters that were used with an external capacitor in measurement of both power frequency and transient voltages. Low to medium range impulse measurements have been observed to be consistent with lab measured results. However, in the next chapter, the non-linear behaviour observed with an increase impulse voltage is addressed.

- What level of analysis can be achieved from online monitoring, and what are the associated corrective actions that can be recommended?

Studies associated with both power frequency and transient behaviour can be performed with the designed Rogowski coil and screen based voltage divider. Recent power shortages in South Africa have highlighted the need for advance monitoring with regards to related benefits that can be achieved if this is in place. The compliance of municipalities with regards to adhering to requested power cuts is one of the key things that can be evaluated by implementing such monitoring systems. Load reduction by end user has been identified as a means of controlling peak load demand. Monitored data can give access to information about electricity consumption patterns and thus highlight areas that are not energy efficient. This information is useful in providing targeted training that helps consumers change their energy consumption profile.

The impact that harmonics have at distribution level are some of the benefits that can be obtained by performing a frequency spectrum of on measured power frequency signals. Areas that are affected by severe harmonics can be identified and thus de-rating of transformers can be performed. Transformers that are experiencing transients can also be monitored with the use of the designed current and voltage sensors. This can be used to identify areas that have faulty surge arrestors. Other benefits also include the ability to monitor areas where energy theft is occurring. This also affects the revenue collected by utilities. Changes to the distribution network brought about by the penetration of intermittent sources such as solar and wind at MV level can be monitored in terms of what transformers are observing.

- To whom should the analysed information be addressed and what communication protocol should be considered?

The level of penetration of the Smart Grid, the availability of Smart equipment and their associated cost limits household customers from participation interactively with the electrical grid at distribution level. The current research focused on providing electricity distribution centres with the capability of monitoring currents and voltages observed on the MV side distribution transformers. Identified stresses can be sent to owners of the monitored transformers, thus identifying the observed stress and the impact that this has on the transformer.

- Can online monitoring lead to optimum tap selection in distribution transformers?

MV voltage regulation within the South African network has predefined Tap Zone that sets operating voltage limits for both normal and abnormal operating conditions (Carter-Brown, 2012). LV/MV transformers are installed with a set voltage tap and changes are made if the end user at the point of supply complains of unacceptable voltage regulation. The availability of online monitoring system at MV level provides an opportunity for monitoring whether transformers are operating within the specified the Tap Zone limits.

Chapter 8

8 Prototype construction and performance evaluation

The combined performance of the above mentioned current and voltage sensors is of interest. In this chapter, a 24 kV epoxy resin bushing enclosed with silicone rubber was constructed. The bushing was designed such that it can be used outdoors. The performance on both MV current and voltage measurements was evaluated. A comparison between simulated and measured performance was done. Appendix B lists the steps taken whilst constructing the bushing.

8.1 Design requirements

Harlow (2012) defines bushings as insulating structures that are used to transmit power in or out enclosures, i.e. barriers, of electrical apparatus such as transformers, circuit breakers, and power capacitors. Critical design parameters are considered to be maximum current and voltage that the bushing can safely transmit without insulation failure. The design specifications for the prototype bushing in line with SANS 60137(2008) were as follows:

- Rated power frequency voltage rating = 24 kV
- Lightning impulse withstand voltage (BIL) = 150 kV
- Power frequency withstand voltage in dry conditions= 50 kV
- Power frequency withstand in wet conditions = 55kV
- Rated power frequency current = 250 A

Other specifications included:

- Minimum creepage distance (Coastal specification) = 760 mm (i.e. 31 kV/mm)
- Power frequency current and voltage measurement capability
- Impulse current and voltage measurement capability
- Outdoor operating capability

8.2 Bushing design limiting factors

The construction of the bushing had key limiting factors that included the unavailability of the following:

- Moulds that could match theoretical sheds design
- Precast Rogowski coils that are embedded in resin
- Vacuum chamber used to reduce air bubbles whilst casting the insulating material

8.3 Material selection

The material used in bushings is related to the application in which they are used. Factors such as required functionality, environmental operating conditions, breakdown strength of the insulating the material, the current and voltage rating are some of the factors that are used in the selection of the type bushing to be used. Based on the requirement of adding both current and voltage sensing equipment, an electrical insulating resin was chosen as different structured moulds could be made. The chosen resin offers a dielectric strength of 21kV/mm. The resin in this case was coated with silicone rubber so as to increase the hydrophobicity of the bushing (Vosloo et. al, 2006).

8.4 Bushing design

Non condenser bushings such as cast resin bushings are subjected to both axial and radial stresses. High axial stresses may lead to surface tracking (Ryan, 2001). The presence radial stresses may lead to insulation breakdown such that insulation punctures occur (Illias, 2012). In this study the bushing screen that is used for stress control and also served the purpose of providing voltage measurements. The designed bushing consists of one main screen surrounding the bushing conductor; this screen is connected to an externally earthed capacitor. The bushings also consist of a screened Rogowski coil that

is insulated with epoxy resin before being placed around the insulated main screen as shown in Figure 8.1. Both the output of the screened Rogowski coils and the externally earthed capacitor were terminated on two BNC connectors. Such connectors can be varied based on the environmental condition and type of connection required.

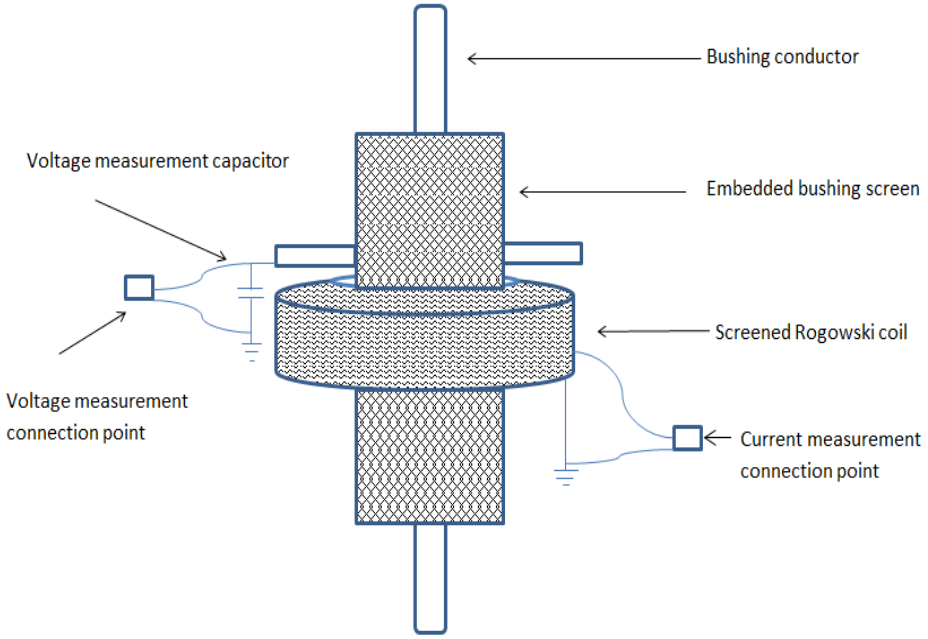

Figure 8.1: Resin cast embedded current and voltage measurements components

The current voltage and current measurement components form part of a bushing with physical properties shown in Figure 8.2 below.

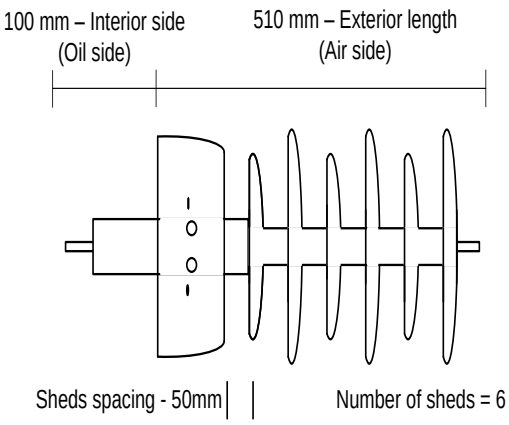

Figure 8.2: Cast resin bushing with embedded current and voltage measuring components

The designed bushing consists of a square toroid profile shown in Figure 8.3 below. The square profile was selected over the circular profile due to the unavailability of circular moulds. The new number of turns obtained with the square profile was 668. The calculated mutual inductance, based of Rogowski coil properties shown in Table 8.1 and Figure 8.3, is given by:

$$M = \frac{\mu_0 N_2}{2\pi} h ln\left(\frac{b}{a}\right) \tag{8.1}$$

-where:

M is the coil mutual-inductance [nH]

$\mu_0 = 4\pi \times 10^{-7}[\mathrm{H/m}]$, Permeability of air

N_2 is the number of turns

a is the toroid coil inner diameter [mm]

b is the toroid coil outer diameter [mm]

h is the toroid coil height [mm]

The corresponding self-inductance is given by:

$$L = \frac{\mu_0 {N_2}^2}{2\pi} h ln\left(\frac{b}{a}\right) \tag{8.2}$$

-where:

L is the coil self-inductance [mH]

The coil lumped capacitance is given by:

$$C = \frac{2\pi^2 \varepsilon_0^2 (a+b)}{\log[(a+b)/(b-a)]} \tag{8.3}$$

-where:

C is the coil lumped capacitance [F]

ε_0 is the permittivity of free space$[\mathrm{F/m}]$

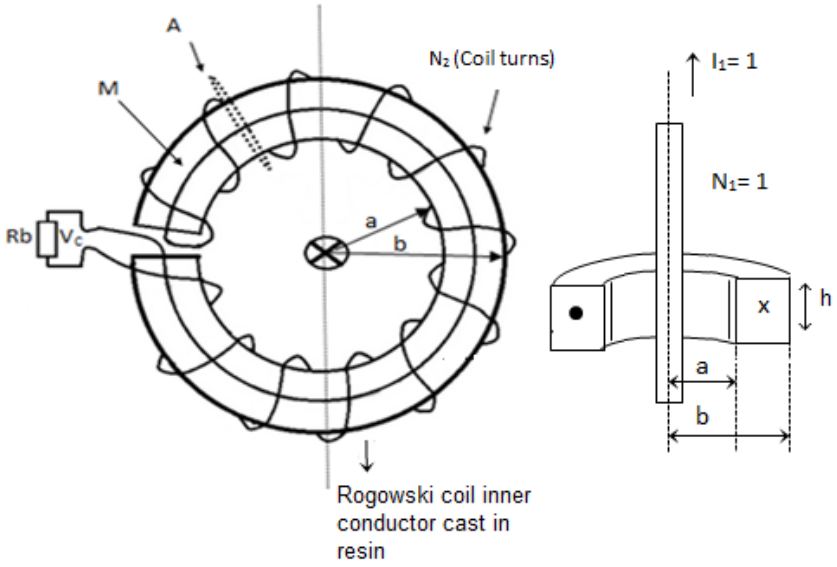

Figure 8.3: Bushing embedded Rogowski coil with a square toroid profile

Table 8.1: Bushing embedded Rogowski coil physical dimension

Parameter	*Description*	*Value*
$d_w[mm]$	Wire diameter	0.25
$R[\Omega]$	Wire resistance	18.5
a[mm]	Inner radius	40
b[mm]	Outer radius	60
h[mm]	Coil height	20
I[mm]	Core length	390
A[mm^2]	Coil area	400
N_2	Number of turns	668

The calculated electrical properties are given in Table 8.2. The measured parameters obtained using the methodology defined in chapter 4 gives electrical parameters in Table 8.3. The measured parameters are smaller than the calculated parameters similar to the parameters obtained whilst analysing Rogowski coils with a circular profile.

Table 1.2: Bushing embedded Rogowski coil calculated parameters

Parameter	*Parameter*	*Value*
M[nH]	Mutual Inductance	861
L [mH]	Coil self-inductance	2.17
C [pF]	Coil capacitance	50.2

Table 8.3: Bushing embedded Rogowski coil calculated parameters

Parameter	*Parameter*	*Value*
C_{T1} [pF]	Tank known capacitance 1	11
C_{T2}[pF]	Tank known capacitance 2	56.25
F_{r1} [kHz]	Resonance frequency ($C_{T1} + C_p$)	480
F_{r2} [kHz]	Resonance frequency ($C_{T2} + C_p$)	397
F_{r21} [kHz]	Resonance frequency ($C_{T1} + 2C_p$)	405
F_{r22} [kHz]	Resonance frequency ($C_{T1} + 2C_p$)	326
C_p[pF]	Probe capacitance	8
C_m[pF]	Coil capacitance	4.1
L_m[mH]	Coil inductance	5.37
M[nH]	Mutual Inductance	510

The insulation based bushing screen capacitance was obtained using an LCR meter and the measured capacitance was found to be 22.23 pF. The screen that was used has the same dimensions as the one used earlier. This screen was then connected to a 47 nF capacitor giving an overall division ratio of 2115:1. Different voltage division ratio can be obtained by using capacitors with different ratings. Appendix B gives details of the bushing construction process.

8.5 Bushing acceptance tests

8.5.1 Impulse withstand test

The designed bushing has a rating of 24 kV. The bushing was subjected to 15 positive standard 1.2/50 μs 150 kV impulses followed by negative impulses at the same rating. The designed bushing did not flashover on either polarity at both the oil side and the air side. Further analysis showed that the designed bushing did not puncture during the test. The impulses that were applied are listed in Appendix A together with corresponding correction factors taken into consideration.

8.5.2 Dry and wet power frequency test

Tests that were conducted on the bushing also included the dry and wet power frequency test. The dry power frequency test was conducted by applying a 50 kV 50 Hz voltage for a minute as stated in SANS 60137(2008). The bushing did not puncture of flashover

during the test. The wet power frequency test required the bushing to withstand an overvoltage of 55 KV for a minute. The air side of the bushing was sprayed with water prior to the application of the 50 Hz 55 kV signal. The bushing did not puncture of flashover during the test. Power frequency voltage tests conducted prior to the test and those conducted after the test remained consistent proving that the capacitance of the bushing had not been changed by the either the dry or wet power frequency test. There was however some corona that was observed during this test. Figure 8.4 shows infrared (IR) scans of the bushing taken during power frequency test. The IR scans show that there were surface discharges in the areas above the measurement unit and just before the first shed. This is the area where the upper end of the bushing screen is located. Other areas of the bushing did not severe deviation in temperature.

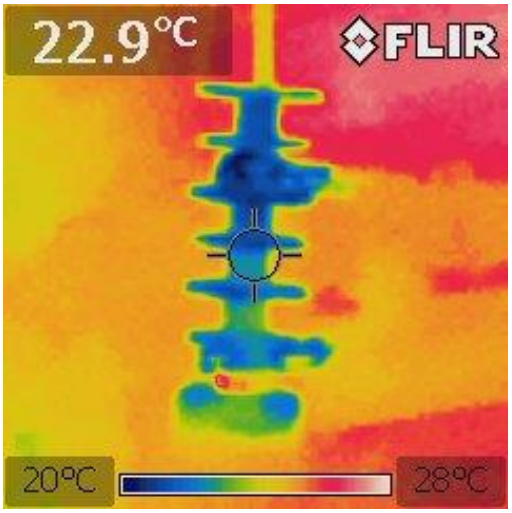

Figure 8.4: Infrared scans of the bushing during power frequency test

8.5.3 Partial discharge test

Partial discharge, as defined in SANS 60270(2000), is the localized electrical discharge that only partially bridges the insulation. SANS 60137 specifies the maximum acceptable partial discharge level at rated operating voltage as 10 pC. Figure 8.5 shows that partial discharge test results obtained at 22 kV. The bushing fails to meet the specified maximum partial discharge level of 5 pC. The partial discharge pattern shows that the bushing is dominated by surface discharge or corona. A FEMM simulation of the designed bushing shows that the bushing has a high stress zone at the first stage of the bushing due to the end position of the screen being close to the surface of the bushing thus resulting in

surface discharges as shown in Figure 8.6. An improvement to the designed bushing can be achieved by having the ends of the screen that are deeply embedded into the bushing.

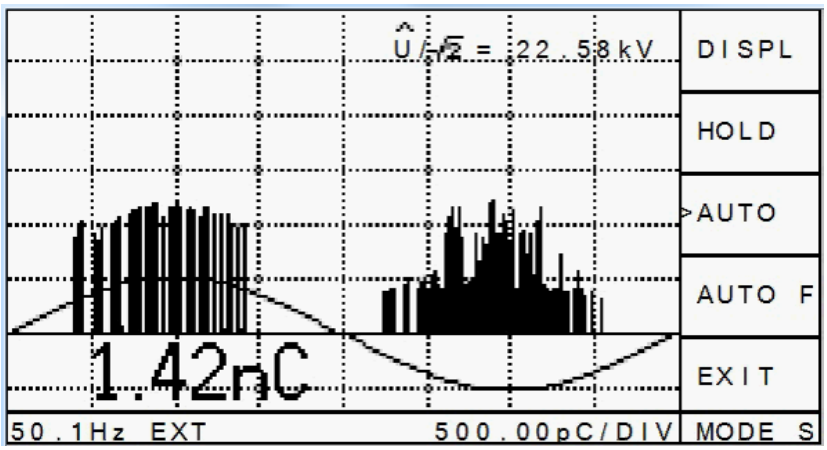

Figure 8.5 PD tests with 22.58 kV applied on the bushing

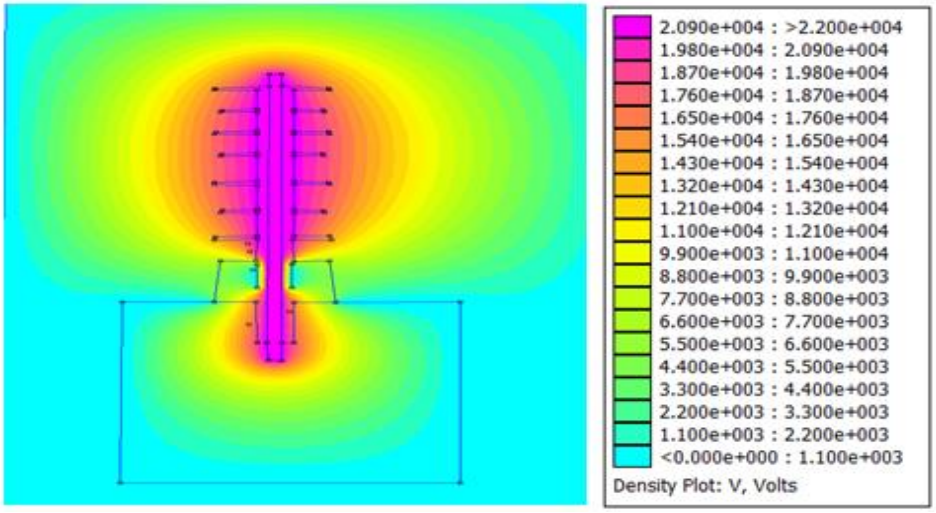

Figure 8.6 FEMM simulation of the designed bushing

8.6 Current measurement results and discussion

8.6.1 Power frequency currents

Figure 8.7 shows the measurement of 242 A primary current with the bushing embedded square cross-section 668 turns toroid Rogowski coil. A comparison between the power

frequency current measurement and Rogowski coil output voltage showed that the 668 turns Rogowski coil has a sensitivity that gives a ratio of 2630:1 as compared to 335:1 and 3333:1 for the 418 turns and the 875 turns Rogowski coils respectively. The large cross sectional area on the bushing embedded 686 turns and the free standing 875 turns coil thus results in improved sensitivity to primary currents. Numerical integration of the 668 turns Rogowski coil output voltage also gives results that are consistent with the primary current as shown in Figure 8.8.

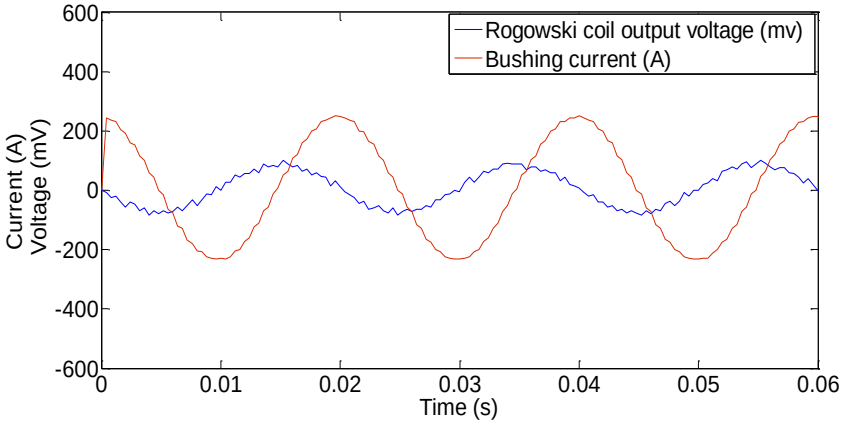

Figure 8.7: Current measurement with the bushing embedded 668 turns Rogowski coil

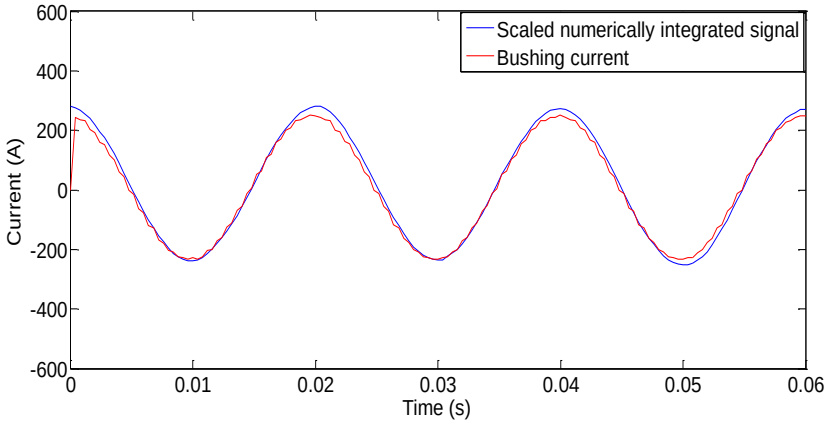

Figure 8.8: Comparison between numerically integrated signal and output of the Rogowski coil

8.6.2 Impulse currents measurement results

The numerically integrated output of the 686 turns Rogowski coil obtained whilst measuring a 5.5 kA 8/20 impulse current, is shown in Figure 8.9. Simulations based on

calculated parameters yields results that are an over-estimation of the measured coal output voltage whilst measured impulses yielded results that are closely approximated to the measured voltage. The observed results shown in Figure 8.10 further emphasize the importance of measuring coil parameters. Simulated results based on the measured coil parameters can thus be used in evaluating the behaviour of the coil whist measuring impulses that are of ranging magnitude.

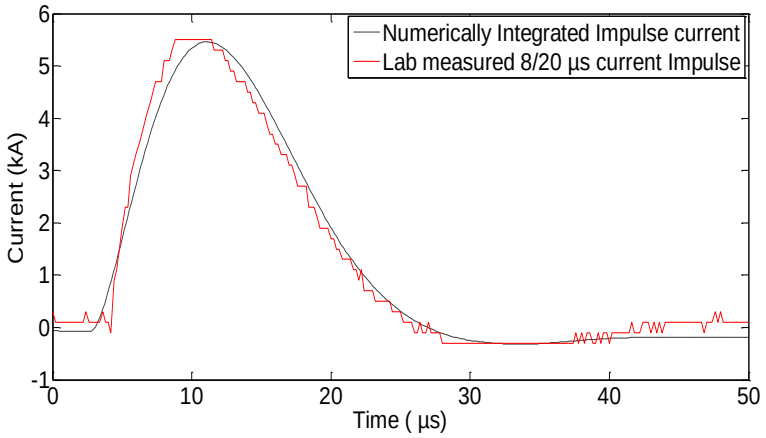

Figure 8.9: Measured 8/20 5.5 kA current impulse

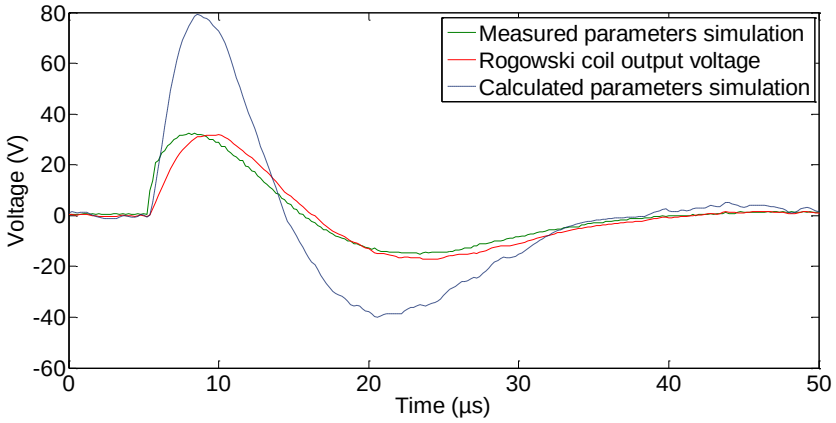

Figure 8.10: Coil output voltage whilst measuring 5.5 kA current impulses

8.6.3 Power frequency voltage measurement results

A comparison between a commercially available 1000:1 capacitive voltage divider and the designed screen based CVD results in voltage measurements that are in phase as depicted in Figure 8.11 and Figure 8.12. The screen based screen based CVD offers a

2115:1 ratio. The screen based CVD voltage measurements remained linear for voltages as low as 1 kV up to the rated voltage.

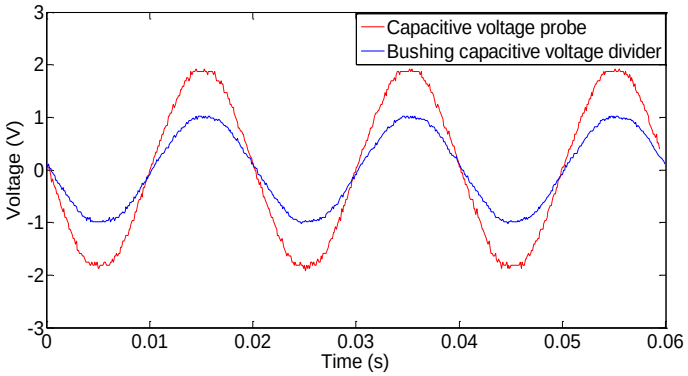

Figure 8.11: Measured 2 kV 50 Hz voltage signal

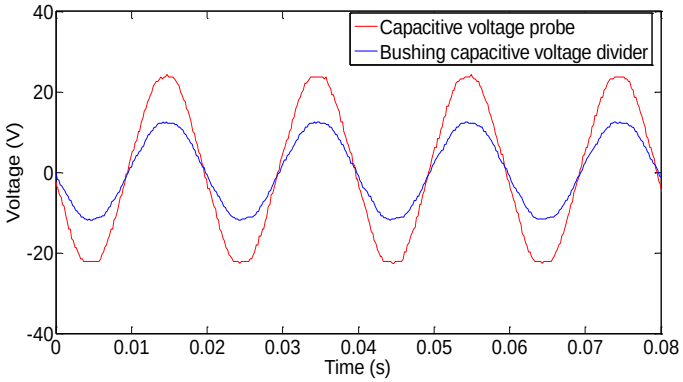

Figure 8.12: Measured 24 kV 50 Hz voltage signal

8.6.4 Impulse voltage measurements

The capability of the designed bushing in capturing impulse voltages was determined by measuring 1.2/50 μs impulse voltages limited to the BIL rating of 150 kV. Impulse measurements performed before and after the Lightning Impulse Withstand test remained consistent. The designed bushing was able to output impulses that were a scaled multiple for impulse voltages lower than 60 kV. Figure 8.13 shows the measurement of a 56 kV impulse and the resultant screen CVD results.

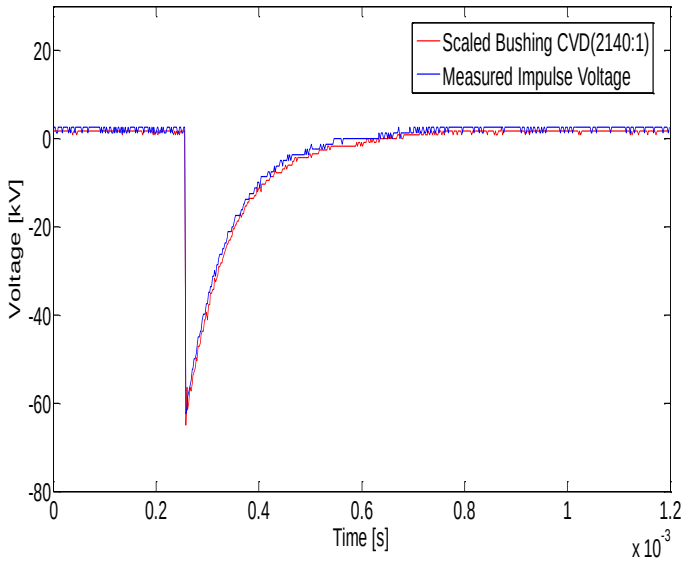

a. Applied voltage

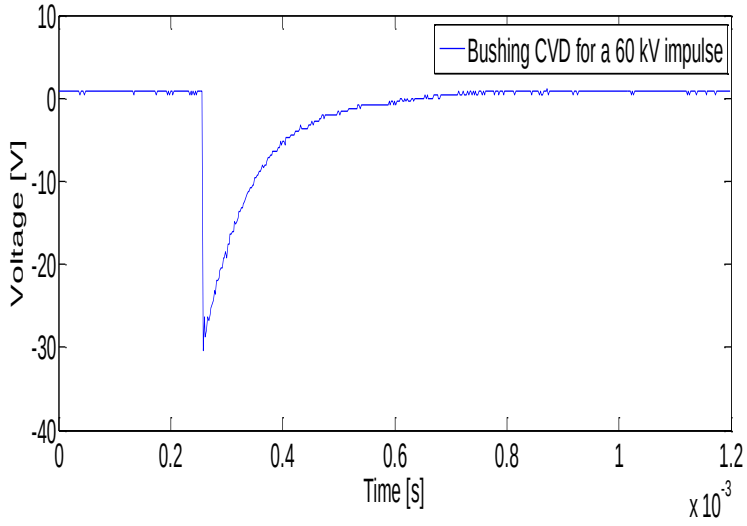

b. Bushing output voltage

Figure 8.13: Applied 60 kV impulse voltage (a) and the corresponding bushing CVD output (b)

Observations however showed that impulses higher than 60 kV resulted in some nonlinearity on the output screen of the CVD. A revisit of the ATPdraw model of the screen based capacitive voltage divider showed that the observed non-linearity could be explained by simulation that included the presence of the non-linear resistor as shown in Figure 8.14 below. The non-linear resistor with current and voltage characteristics that gave better results for a 130 kV impulse was used in simulating the bushing CVD behaviour for voltages higher than 60 kV. Figure 8.15 shows a 150 kV 1.2/50 μs with the corresponding bushing output voltage. Observations show that the output of the bushing CVD could be closely approximated by the simulations that included the non-linear

resistor as compared to a model that excludes the non-linear resistor as shown in Figure 8.14.

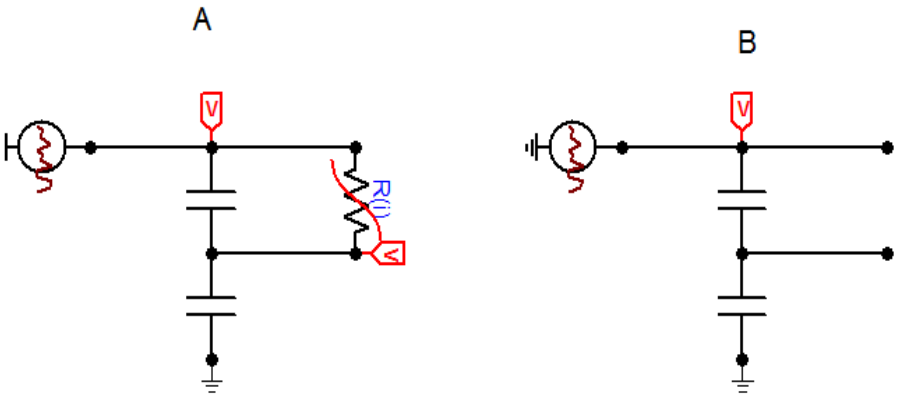

Figure 8.14: Measured 8/20 5.5 kA current impulse

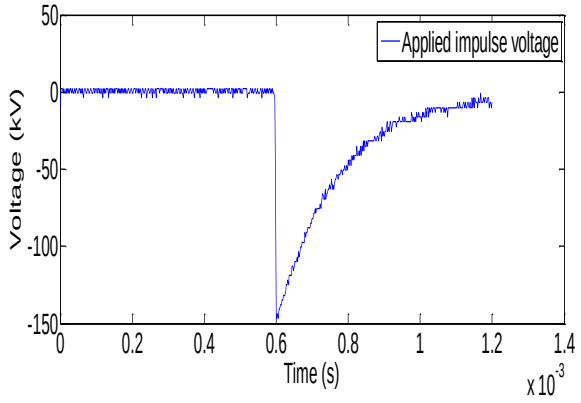

a) Applied Impulse

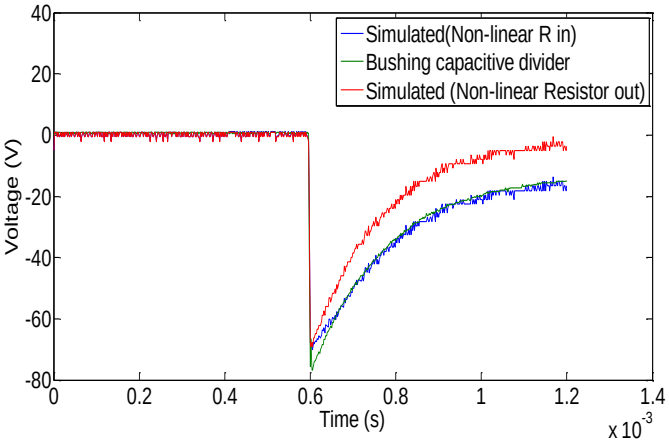

b) Measured and simulated output

Figure 8.15: Applied 150 kV impulse voltage (a) and the corresponding bushing CVD output (b)

8.7 Conclusion

The application of studies conducted with individual components in chapter 3 to chapter 6 resulted in the successful construction of the bushing that can monitor both currents and voltages. The use of a rectangular cross-section toroid Rogowski coil enabled measurements of both power frequency and impulse currents. Bushing embedded capacitor connected to the embedded screen resulted in the successful measurement of both power frequency and transient currents. Embedding both the screen and the capacitor in epoxy resin also resulted in capacitive voltage setup that is able to measure impulse voltages as high as 150 kV. Simulations using the ATPdraw non-linear resistor resulted in the compensation of non-linearity observed for impulses rated 60 kV and above. The performance of wet and dry power frequency test was conducted successfully without any puncture flash over. Surface discharges were however observed on the surface close to the end position of the screen.

9 Conclusion and recommendations

The research focussed on the development of cost effective transducers that can be used to monitor electrical stresses that may cause transformer failure. Studies showed that currently available LV monitoring system could provide more definitive identification of stresses if there were supplemented with affordable MV monitoring systems. The introduction of the Smart Grid together with the associated benefits can only be achieved with effective monitoring that is in place. Assessments performed showed that bushing embedded capacitive voltage dividers and Rogowski coils were viable options for monitoring MV stresses on transformers rated 16 KVA up to 2 MVA.

Studies conducted using Rogowski coils showed that Rogowski coils that have a larger cross-sectional area and an increased number of turns had better current sensitivity. The use of numerical integration also enabled recovery of the primary current under both power frequency and transient conditions. The use of a screen in achieving voltage measurement also showed that the bushing maintained the turns ratio based on the bushing internal capacitance and the capacitance connected between the screen and the earth terminal. The measurement of transient voltages below 60 kV also showed that the bushing turns ratio was maintained. Increasing impulse to voltages above 60kV resulted in non-linearity observed on the screen based bushing CVD output.

Studies conducted enabled the developments of a 24 kV prototype bushing. The designed bushing provided both power frequency and transient current measurements. Studies conducted showed that results from the coils placed around a bushing offered results that were consistent with those of an embedded Rogowski coil. Variation in the sensitivity of the coils was based on the physical dimensions and the number turns of the Rogowski coils. The prototype bushing developed also offered power frequency and transient voltage measurements. Embedding the capacitor used to connect between the screen and the earth terminal did not result in variation of the bushing CVD ratio setup based on the measured bushing screen capacitance. Measurements of impulse

voltages up to the rated BIL of 150 kV were achieved with nonlinearity observed on the high range level measurement.

Simulations using ATPdraw empirical sources were used in simulating the behaviour of the Rogowski coils and the bushing CVD. Observed results showed that the measured coil parameters offered better approximation of the measured impulse currents measurements when compared to calculated parameters. The use on a non-linear resistor resulted in improved approximation of higher range impulse voltages above 60 kV. Such simulations thus enable compensation for errors that may result whilst measuring transients of higher voltage levels.

The conducted study has shown the development of a cost effective bushing that can perform both power frequency and transient voltage and current measurements. Improvements required on the designed bushing include embedding the ends of the screen deeper in insulation so as to decrease the stresses observed just above the measuring area of the bushing thus reducing the possibility of observed surface discharges. Other improvements required include the increased sensitivity of low range 50 Hz currents with the Rogowski coil dimensions fitting within predefined operating area. Further analysis with all three phases on the transformer in place is necessary. Integration of the designed bushing with CVM units may also be a subject for further research.

References

Alam M. J. E., Muttaqi K. M. and Sutanto D.(2013) "A SAX-Based Advanced Computational Tool for Assessment of Clustered Rooftop Solar PV Impacts on LV and MV Networks in Smart Grid", IEEE Transactions on Smart Grid, Volume: 4, Issue: 1, pp. 577 – 585.

Annapoorani K. I. and Umamaheswari D. B. (2012) "Fault Prediction based on Dissolved Gas Concentration from Insulating Oil in Power Transformers using Neural Network", Proc. IEEE 10th International Conference on the Properties and Applications of Dielectric Materials (ICPADM), pp. 1-4.

Argueso M., Robles G., and Sanz J. (2005) "Implementation of a Rogowski coil for the measurement of partial discharges", Review of Scientific Instruments, vol. 76, pp. 065107-065113.

Beckers P. C., Beukes J. H. (2007), The Design of a Self-Regulated and Protected Electrification Transformer, MSc Thesis, University of Stellebosch, South Africa.

Behzadi R, Oskuoee M, Mohammadi D. (2007), "Integrated Electronic Metering Insulator for Medium Voltage Overhead Lines", CIRED. 19th International Conference of Electricity Distribution, pp. 1-4.

Carter-Brown C. G (2012). Distribution Planning Standard-Part l1: Distribution Voltage Regulation and Apportionment Limits. DST 34-192, Eskom Distribution, rev 2.

Elsworth C. G. (2008), The Smart Grid and Electric Power Transmission. Nova Science Pub Incorporated.

Eskom Holdings Ltd (2013). Eskom Integrated Report: Supplementary and Divisional Report for the Year Ended 31 March 2013.

Ghosh D. P. , Schrader D. E. Schulze W. D. and Wicker S.B. (2012) “Economic analysis of privacy aware Advanced Metering Infrastructure adoption”, Innovative Smart Grid Technologies (ISGT), 2012 IEEE PES, pp. 1-4

Hilshey A. D. , Hines P. D. H. , Rezaei P. and Dowds J. R. (2013), "Estimating the impact of electric vehicle smart charging on distribution transformer aging", IEEE Trans. Smart Grid, vol. 4, no. 2, pp. 905 -913

Harlow J. H.(2004) Electric Power Transformer Engineering. CRC Press, 1st Edition. pp. 114-115, 441-445.

Harlow J. H. (2012), Electric Power Transformer Engineering, Third Edition, CRC Press, Volume 2, pp. 13.1-13.24.

Hartmann J. Biela H. Ertl, and Kolar J. W. (2009), "Wideband Current Transducer for Measuring AC Signals With Limited DC Offset", IEEE Transactions on Power Electronics, vol. 24, pp. 1776-1787.

Hashmi G. M., Lehtonen M. and Elhaffar A. (2007), “Modelling of Rogowski Coil for online PD Monitoring in Covered Conductor Overhead Distribution Networks,” CIRED: International Conference on Electricity Distribution. Vienna.

Hewson C. and Ray W. (2004) “The Effect of Electrostatic Screening of Rogowski Coils Designed for Wide-Bandwidth Current Measurement in Power Electronic Applications,” 35th Annual IEEE Power Electronics Specialists Conference.

Henderson R. D. and Rose P. J. (1994), “Harmonics: the effects on power quality and transformers”, IEEE Trans. Ind. Applicat., vol. 30, pp. 528-532.

Hlavacek J., Prochazka R., Draxler K. and Kvasnicka V. (2008), "The Rogowski coil design software", Proc. 16th IMEKO TC4 Int. Symp., pp.295 -300,

IEC/SANS Standard 60137(2010), Insulated Bushings for Alternating Voltages Above 1000 V, ed. 3.

IEC/SANS Standard 60060-1 (1989), High voltage tests: Atmospheric correction factors.

IEEE Standard C37.235 (2007) IEEE Guide for the Application of Rogowski Coils Used for Protective Relaying Purposes.

IEEE STD C57.12.00 (1993) IEEE Standard General Requirements for Liquid-Immersed Distribution, Power, and Regulating Transformers

Illias H., Tunio M. A., Bakar A. H. A and H. Mokhlis (2012) “Distribution of Electric Field in Capacitor and Surge Arrester Bushings", IEEE International Conference on Power and Energy (PECon), Kota Kinabalu Sabah, Malaysia, pp. 461-466.

Javora R., Stefanka M., Mahonen P., Niemi T. and Rintamaki O. (2009), “Protection in MV Networks using Electronic Instrument Transformers”, CIRED 20th International Conference on Electricity Distribution, Prague, pp. 8-11.

Khatri A. (2010), “Evolution of Future Electrical Networks in Eskom”, 62nd AMEU Convention, pp. 113-118.

Kleinhans R. (2011), “Current and Voltage Monitors Combat Theft and Improve Supply Quality”, Energize. Transmission and Distribution, pp. 41-45.

Kojovic L. A. (2005), “Rogowski Coil Transient Performance and ATP Simulations for Applications in Protective Relaying”, Conference on Power Systems Transients (IPST’05) in Montreal Canada.

Masoum M. A. S., Moses P. S. and Deilami S. (2010), "Load management in smart grids considering harmonic distortion and transformer derating", Proc. Int. Conf. Innovative Smart Grid Technol., pp.1 -7.

Mehta A. K., Sharma R. N., Chauham S. and Saho S. (2013), “Transformer Diagnostics under Dissolved Gas Analyses Using Support Vector Machine”, ICPEC, International Conference of Power, Energy and Control, pp 181-184.

Meyer N. L. and Carter-Brown C. G., (2010) Distribution Guide - Part 1: Network Planning Guide for Distribution Transformers. GDL 34-617, Eskom Distribution, rev 1.

Netshiongolwe F.A, Van Coller J., Cormack R. (2014). “Development of Alternative Electrical Stress Monitoring Transducers Applicable to MV/LV Distribution Transformers”, SAUPEC 2014.

Netshiongolwe F.A, Van Coller J., Cormack(2015) Advancements in Distribution Transformer Electrical Transients and Power Frequency Signal Monitoring, SAUPEC 2015.

Petting S.J. and Siersema. J (1983) “A Polyphase 500 kA Current Measurement System with Rogowski Coils”, IEE Proc B Vol. 130, No 5, pp 360-363.

Phillips A., Grobbelaar G., Pritchard C., Melaia R., and Jandrell I. (1996), “Development of a Rogowski Coil to Measure Lightning Current Impulses”, SAIEE Transactions.

Ray W.F. and Davis R. M. (1999), High Frequency Improvements in Wide Bandwidth Rogowski Transducers, EPE 99 Conference Proc., Lauzanne.

Ray W. F. and Hewson C. R. (2000), “High Performance Rogowski CurrentTransducers”, Industry Applications Conference, Vol.5, pp 3083 – 3090.

Ryan M. H. (2001), High Voltage Engineering and Testing, 2nd Edition, IET Publications, pp 405-430.

Schon K. and Schuppel W. (2007) Precision Rogowski Coil used with Numerical Integration, 13th ISH Proc., Ljubljana, paper T10-130.

Shafiq M., Hussain G. A., Kött L. and Lehtonen M. (2014), “Effect of geometrical parameters on high frequency performance of Rogowski coil for partial discharge measurements.” Measurement (49), pp. 126-137, 2014

Shareghi M., Phung B., Naderi M., Blackburn T. and Ambikairajah E. (2012), "Effects of current and voltage harmonics on distribution transformer losses, " in International Conference on Condition Monitoring and Diagnosis (CMD), Bali.

Smith T. B. (2003), "Electricity theft- comparative analysis," Energy Policy, vol. 32, pp. 2067-2076.

Swanson A. G. (2006), High Frequency Current Distribution in a Structure with Application to Lighting Protection Systems, Master's dissertation, University of the Witwatersrand, Johannesburg.

Van Schalkwyk W. J. D. and Van Coller J. (2013), "An Investigation into a More Optimal Choice of BIL on MV Feeders", Cigré 7th South African Regional Conference.

Ward D. A. and J. La T. Exon (1993) Using Rogowski coils for transient current measurements. Engineering Science and Education Journal. pp. 105-113.

Vosloo W. L., Macey R. E and De Tourreil (2004): The practical guide to outdoor high voltage insulators, Crown Publications, Johannesburg.

Appendix A

A1: Impulse voltage measurement

The type C bushing and the prototype bushing used in this study were subjected to 1.2/50 µs impulse voltages of varying magnitude. Figure A.1 shows a typical 1.2/50 impulse voltage as defined by SANS 606001-1(2011)

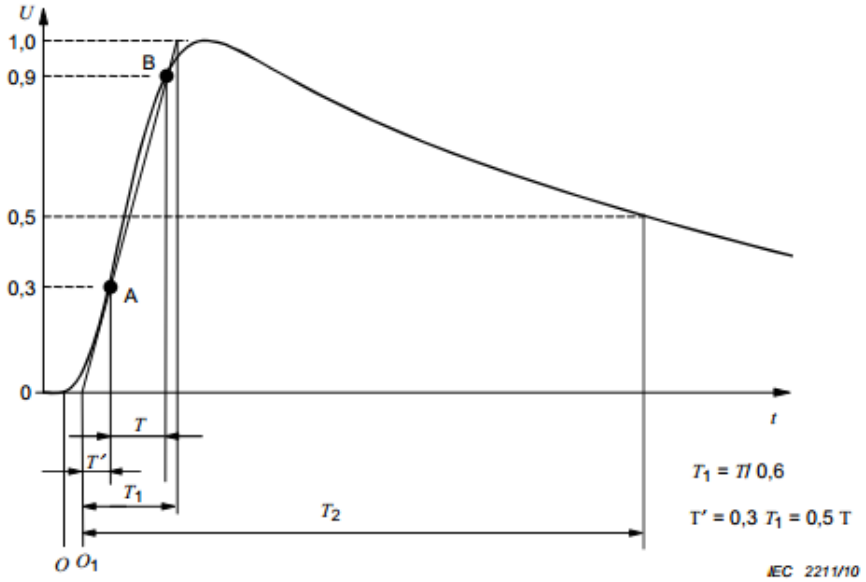

Figure A1: Full wave lightning impulse

The 1.2/50 µs lightning voltage impulse is defined as follows:

- Rise time (10% to 90%): T_1 = 1.2 µs ± 30 %
- Fall time (drop to 50%): T_2 = 50µs ± 20 %

The generator used in this study is shown in Figure A.2. Varying the magnitude of the impulse was done by increasing or decreasing the spark gaps of the generator. Correction factors as prescribed in SANS 606001-1(2011) were used in determining the corrections for atmospheric conditions. The measured impulses had to be corrected using correction factors that are calculated as a function of temperature, humidity and pressure.

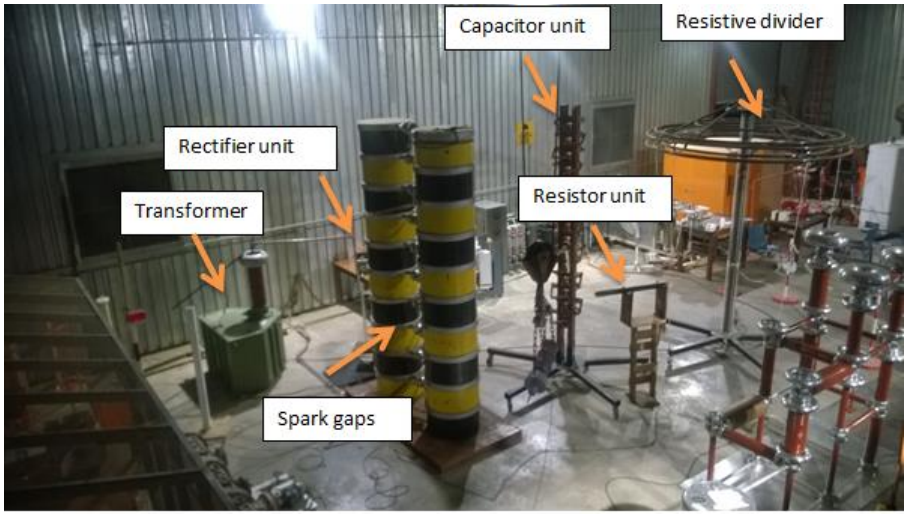

Figure A2: 1.2/50 µs impulse generator components

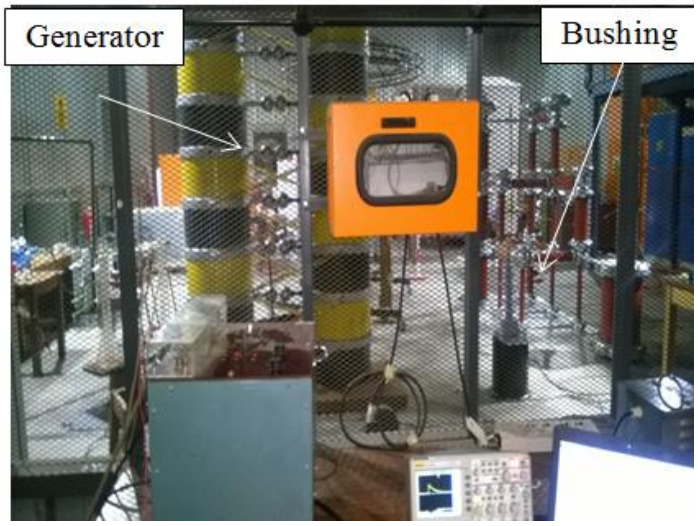

Figure A3: Prototype bushing Impulse withstand test

The corrected impulse voltage is given by:

$$U_0 = \frac{U}{K_t} \tag{A.1}$$

-where

U_0 = Corrected voltage [V]

U = Measured voltage [V]

K_t = Correction factor

$$K_t = k_1 \times k_2 \tag{A. 2}$$

-where

k_1 = The air density correction factor

k_2 = The humidity correction factor

$$k_1 = \delta^m = \left(\frac{p}{p_0} \times \frac{273 + t_0}{273 + t}\right)^m \quad \text{(A. 3)}$$

-where

δ = Relative air density

p = Measured pressure

t = Measured temperature

m = Air density correction factor

IEC60060-1(2011) defines standard reference atmosphere as:

Temperature t_0 = 20 °C

Absolute pressure p_0 = 1 013 mbar

Absolute humidity h_0 = 11 g/m^3.

The humidity density factor k_2 is evaluated by:

$$k_2 = k^w \quad \text{(A. 4)}$$

To parameters w and m, we need to first evaluate the parameter g, given by:

$$g = \frac{U_{50}}{500 L \delta k} \quad \text{(A. 5)}$$

-where

U_{50} is equal to 1.1 times the test voltage in V

L is the minimum discharge path in m

δ is the relative air density

k is a dimensionless constant

The absolute humidity is determined from the relative humidity by:

$$h = \frac{6.11 \times R \times e^{\frac{17.6xt}{243+t}}}{0.4615 \times (273 + t)} \quad (A.6)$$

The dry impulse tests was conducted under the following conditions

Measured temperature t = 25 °C

Measured pressure p = 831 mbar

Relative humidity (R) = 36 %

Based on equations A.1 up to A6, and curves given in SANS 60060-1(2011), k_1 was found to be 0.947 whilst k_2 was found to be 0.997 for impulse tests resulting in impulse values shown in Table A1 for tests conducted on the prototype bushing.

Table A1: Dry lightning 1.2/50 µs voltage impulse testing of the prototype

Impulses	*Positive Impulse*	*Negative Impulse*
1	161.74	155.13
2	158.43	155.13
3	158.43	158.43
4	158.43	158.43
5	158.43	158.43
6	158.43	155.13
7	161.74	158.43
8	161.74	155.13
9	161.74	158.43
10	151.83	158.43
11	161.74	158.43
12	161.74	158.43
13	161.74	161.74
14	161.74	161.74
15	161.74	158.43

Appendix B

B1: Epoxy resin bushing construction process

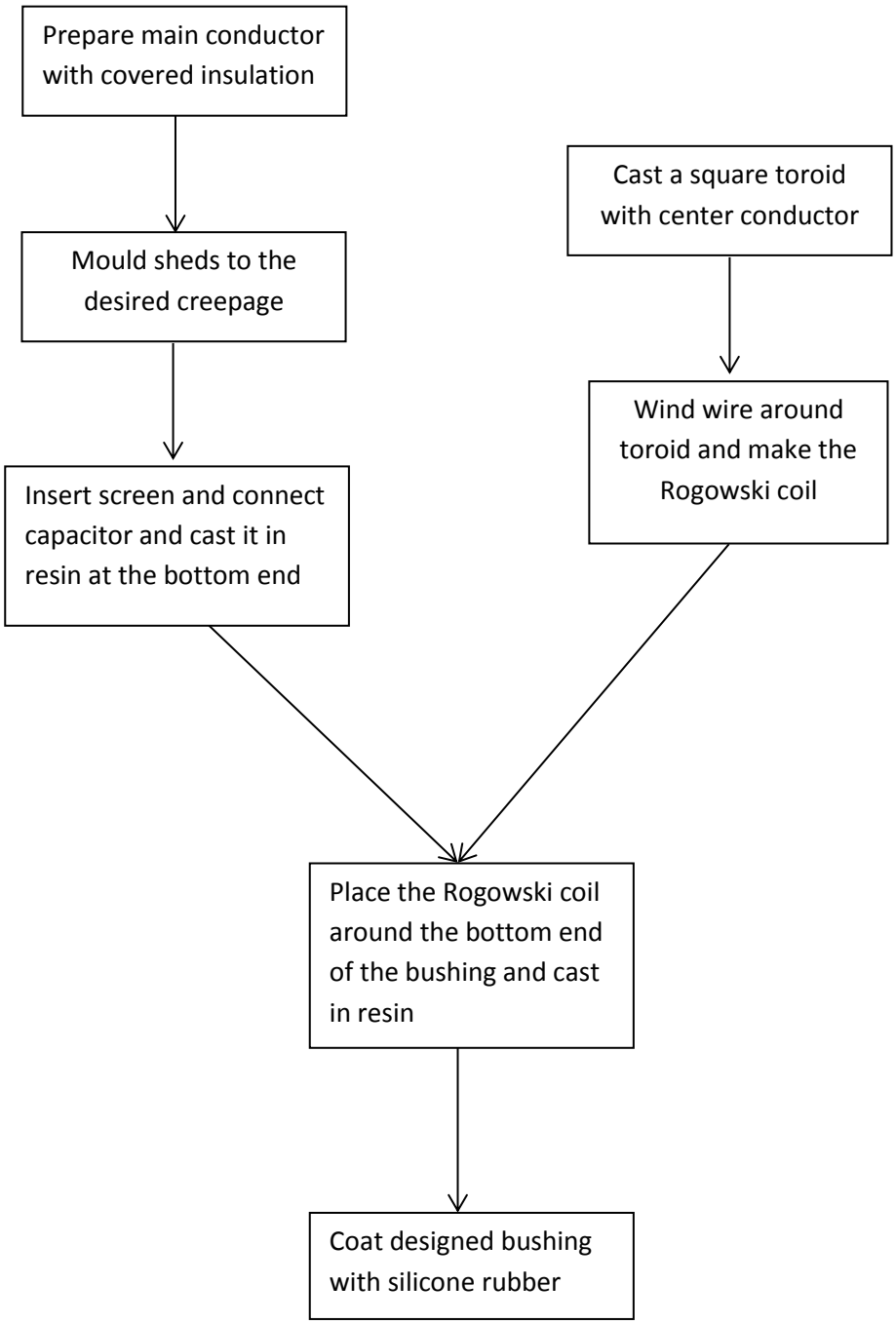

Figure B1: Steps followed in making the bushing prototype

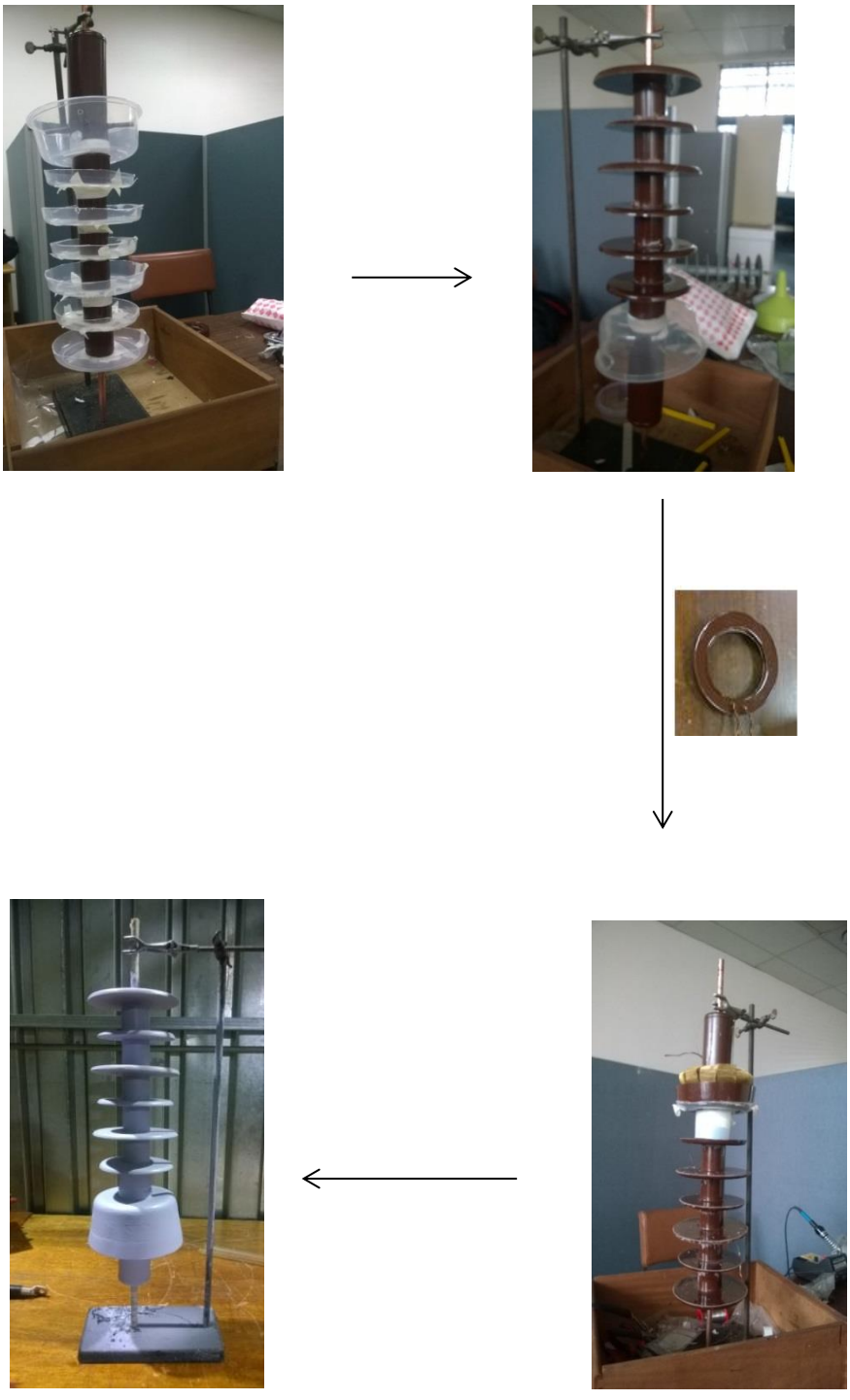

Figure B2: Prototype construction photos

Appendix C

C1: Impulse current tests measurement

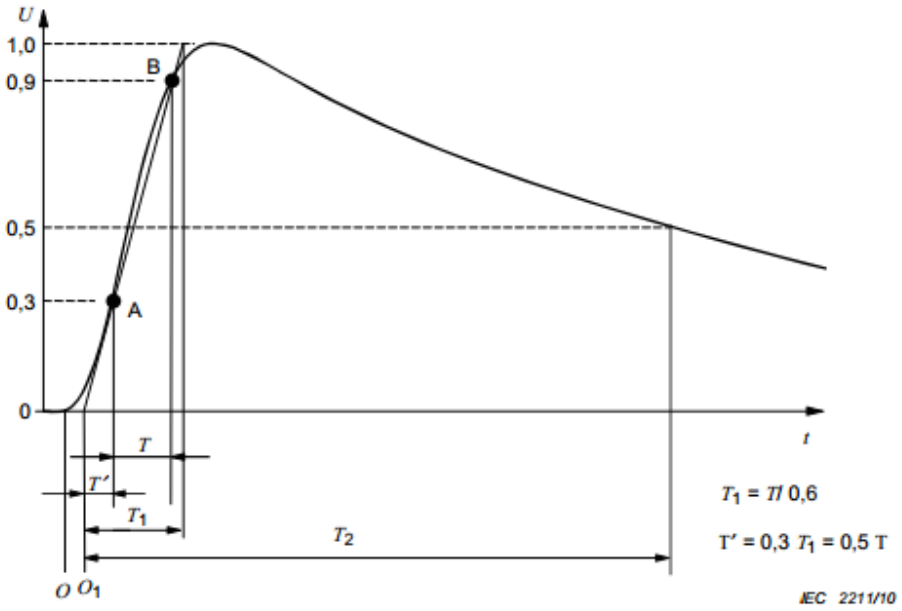

Figure C1: Full wave lightning impulse

The 8/20 µs current impulse is defined as follows:

- Rise time (10% to 90%): T_1 = 8 µs ± 30 %
- Fall time (drop to 50%): T_2 = 20 µs ± 20 %

Figure C2: Current impulse tests with type C bushing measured with 418 turns and 875 Rogowski turns coil

Appendix D

D1: Conference submissions:

- A paper titled: **Electrical Stress Monitoring of Distribution Transformers using Bushing Embedded Capacitive Voltage Dividers and Rogowski Coils.** Submitted to the International Conference Power Systems Transients (IPST2015), Cavtat, Croatia, June 2015

- A paper titled: **Advancements in Distribution Transformer Electrical Transients and Power Frequency Signal Monitoring.** Submitted to the South African Universities Power Engineering Conference, Johannesburg, South Africa, January 2015.

- A paper titled: **Development of Alternative Electrical Stress Monitoring Transducers Applicable to MV/LV Distribution Transformers.** Submitted to the South African Universities Power Engineering Conference, Kwazulu Natal, South Africa, January 2014.

Electrical Stress Monitoring of Distribution Transformers using Bushing Embedded Capacitive Voltage Dividers and Rogowski Coils

Fulufhelo Andrew Netshiongolwe and John Michael van Coller

***Abstract*-- Premature failure of distribution transformers has prompted the need to measure the electrical stresses that may be causing such failures. This paper presents a non-intrusive alternative means of monitoring electrical stresses on the medium voltage (MV) side of distribution transformers rated 16 kVA up to 2 MVA with the aim of curbing premature transformer failure. An electric field control screen embedded in a 24 kV bushing is used to form a capacitive voltage divider measuring both power frequency and transient voltages. A shielded Rogowski coil placed around the bushing screen measures both power frequency and transient currents. Simulation models are able to recreate the laboratory measured results.**

***Keywords*: Rogowski coil, impulse currents, impulse voltage, capacitive voltage divider, Smart Grids**

I. Introduction

The presence of transients, harmonics, ever increasing changes in loads and load profiles increases the electrical stresses experienced by transformers at the distribution level. Due to the low capital cost of distribution transformers, minimal condition monitoring is installed. Colour coded thermal stickers that require field inspection are currently used for overload monitoring on Eskom distribution transformers rated up to 2 MVA [1]. The increase in the premature failures of these transformers has prompted the need to seek alternative monitoring techniques.

The introduction of Smart Grids affords utilities the ability to better manage load profiles, monitor and manage electrical stresses and improve electrical equipment availability [2]. This research focuses on the development of a low cost bushing with embedded current and voltage transducers capable of monitoring wideband electrical stresses on the MV side of distribution transformers. The operating principle of the designed bushing capacitive voltage divider and Rogowski coil is given. Various tests were performed to evaluate the performance of the designed bushing against commercially available current and voltage probes. A comparison between simulated and measured results is also presented.

This work was funded by Eskom through the Eskom Power Plant Engineering Institute (EPPEI) program. F.A. Netshiongolwe is with Eskom Generation and is studying towards an MSc in Electrical Engineering at the University of the Witwatersrand (e-mail: netshifa@eskom.co.za). J. M. Van Coller is with the University of Witwatersrand and is a Senior Lecturer who has been with University for many years and holds the Eskom Chair of High Voltage (e-mail: john.vancoller@wits.ac.za).

Paper submitted to the International Conference on Power Systems Transients (IPST2015) in Cavtat, Croatia June 15-18, 2015

II. Background

A. Electrical stress monitoring

Premature failure of distribution transformers may be caused by unmonitored transient and power frequency electrical stresses. Current and voltage monitoring on the low voltage (LV) side of pole-mount transformers within Eskom distribution networks has led to the identification of transformers that are subjected to stresses that include overloading, severe load unbalances and overcurrent conditions [3]. Such findings prompted the need to develop low cost electrical transducers that could be used to identify other electrical stresses that could lead to premature transformer failure. Another example is where failed surge arresters allow large transient voltages to appear across transformers which may result in their premature failure [4]. The presence of harmonics introduced by the increased use of nonlinear loads increases the risk of transformer over-temperatures [5].

In this study, focus is on the development of low cost electrical stress monitoring sensors suitable for use on the medium voltage (MV) side of distribution transformers. Information obtained from such sensors can then be used to identify transformers that are exposed to excessive electrical stresses that may lead to premature failure.

B. Rogowski coil current sensor

Rogowski coils with a non-magnetic core, such as the one depicted in Fig.1, have been shown to have the following superior features [6]-[8]:

- High bandwidth (suitable for transients)
- Multiple primary current measurement ranges
- Non-intrusive to the primary circuit
- Modular in size
- Linear

The Rogowski coil output voltage is a function of the time derivative of the measured primary current. The coil output voltage based on the properties in Fig. 1 and Table 1 is given by [6], [8]:

$$V_c = -\frac{d\varphi}{dt} = -\mu_0 NA\frac{di}{dt} = -M\frac{di}{dt} \quad (1)$$

-where:

V_c is the coil output voltage [V]

φ is the coil flux linkage [Weber-turns]

μ_o is the permeability of free space [$4\pi \times 10^{-7}$ H/m]

N is the number of turns
A is the coil area [m^2]
i is the current in the primary conductor [A]
M is the mutual inductance [H]

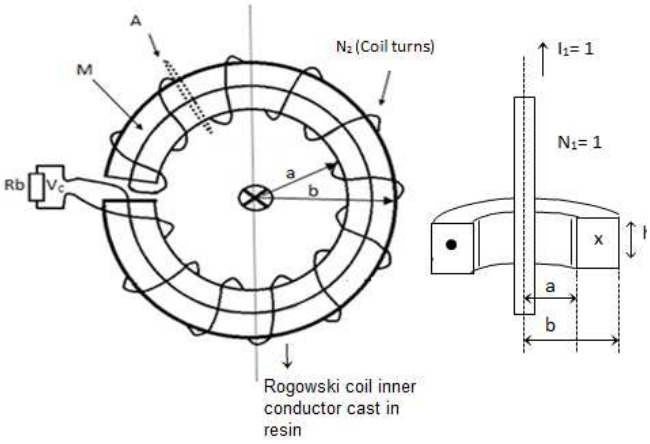

Fig. 1. Rogowski coil cast in resin

TABLE 1
DESIGNED ROGOWSKI COIL SPECIFICATION

Parameter	Description	Value
$d_w[mm]$	Wire diameter	0.25
$R[\Omega]$	Wire resistance	18.5
a[mm]	Inner radius	40
b[mm]	Outer radius	60
h[mm]	Coil height	20
I[mm]	Core length	390
A[mm^2]	Coil area	400
N_2	Number of turns	668

A widely accepted lumped parameter model for the Rogowski coil is shown in Fig. 2 below. The calculated mutual inductance of the Rogowski coil with properties in Table 1 and Fig. 1 is given by [9]:

$$M = \frac{\mu_0 N_2}{2\pi} hln\left(\frac{b}{a}\right) \quad (2)$$

The corresponding self-inductance is given by:

$$L = \frac{\mu_0 {N_2}^2}{2\pi} hln\left(\frac{b}{a}\right) \quad (3)$$

The coil lumped capacitance is given by:

$$C = \frac{2\pi^2 \varepsilon^2 (a+b)}{\log[(a+b)/(b-a)]} \quad (4)$$

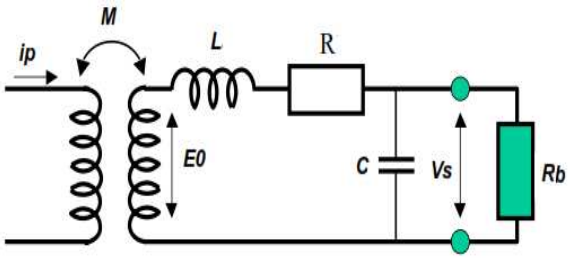

Fig. 2. Rogowski coil electrical model [6]

TABLE 2
CALCULATED COIL PARAMETERS

Parameter	Description	Value
M (nH)	Mutual Inductance	861
L (mH)	Coil self-inductance	2.17
C (pF)	Coil capacitance	50.2

Calculated coil parameters have been shown to differ from the measured parameters at high frequencies. Because of this, the decision was made to rather base the model on measurements. Hashmi et al used coil parameters measured at 1 kHz to simulate Rogowski coil behavior whilst measuring partial discharges [10]. Shafiq et al. developed a parameter identification method that involves measuring impulse waveforms with a Rogowski coil whose output is sensed with the use of a differential probe [11]. A Fast Fourier transform of the output of the differential probe was then used to find the resonant frequencies for different configurations. The resonant frequencies were then used to determine the relationship between the inductances and capacitances of the coil.

In this study a 20 MHz function generator, an oscilloscope and tank circuits were used to determine the coil parameters using the resonance frequency calculations given in (5)-(10) below. The output of the function generator is applied across a resistor in series with a coil that is in parallel with a known capacitor C_T. The measured voltage across the coil reaches a peak at the point of resonance where the relationship between the total circuit capacitance and the inductance is given by:

$$F_r = \frac{1}{\sqrt{L_T(C_m + C_p + C_T)}} \quad (5)$$

- where:

F_r is the tank circuit resonant frequency [Hz]
L_m is the coil inductance [H]
C_m is the coil stray capacitance [F]
C_p is the probe capacitance [F]
C_T is the capacitance of the known capacitor [F]

Based on (5), given the capacitance of the known capacitor 1, C_{T1}, which gives a measured tank resonant frequency F_{r1} when combined with the designed coil, (5) can be rearranged such that:

$${F_{r1}}^2 L_m (C_p + C_m + C_{T1}) = 1 \quad (6)$$

For the capacitance of the known capacitance 2, $C_{T2,}$ and

measured tank resonant frequency, F_{r2}, the above equation becomes:

$$F_{r2}{}^2 L_m(C_p + C_m + C_{T2}) = 1 \quad (7)$$

Taking a ratio of (6) and (7) results in the following expression:

$$(C_p + C_m + C_{T1}) = \frac{F_{r1}{}^2}{F_{r2}{}^2}(C_p + C_m + C_{T2}) \quad (8)$$

From the above expression the coil stray capacitance and probe capacitance are given by:

$$C_m + C_p = \frac{C_{T2}\left(\frac{F_{r1}{}^2}{F_{r2}{}^2}\right) - C_{T1}}{1 - \frac{F_{r1}{}^2}{F_{r2}{}^2}} \quad (9)$$

Shafiq et al suggest taking other measurements with two probes in order to determine the probe capacitance [6]. The above expression is then modified such that:

$$C_m + 2C_p = \frac{C_{T2}\left(\frac{F_{r21}{}^2}{F_{r22}{}^2}\right) - C_{T1}}{1 - \frac{F_{r21}{}^2}{F_{r22}{}^2}} \quad (10)$$

- where $F_{r21}$and F_{r22} are the new resonance frequencies that result due to the additional probe capacitance. The probe capacitance is calculated by subtracting the value obtained from (9) from that obtained from (10). Once the probe capacitance is calculated, the coil capacitance is then obtained from (9). The coil inductance is found by averaging the calculated inductance at the different resonance frequencies above. Table 2 gives all the corresponding measured and calculated coil parameters of the designed Rogowski coils. The accuracy of both measured and calculated parameters in modelling the designed Rogowski coils performance is evaluated by comparing simulated and measured results in the subsequent sections.

TABLE 3
MEASURED COIL PARAMETERS

Parameter	Parameter	Value
C_{T1} [pF]	Tank known capacitance 1	11
C_{T2}[pF]	Tank known capacitance 2	56.25
F_{r1} [kHz]	Resonance frequency ($C_{T1} + C_p$)	480
F_{r2} [kHz]	Resonance frequency ($C_{T2} + C_p$)	397
F_{r21} [kHz]	Resonance frequency ($C_{T1} + 2C_p$)	405
F_{r22} [kHz]	Resonance frequency ($C_{T1} + 2C_p$)	326
C_p[pF]	Probe capacitance	8
C_m[pF]	Coil capacitance	4.1
L_m[mH]	Coil inductance	5.37
M[nH]	Mutual Inductance	510

C. Voltage monitoring using bushing screen

Non-condenser bushings such as cast resin MV bushings are subjected to both axial and radial stresses. High axial stresses may lead to surface tracking [12]. The presence of high radial stresses may lead to partial discharges or even insulation breakdown [13]. In this study the bushing screen is used for electric field stress control as well as voltage measurement. The designed bushing consists of one screen surrounding the bushing conductor. This screen is connected to an external capacitor to form a capacitive voltage divider. The insulation between the screen and the bushing conductor can be represented by a resistor in parallel with a capacitor as shown in Fig. 3. The position of the screen in relation to the bushing conductor suggests a cylindrical geometry. The insulation capacitance between the conductor with reference to Fig 3 and Table 4 parameters is given by Kuffel et al. [14]:

$$C_1 = \frac{2\pi\varepsilon_0\varepsilon_r' h}{\ln\frac{b}{a}} \text{ [F/m]} \quad (11)$$

The corresponding insulation resistance at angular frequency w is given by:

$$R_1 = \frac{h \ln\frac{b}{a}}{w 2\pi\varepsilon_0\varepsilon_r''} [\Omega/m] \quad (12)$$

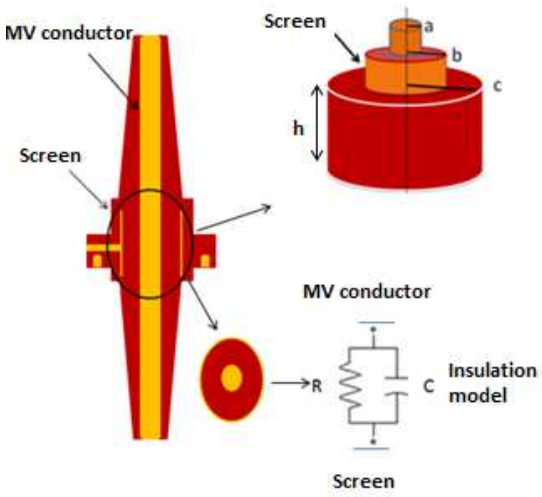

Fig. 3. Cross-section of a screened 24 kV epoxy resin bushing with emphasis on the position of the screen relative to the bushing conductor

The dielectric resistance at power frequency is large enough such that the measured bushing voltage is given by:

$$V_{out} = \frac{C_1}{C_1 + C_2} V_{in} \quad (13)$$

- where:

C_1 is the capacitance between the bushing screen and the bushing conductor [F]

C_2 is the capacitance of the external capacitor [F]

V_{in} is the input voltage [V]

V_{out} is the output voltage [V]

TABLE 4
EPOXY RESIN 24 KV BUSHING PARAMETERS

Parameter	Parameter description	Value
ε_0(F/m)	Free space permittivity	8.854E-12
ε_r'	Relative permeability	3.8
ε_r''	Relative permeability	0.038
Tan delta	Epoxy resin tan delta	0.01
a(mm)	Conductor radius	6
b (mm)	Screen radius	30
h (mm)	Screen height	60

The measured capacitance between the bushing screen and the bushing conductor was 22.23 pF. The capacitance of the external capacitor connected between the bushing screen and the external earth was 47 nF. Based on (13), the voltage division ratio was calculated as 2115:1. A different voltage division ratio can be obtained by using a different external capacitor C_2.

III. EXPERIMENTAL SETUP

The designed bushing was subjected to a voltage impulse corresponding to its rated BIL of 150 kV. The designed bushing was coated with silicone rubber to improve its pollution performance [15]. Other tests included wet and dry power frequency withstand tests as described in SANS/IEC 60137 [16]. The designed bushing did not puncture or flashover when these tests were performed. The experimental setup for tests related to the performance of the embedded Rogowski coil and the capacitive voltage divider are described below.

A. Power frequency current measurement

The designed bushing was tested with a high power frequency current source as shown in Fig. 4 below. The current flowing through the bushing was varied using the variac. The measured current value was compared with that obtained using a 100/1 commercial wideband current probe. Currents were varied up to the 250 A rating of the bushing. Further measurements were made at 160% of the rated current.

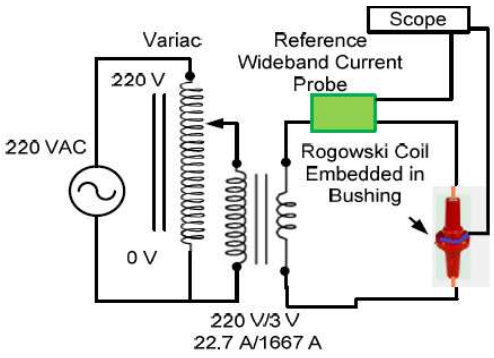

Fig. 4. Power frequency current measurements

B. Impulse current measurements

An 8/20 μs current impulse generator shown in Fig 5 was used to generate current impulses that were passed through the designed bushing. The measured current value was compared with that obtained using the same 100/1 commercial wideband current probe. Impulse currents of different amplitudes were obtained by varying the input AC source voltage which charged the capacitors to the desired level before discharging the current impulse through the bushing.

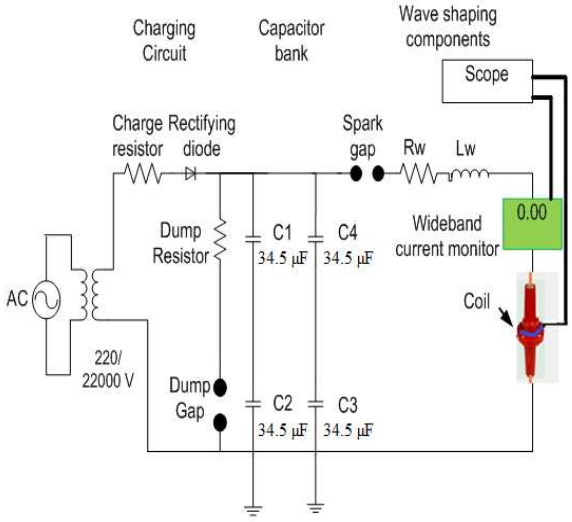

Fig. 5. Impulse current measurements circuit

C. Power frequency voltage measurement

Power frequency voltage measurements were performed by connecting the designed bushing to the output of a 0.22/60 kV transformer on the high voltage side. The output voltage of the transformer was varied using the variac as shown in Fig. 6. The measured voltage from the bushing capacitive voltage divider was compared with that obtained using a commercially available 1000/1 capacitive voltage probe.

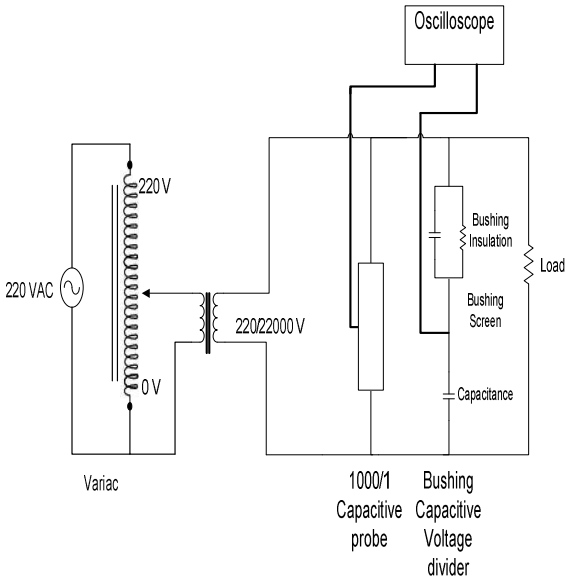

Fig. 6. Power frequency voltage measurement

D. *Impulse voltage measurement*

An 8 stage 1.2/50 µs voltage impulse generator was used to generate impulse voltages that were applied on the bushing. The bushing was subjected to voltages up to the rated BIL of 150 kV. The output of the bushing divider was compared to that of a wideband resistive divider. Each of the measured impulses were adjusted using correction factors as prescribed in SANS/IEC 60060-1[17].

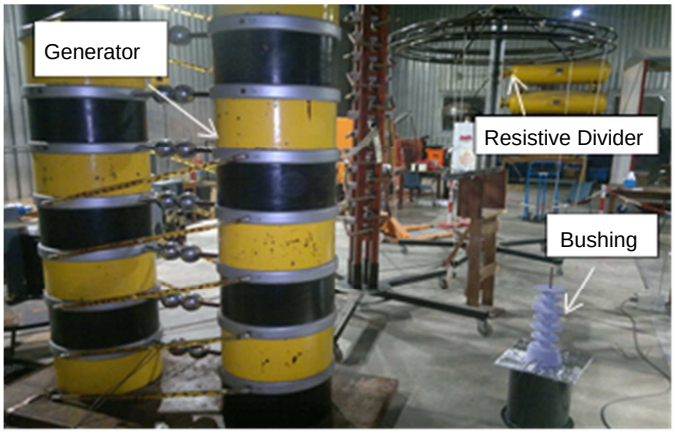

Fig. 7. Impulse voltage measurement setup

IV. Simulation and Measured Results

An accurate simulation model is required since this allows compensation to be designed for any observed nonlinearity. Simulation models of the current and voltage sensors were developed using the simulation package ATPDraw.

A. *Current measurements*

Several authors have used the modified version of the ATPDraw saturable transformer model in the simulation model of Rogowski coils [8, 10]. This is achieved by modifying the non-linear saturable transformer flux versus current relationship such that it becomes linear as depicted in Fig. 8. In this study the parameters found in Tables 2 and 3 were used to develop the simulation model that reproduced the laboratory measured results. The accurately measured impulse currents were used as input currents to the circuit model shown in Fig 9. A 10/1 passive voltage probe was used as an interconnection between the oscilloscope and the Rogowski coil.

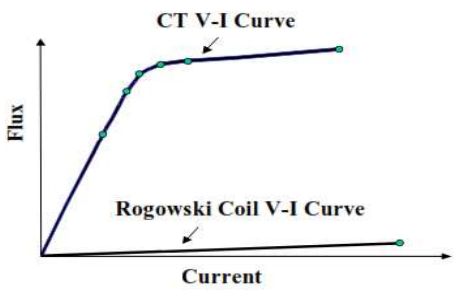

Fig. 8 Transformation of ATPDraw saturable transformer model to a Rogowski coil model [8]

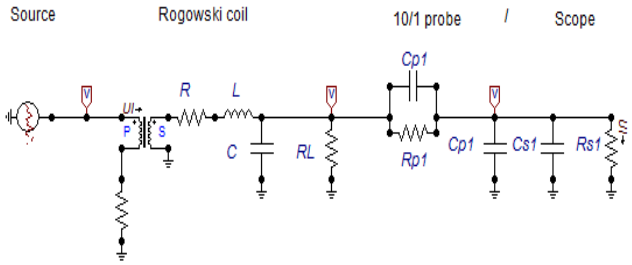

Fig. 9. Simulated current measurement circuit

A comparison between the unintegrated output of the Rogowski coil and the simulated behaviour is shown in Fig. 10. The measured Rogowski coil output voltage waveform is consistent with the voltage waveform obtained by [18].The results were obtained whilst measuring an 6 kA 8/20 µs current impulse shown in Fig. 11 below. The simulated behaviour based on measured parameters closely approximated the measured unintegrated output of the Rogowski coil. Calculated parameters based on the physical properties result in an overestimation of the coil output. The numerically integrated output of the Rogowski coil shown in Fig. 11 closely approximates the measured impulse waveform. Observed results when measuring 9 kA and 15 kA current impulses remain consistent with the behaviour illustrated in Fig. 10 and Fig. 11.

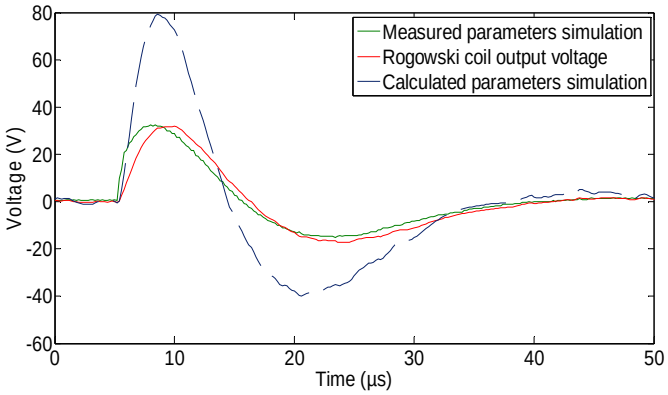

Fig. 10 Comparison between the designed Rogowski coil measured output voltage and the simulated output voltage

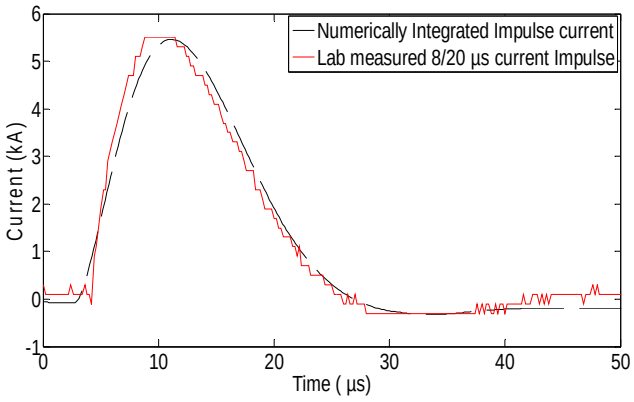

Fig. 11. Comparison between 6 kA wideband current probe measurement with the numerically integrated Rogowski coil

output voltage.

The output of the designed Rogowski coil when measuring rated 50 Hz current is shown in Fig. 12. The unintegrated current is 90 degrees out of phase with the output of a commercial wideband probe as shown in Fig. 13 – as expected.

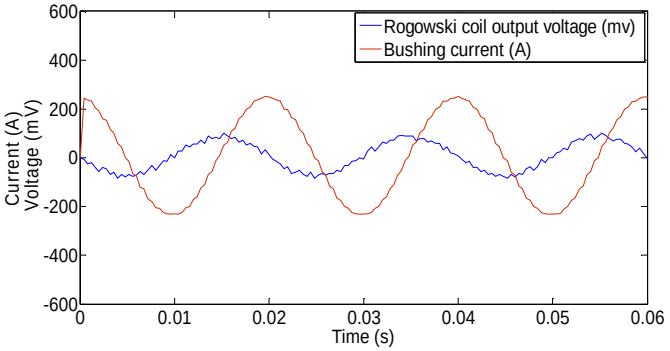

Fig. 12. Performance of the Rogowski coil whilst measuring rated current

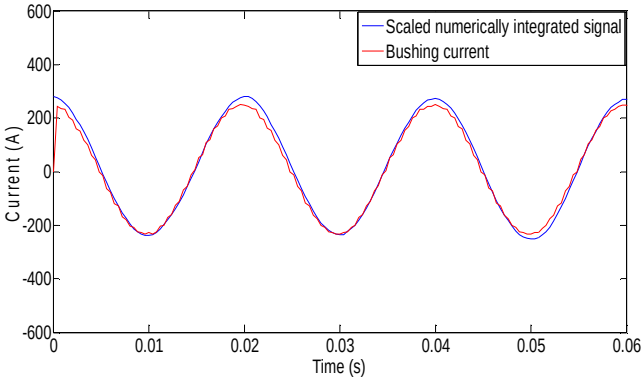

Fig. 13. Scaled numerically integrated output of the designed Rogowski coil

B. Voltage measurements

The output of the bushing capacitive voltage divider was observed to offer linear results comparable with that of a commercial capacitive voltage probe when measuring 50 Hz power frequency voltages. Observed results were measurable from 1 kV upwards. They were also consistent with the calculated 2115:1 transformation ratio. Fig. 14 shows the measurements that were taken at 2 kV and Fig. 15 shows those taken at 24 kV.

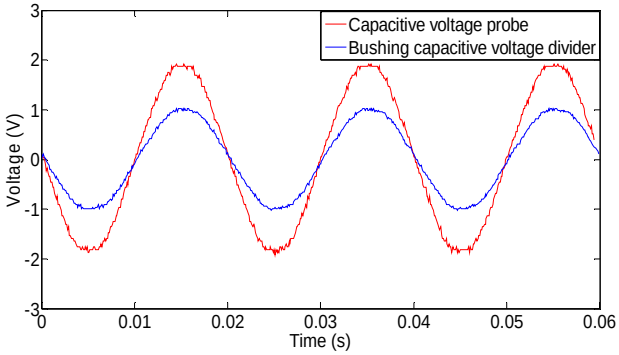

Fig. 14 Low voltage measurements

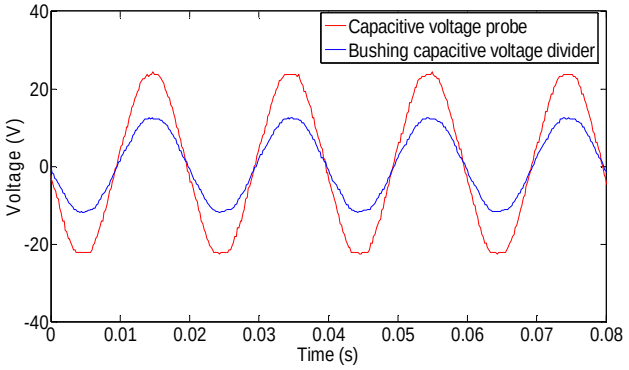

Fig. 15. High voltage measurement

When measuring impulse voltages, nonlinearity was observed when measuring impulse voltages larger than 60 kV. This nonlinearity was also found with other capacitive dividers that used epoxy resin as a dielectric. This behaviour suggested a simulation model as shown in Figure 16 below

The ATPdraw nonlinear type 92 resistor was used to simulate the nonlinearities introduced by the epoxy resin dielectric when subjected to impulses larger than 60 kV. The non-linear resistor current versus voltage characteristic was chosen to give good results for a 130 kV voltage impulse. Fig. 17 to 19 show comparisons between the simulated and measured voltage impulses using the model with the optimized non-linear resistor and those without.

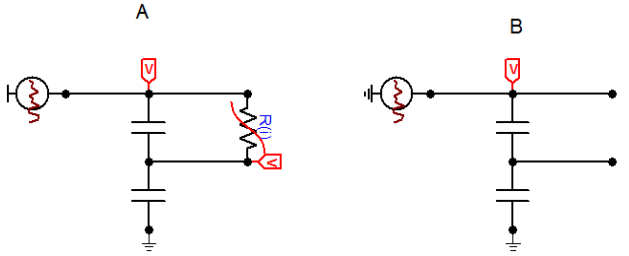

Fig. 16. Simulated bushing capacitive voltage divider model.

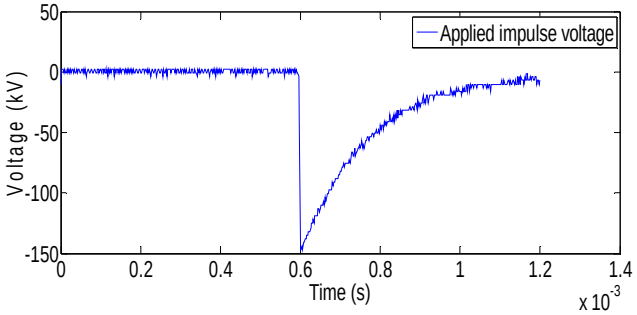

Fig. 17. Applied rated BIL 150 kV 1.2/50 µs impulse voltage

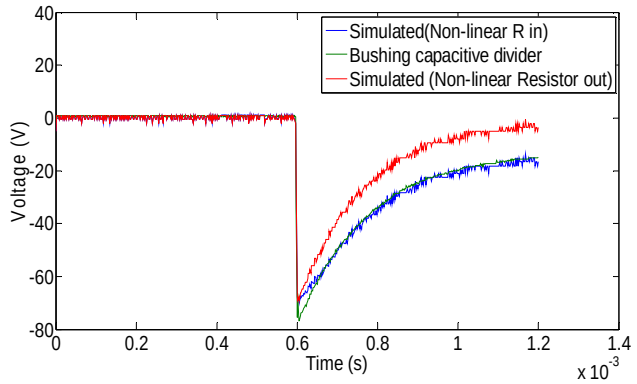

Fig. 18. Bushing capacitive voltage divider output at the rated BIL

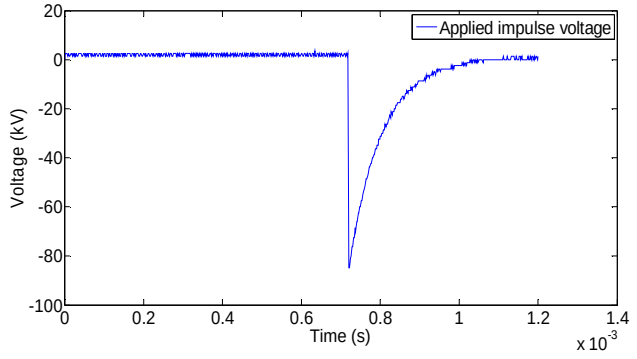

Fig. 19. Applied 80 kV 1.2/50 µs impulse voltage

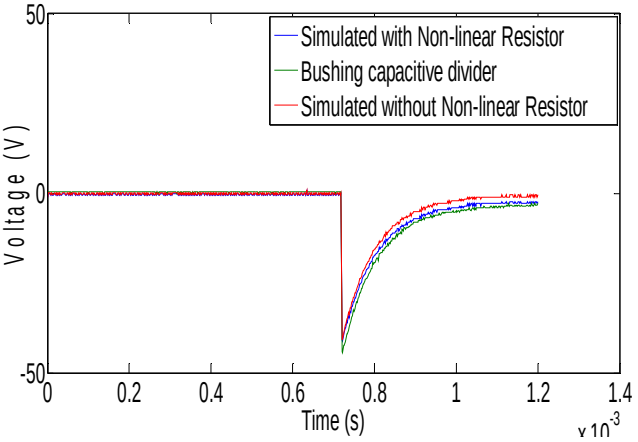

Fig. 20. Bushing capacitive voltage divider output for the applied 80 kV 1.2/50 µs impulse voltage

V. Industry Benefits

The study conducted showed the possibility of using a low cost screen-based bushing capacitive voltage divider and a bushing embedded Rogowski coil for performing MV side measurements. These transducers can be used for identifying transformers that are subjected to severe electrical stresses on the MV side and thus can help in the prevention of premature transformer failure. With refined sensitivity of the designed Rogowski coils, the bushing with embedded voltage and current probes can assist in reducing costs associated with the measurements required for implementing the Smart Grid of the future.

VI. Conclusion

This paper presented the design, testing and modelling of an MV transformer bushing with embedded voltage and current probes for use with distribution transformers. Simulated results obtained using measured parameters were consistent with laboratory measured results for both power frequency and impulse current measurements. Power frequency voltage measurements using the bushing capacitive voltage divider showed a constant 2115:1 voltage transformation ratio for the range 1 kV up to 24 kV. Observations showed nonlinearities when 1.2/50 µs impulses with magnitude larger than 60 kV were applied. With an accurate nonlinear model of this behaviour, a compensation circuit can be designed to cancel out this non-linearity.

VII. References

[1] Distribution Guide– Part 1: Network Planning Guideline for Transformers, Eskom Guideline 34-542, Nov. 2010.

[2] C. G.Elsworth, *The Smart Grid and Electric Power Transmission*, Nova Science Pub. Incorporated, 2008, p1-45.

[3] R Kleinhans, "Current and Voltage Monitors Combat Theft and Improve Supply Quality", *Energize: Transmission and Distribution*, pp. 41-45. Sep. 2011.

[4] W. J. D. van Schalkwyk and J. van Coller, "An Investigation into a More Optimal Choice of BIL on MV Feeders", *in 2013 Proc.Cigré 7th South African Regional Conf.*

[5] M. Sharengi, B. Phung, M. Naderi, T. Blackburn and E. Anbikairajar, "Effects of Current and Voltage Harmonics on Distribution Transformer Losses", *in 2012 Proc. International Conf. on Condition Monitoring and Diagnosis(CMD)*, Bali, pp. 633-636, 2012

[6] *IEEE Guide for the Application of Rogowski Coils Used for Protective Relaying Purposes*, IEEE Standard C37.235, Sep. 2007.

[7] W. F. Ray and R .M. Davis, "High frequency improvements in wide bandwidth Rogowski transducers", *in 1999 Proc. EPE 99 Conf.*

[8] L. A. Kojovic. "Rogowski Coil Transient Performance and ATP Simulations for Applications in Protective Relaying", *in 2005 Proc. International Conf. on Power Systems Transients International (IPST'05).*

[9] M. Argueso , G. Robles and J. Sanz, "Implementation of a Rogowski coil for the measurement of partial discharges", *Rev. Sci. Instrum.*, vol. 76, no. 6, pp. 065107-1 -065107-7, May 2005.

[10] G. M. Hashmi, M. Lehtonen, and M. Nordman, "Modeling and Experimental Verification of On-line PD Detection in MV Covered-conductor Overhead Networks", *IEEE Transaction on Dielectrics and Electrical Insulation*, vol. 17,Issue 1, pp. 167-180, Feb 2010.

[11] M Shafiq, G. Amjad Hussain, L Kütt and M Lehtonen. "Effect of geometrical parameters on high frequency performance of Rogowski coil for partial discharge

measurements.” *Measurement (49)*, pp. 126-137, 2014.
[12] M. H. Ryan, *High Voltage Engineering and Testing*, 2nd ed., IET Publications, 2001, pp. 405-430.
[13] H. Illias, M. A.Tunio, A. H. A Bakar and H. Mokhlis, “Distribution of Electric Field in Capacitor and Surge Arrester Bushings" *in 2012 Proc. IEEE International Conf. on Power and Energy (PECon)*, pp. 461-466. (2012)
[14] E. Kuffel, W. S. Zaengle and J. Kuffel, *High Voltage Engineering- Fundamentals,* Butterworth-Heinemann, 2nd ed., 2000
pp. 201-241.
[15] W. L. Vosloo, R. E. Macey and C. de Tourreil, *The Practical Guide to Outdoor High Voltage Insulators*, Crown Publications, Sep 2006, pp. 186-187
[16] Insulated Bushings for Alternating Voltages Above 1 000 V, SANS Standard 60137, ed. 3, 2010.
[17] High voltage tests: Atmospheric correction factors, SANS Standard 60060-1, 1989.
[18] K. Schon. *High Impulse Voltage and Current Measurement Techniques: Fundamentals, Measuring Instruments, Measuring Method*, Springer International, Jan 2012, p. 195.

ADVANCEMENTS IN DISTRIBUTION TRANSFORMER ELECTRICAL TRANSIENTS AND POWER FREQUENCY SIGNAL MONITORING

F. A. Netshiongolwe[1], R. Cormack[2], J. M. van Coller[1]

[1]Eskom Power Plant Engineering Institute (EPPEI)-High Voltage (HV), School of Electrical and Information Engineering, University of the Witwatersrand, Private Bag 3, Wits 2050, South Africa Email: netshifa@eskom.co.za, John.VanColler@wits.ac.za
[2]Eskom, PO Box 1091, Johannesburg, 2001, South Africa Email: CormacR@eskom.co.za

Abstract. This paper presents the use of a designed Rogowski coil current sensor and a capacitive voltage divider for both transient and power frequency monitoring in distribution networks. Limitations to presently available monitoring systems that use conventional ferromagnetic core current transformers are presented. The designed 875 turns coil was used in successfully measuring currents rated up to 600A. The integrated output of the designed Rogowski coil was consistent with measured 6 kA 8/20 µs impulse current. An embedded screen on a 24 kV rated bushing was used in capturing power frequency voltages ranging from 1 kV up to 27 kV. Non-linearity have however been observed when measuring1.2/50 µs impulse voltage beyond 80 kV.

Key Words: Rogowski coils; capacitive voltage divider, impulse current, impulse voltage

1. INTRODUCTION

Advancements in the distribution network have resulted in the need for increased electrical monitoring. The increased use of compact fluorescent lamps, computers and PV generation sources with power electronic interfaces have also led to an increase in the level of harmonics at the distribution level [1]. Transients introduced by faults and lightning strikes can cause significant damage to distribution transformers. Failed surge arrestors on pole-mount transformers are often not identified in time, resulting in premature transformer failures [2]. All this highlights the need to have reliable monitoring that enables effective management of distribution-level equipment.

Monitoring technology applied to distribution transformers is often limited due to the unavailability of low cost sensors. This paper presents a low cost approach to monitoring distribution transformers using an existing bushing screen and a Rogowski coil embedded in the bushing. An overview of the potential electrical stresses observed at distribution level is given. The operating principles of the capacitive voltage divider and the Rogowski coil are given. Both the power frequency and the transient measurement capabilities of the above sensors are evaluated.

2. BACKGROUND

2.1 Electrical stresses

The premature failure of distribution transformers (rated up to 2 MVA) has led to the use of current and voltage monitoring systems on the low voltage (LV) side of Eskom distribution transformers [3]. The use of such monitors coupled with temperature sensors has shown that some transformers are subjected to severe system faults, severe overloading and load unbalance. Such stresses often lead to transformers operating at significantly higher temperatures resulting in insulation damage. Overloading has been shown to have the following effects on transformers [4]:

- Damage to tap changers and bushings
- Paper insulation degradation when the winding temperature (i.e hot spot temperature) is in excess of 90^0C. Observations show that paper insulation life is halved for every 6^0 C the hot spot temperature exceeds 98^0 C

Non-linear loads such as compact fluorescent lamps (CFLs) battery chargers, uninterruptable power supplies (UPSs), television sets, inverter-controlled air conditioners and refrigerators are becoming more common in South Africa. Such non-linear loads cause harmonic currents that also produce harmonic voltages that increase the losses in the utility equipment. Sharengi et al. showed that the loading capacity of a transformer had to be reduced by 35 % when supplying CFLs compared to linear loads such as incandescent lamps [5]. Monitoring harmonics at transformer level can thus lead to more accurate derating of such transformers.

Electrical stresses in the form of lightning transients also contribute towards premature failure of transformers. In Eskom, pole-mounted transformers are protected using fuses and surge arresters. Fuses isolate faulty transformers. Surge arrestors offer protection against lightning or switching transients. Table 1 shows lightning related transformer failures that were reported in the Eskom Free State Operating Unit. Such a failure rate highlights the need for monitoring systems capable of quantifying these stresses.

Monitoring systems developed within Eskom for pole-mounted transformers currently measure only the power frequency stresses on the LV side of pole-mounted transformers. The developed system already has a communication infrastructure that sends

measured parameters to the network operators. The MV side is not monitored. Transients are also not monitored. This paper looks at the use of Rogowski coils and bushing screen capacitive voltage dividers for wideband monitoring on the MV side of distribution transformers.

Table 1: Financial year 2013/2014 MV/LV pole-mounted transformer equipment failures in the Free State Operating Unit [2]

Average failures (per year)	*Total*	*Due to lightning*	*Percentage*
MV fuses	7895	6160	78%
Pole-mounted transformers	638	497	77.9%
MV surge arrestors	2312	2312	100%

2.2 Rogowski coil current monitoring

Saturation and limited bandwidth have led to the switch from using ferromagnetic core current transformers to air-cored Rogowski coils. Rogowski coils such as the one depicted in Figure 1 sense the current flowing through the conductor. A Rogowski coil with physical properties shown in Table 2 was designed and studied. The 875-turn coil was terminated with a 179 Ω resistor. Rogowski coil operation is based on Ampere's law, where the coil senses the magnetic field around the conductor. The respective equation is [6]:

$$i = \oint H cos\alpha . dl \qquad (1)$$

Where:

i = primary current [A]
H = magnetic field strength [A/m]
dl = small element along the coil path [m]
α = angle between the magnetic field and the element

The flux linking the entire coil given by [7, 8]:

$$\varphi = \int d\varphi = \int \mu_0 nAHcos\alpha dl = \mu_0 nAi \qquad (2)$$

Where:

φ = Total flux linkage [Wb]
$d\varphi$ = Flux linkage within a section dl
μ_0 = $(4\pi \times 10^{-7}[\mathrm{H.m^{-1}}]$, Permeability of air
n = Number of turns per metre $[\mathrm{m^{-1}}]$
A = coil cross-sectional area [m]

The voltage induced in the coil is a function of both the time derivative of the measured primary current and the mutual inductance of the coil as expressed in equation (3) below [7,8]:

$$V_c = \frac{d\varphi}{dt} = -\mu_0 nA\frac{di}{dt} = -M\frac{di}{dt} \qquad (3)$$

Where

V_c = Coil voltage [V]
M = Mutual inductance [H]

The corresponding mutual inductance based on the parameters in Table 2 can be calculated as [9]:

$$M = \mu_0 \frac{N_2}{L} A \qquad (4)$$

The current in equation (3) is obtained by integrating the coil output voltage using active integration circuits [6, 10]. The current can also be calculated using numerical integration techniques [11]. In this study, numerical integration techniques are used for both power frequency and transient measurements.

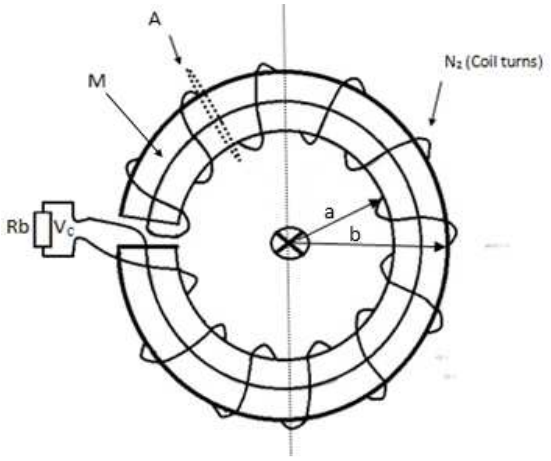

Figure 1: Rogowski Coil: the current to be measured flows through a conductor centrally located at X

Table 2: Designed Rogowski coil specification

Parameter	**Parameter description**	**Value**
d_w[mm]	Wire diameter	0.375
$R[\Omega]$	Wire resistance	18.66
a[mm]	Toroid inner radius	33.5
b[mm]	Toroid outer diameter	57.5
L[m]	Wire length	65
A[$\mathrm{mm^2}$]	Coil area	452.39
N_2	Number of turns	875
M[nH]	Mutual inductance	497

The Rogowski coil designed in this study will be embedded in 22 kV bushing. The power frequency performance of the Rogowski coil was evaluated as

shown in Figure 2 below. The transient performance was evaluated using an 8/20 µs current impulse generator as shown in Figure 3. A wideband current monitor was used as a reference in both the power frequency and the impulse measurements. Both coil voltages were integrated numerically so as to evaluate the primary current.

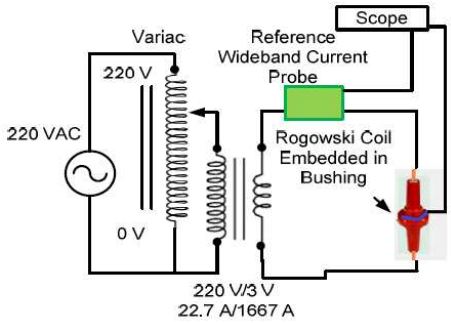

Figure 2: Power frequency test circuit

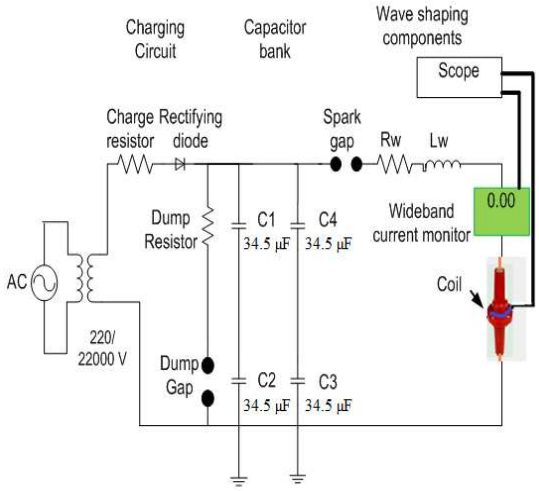

Figure 3: Impulse current test circuit

2.3 Screened bushing voltage monitoring

The 22 kV epoxy resin bushing with embedded screen for internal electric field control is shown in Figure 4 and has been successfully used for measuring power frequency voltages [11]. In this study the performance of the bushing was evaluated for measuring both power frequency and impulse voltages. A comparison between the voltage obtained using the bushing screen and a wideband 1000/1 capacitive probe for power frequency measurements was made. The capacitance between the bushing conductor and the screen was measured as 22 pF.

Both the power frequency and the transient output voltages were measured across the external capacitor connected between the screen and earth. The ratio of the bushing divider was determined by varying the input voltage from 1 kV up to 22 kV. Impulse voltages were also applied using a 1.2/50 µs voltage impulse generator. If the insulation conductance can be ignored

$$V_{out} = \frac{C_1}{C_1 + C_2} V_{in} \qquad (5)$$

Where:

C_1 = Capacitance between the bushing screen and the bushing MV conductor [F]

C_2 = External Capacitor [F]

V_{in} = Input voltage [V]

V_{out} = Output voltage [V]

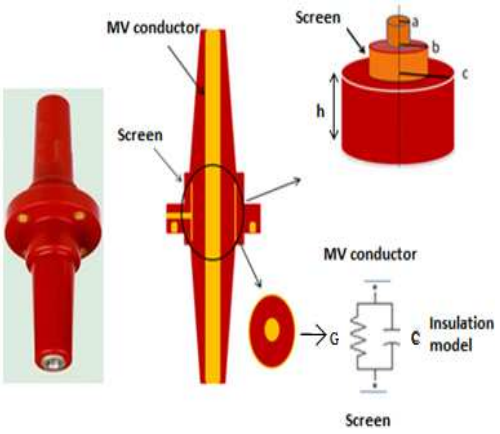

Figure 4: Cross-sectional view of a 22 kV epoxy resin bushing with embedded screen with emphasis on the position of the screen relative to the MV conductor [14].

The external capacitor had a value of 47 nF. Based on equation 5, the voltage division ration was

$$\frac{V_{out}}{V_{in}} = \frac{1}{2137.36} \qquad (6)$$

3. CURRENT MEASUREMENT RESULTS

3.1 Power frequency current measurement

Low range and high range currents measured with the Rogowski coil are shown in Figure 5 and 6 respectively. The corresponding scaled numerically integrated current shown in Figure 7 and 8 respectively and is compared with the reference wideband current monitor. Kojovic however suggests that numerical integration is not necessary for power frequency measurement since it is known that the measured signal is shifted by 90^0 [9]. Though numerical integration is performed in this study, analysis of measured coil data can also be done without going through the complexities of integrating provided power frequency signals are the only signals of interest. The measured voltage signal would simply be related to the primary current through a scaled multiplying factor.

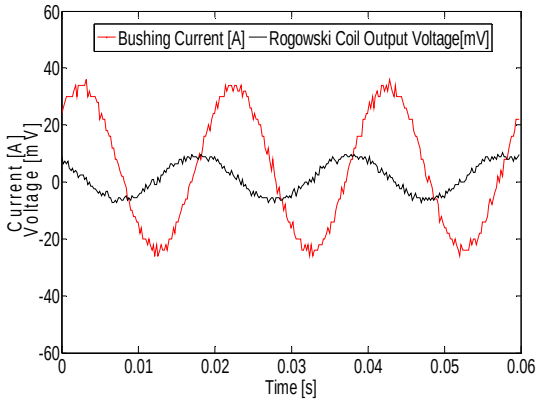

Figure 5: Unintegrated low range 50 Hz current signal

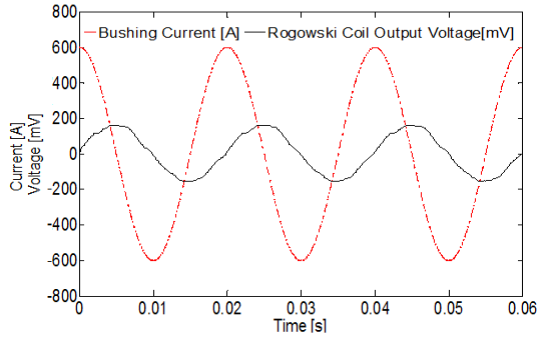

Figure 6: Unintegrated high range 50 Hz current signal

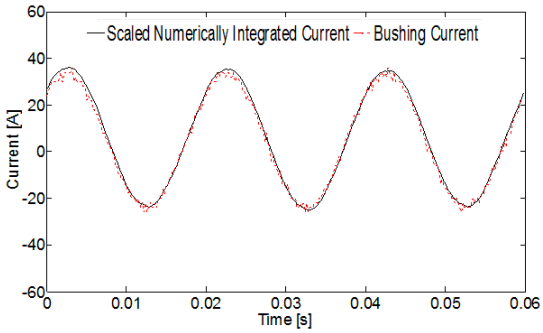

Figure 7: Integrated low range current 50 Hz

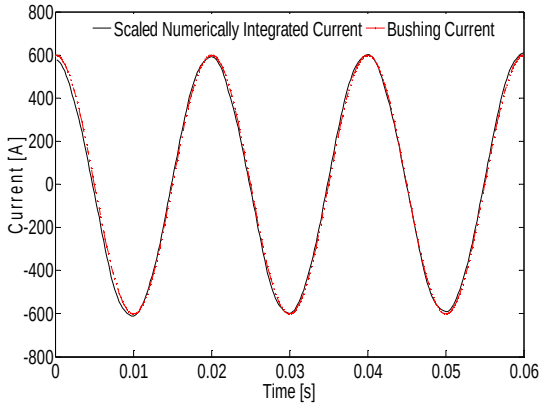

Figure 8: Integrated high range current 50 Hz

3.2 Impulse current measurement

The output voltage of the Rogowski coil when subjected to a 6 kA current impulse is shown in Figure 9. The measured signal was taken with a 10/1 passive probe with the Rogowski coil terminated with the same resistor used in power frequency measurement. Figure 10 shows the current signal that was measured with a wideband current monitor and the corresponding scaled numerically integrated signal based on the output in Figure 9. There is however a 4µs time shift introduced by the numerically integrated signal with the reference wideband current monitor output.

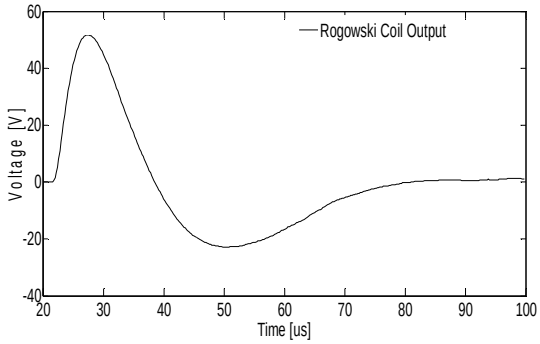

Figure 9: Rogowski coil voltage output under impulse current measurement conditions

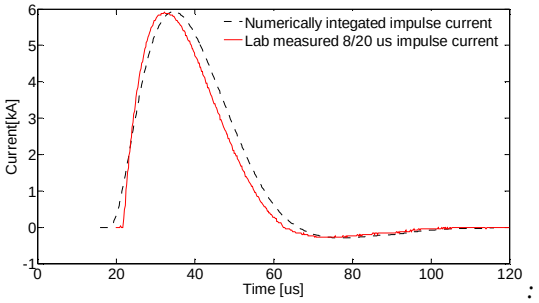

Figure 10: Integrated impulse current signal

4. VOLTAGE MEASUREMENT RESULTS

4.1 Power frequency voltage measurement

Comparison between the measured output voltage of the reference wideband capacitive divider probe and the bushing voltage divider are shown in Figures 11, 12 and 13. Figure 11 shows the use of the bushing divider in measuring a 1.5 kV power frequency voltage. The corresponding bushing voltage divider output in this case was 0.7 V. A scaled version of the bushing voltage divider output termed Scaled CVD shows that the measured waveform is in phase with the wideband capacitive probe output. The division ratio is consistent with the calculations in equations 5 and 6. The scaling factor used for the Scaled CVD signal is 2.137 instead of 2137 so as to match with

the division by a factor of a 1000 introduced by the wideband capacitive voltage probe.

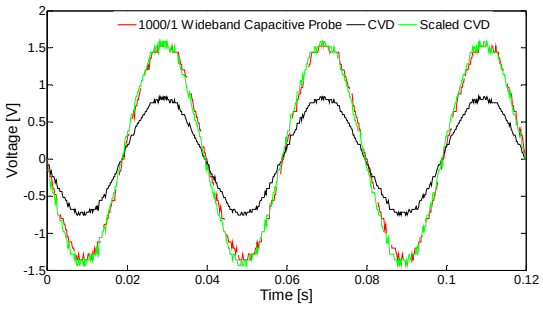

Figure 11: Low range 50 Hz voltage measurement. Measured signal in green has a magnitude of 1.5 kV scaled by a factor of 1000 which enables comparison with the measured bushing voltage divider output termed CVD.

Analysis of the measured waveforms shows that the ratio given in equation 6 is still applicable at a midrange voltage of 13 kV as well as at 27 kV with the bushing voltage divider output equal to 6 V and 12.6 V respectively. The output voltages of both the reference capacitive divider and the bushing voltage divider are shown on the Figures 12 and 13 below.

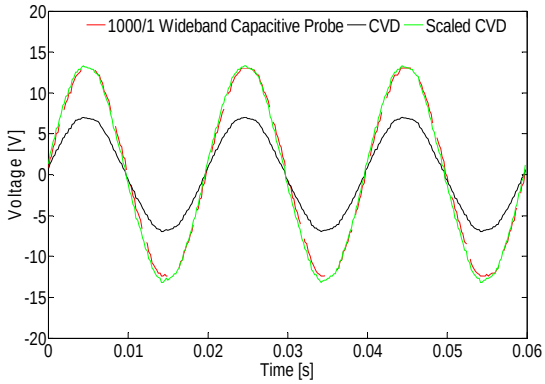

Figure 12: Mid-range 50 Hz voltage measurement. Measured signal in green has a magnitude of 13 kV scaled by a factor of 1000.

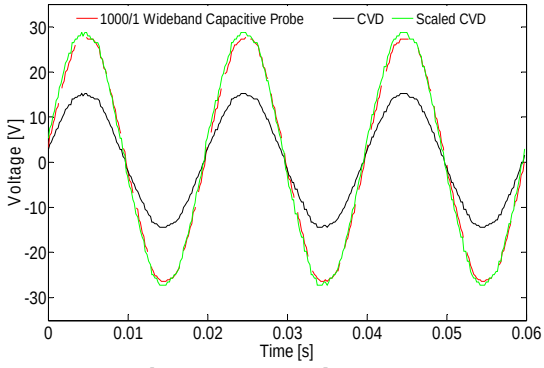

Figure 13: High range 50 Hz voltage measurement Measured signal in green has a magnitude of 27 kV scaled by a factor of 1000.

4.2 Impulse current measurement

The measurement of voltage transients using the same bushing screen divider was also evaluated where voltage transients up to the Basic Insulation Level (BIL) of 125 kV is of interest. A comparison of the bushing divider and a reference resistive divider showed that 1.2/50 µs lightning voltage impulses can also be measured with the bushing divider. The bushing divider has the capability of accurately measuring both the rise time and the fall time of the 54 kV impulse shown in Figure 14 below. Non-linearity is however observed when the impulse voltage is increased beyond 80 kV. Laboratory results also showed that earthing and shielding play an important role in obtaining accurate results. Further investigations will revolve round identifying parameters responsible for the observed nonlinearities as suggested in [13].

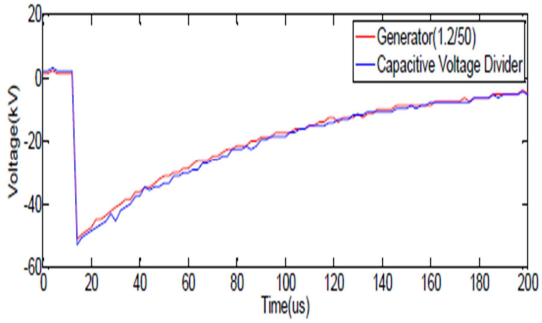

Figure 14: Impulse voltage measurements

5. Conclusion

The presence of both power frequency and transient electrical stresses leads to premature failure of distribution transformers. Both low range and high range currents were successfully measured with the designed embedded Rogowski coil. The current obtained by numerically integrating the output voltage of the Rogowski coil gave results that were consistent with both the power frequency and the transient primary current captured by the reference wideband current probe. Low range and mid-range voltage measurements taken with the bushing divider were consistent with the output of the reference divider. Further work will involve investigating possible causes for nonlinearities of the bushing divider.

REFERENCES

[1] MAS Masoum, PS Moses and S Deilami, "Load Management in Smart Grids Considering Harmonic Distortion and Transformer Derating", *Proc. Int. Conf. Innovative Smart Grid Technology*, pp. 1-7, 2010.

[2] WJD Van Schalkwyk and J van Coller, "An Investigation into a More Optimal Choice of BIL

on MV Feeders", *Cigré 7th South African Regional Conference*, 2013.
[3] R Kleinhans, "Current and Voltage Monitors Combat Theft and Improve Supply Quality", *Energize: Transmission and Distribution*, pp. 41-45. 2011.
[4] NL Meyer, *Distribution Guide-Part 1: Network Planning Guideline for Distribution Transformers*, Eskom Distribution, 2010.
[5] M Sharengi, B Phung, M Naderi, T Blackburn and E Anbikairajar, "Effects of Current and Voltage Harmonics on Distribution Transformer Losses", *International Conference on Condition Monitoring and Diagnosis(CMD)*, Bali, 2012
[6] WF Ray and RM Davis, "High Frequency Improvements in Wide Bandwidth Rogowski Transducers", *EPE 99 Conference Proc.*, Lauzanne. 1999.
[7] DA Ward and J La T Exon, "Using Rogowski Coils for Transient Current Measurements", *Engineering Science and Education Journal*, pp 105-113, 1993.
[8] A Phillips, G Grobbelaar, C Pritchard, R Melaia, and I Jandrell. "Development of a Rogowski Coil to Measure Lightning Current Impulses", *SAIEE Transactions*, 1996.
[9] LA Kojovic, "Rogowski Coil Transient Performance and ATP Simulations for Applications in Protective Relaying", *Conference on Power Systems Transients, IPST'05*, Montreal, Canada, 2005.
[10] SJ Petting and J Siersema, "A Polyphase 500 kA current measurement system with Rogowski coils", *IEE Proc. B*, Vol. 130, No. 5, pp. 360-363, 1983.
[11] K Schon and W Schuppel, "Precision Rogowski Coil used with Numerical Integration", *13th ISH*, Ljubljana, paper T10-130, 2007.
[12] FA Netshiongolwe, J Van Coller and R Cormack, "Development of Electrical Stress Monitoring Transducers Applicable to Distribution Transformer," *SAUPEC*, UKZN, 2014.
[13] JA Martinez-Velasco, *Power System Transients: Parameter Determination*, CRC press, pp. 111-115, 2009.

DEVELOPMENT OF ALTERNATIVE ELECTRICAL STRESS MONITORING TRANSDUCERS APPLICABLE TO MV/LV DISTRIBUTION TRANSFORMERS

F. A. Netshiongolwe[1], R. Cormack[2], J. M. van Coller[1]

[1]Eskom Power Plant Engineering Institute (EPPEI)-High Voltage (HV), School of Electrical and Information Engineering, University of the Witwatersrand, Private Bag 3, Wits 2050, South Africa Email: netshifa@eskom.co.za, John.VanColler@wits.ac.za
[2]Eskom, PO Box 1091, Johannesburg, 2001, South Africa
Email: CormacR@eskom.co.za

Abstract. This paper presents an alternative means of monitoring power frequency, harmonic frequency and surge currents and voltages and hence the associated electrical stresses on the medium voltage (MV) side of distribution transformers with a rating of 16 kVA up to 500kVA. Limitations of conventional ferromagnetic core current transformers and voltage transformers are presented. The design of a wideband Rogowski coil current transducer with a three stage integrator is presented. The use of an electric field control screen, embedded in a 24 kV bushing, as a means of attaining capacitive voltage division is presented.

Keywords: bushing, capacitive voltage divider, electrical stress, measurement, Rogowski coils.

1. INTRODUCTION

Electrical stresses on the medium voltage (MV) side of distribution transformers rated 16 kVA up to 500 kVA remain unevaluated. Studies show that a run to failure maintenance strategy has been adopted as costs for monitoring of such transformers often outweighs purchase costs. Increased failures of pole-mount transformers in the Eskom Distribution network has resulted in annual replacement costs of over R71 894 000 [1]. Such costs coupled with the need to ensure quality of supply to consumers have resulted in the need to develop alternative cost effective monitoring techniques that will maximize transformer availability. The dawn of the Smart Grid concept in South Africa's distribution network will include improved restoration times, improved line monitoring and improved transformer monitoring [2]. Such goals can only be met with cost effective monitoring technology capable of relaying actual field information. This paper reviews monitoring techniques that can be employed on pole- mount transformers within the distribution networks. The use of capacitive voltage monitoring and Rogowski current coil monitoring in power systems is also reviewed. The design of a voltage and current monitoring bushing is described. The observed results are discussed and a conclusion is given.

2. BACKGROUND

2.1 Distribution transformer monitoring

Distribution transformers rated 16 kVA up to 500kVA are common in the South African network. Failures of such transformers are however also common. Traditional forms of condition monitoring, such as dissolved gas analysis (DGA), are not applied to such transformers due to cost considerations. The recent introduction of low voltage (LV) current and voltage monitoring (CVM) units has shown that electrical stresses such as overloading, severe current unbalance and general overcurrent conditions are some of the causes of failures of such transformers [1]. The LV CVM units have been designed such that observable stresses produce alarms that are sent through to end users, affording them the opportunity to take corrective action. Alarms provided by LV CVM units have assisted end users in diagnosing some of the risks that may lead to premature transformer failure, which marked the evolution from reactive to proactive maintenance response.

The benefits that can be obtained by monitoring electrical stresses observed on the medium voltage (MV) side of such transformers have not been explored. Other electrical stresses that cause transformer failure such as harmonics and transients are presently not monitored. Limitations of observing stresses being monitored are often brought about by the lack of availability of cost effective MV electrical transducers. Figure 1 gives an overview of the proposed MV side monitoring system. This paper focusses on the construction of the electrical stress monitoring transducers that can be embedded in the MV transformer bushing with minimal intrusion to the transformer operation.

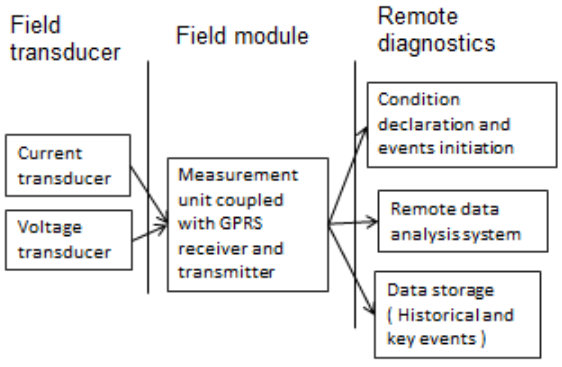

Figure 1: Proposed MV monitoring system

2.2 Current and voltage monitoring transducers.

Current and voltage monitoring has traditionally been performed using ferromagnetic current transformers (CTs) and ferromagnetic voltage transformers (VTs) Such CTs and VTs however have limited bandwidth, phase and magnitude errors, and exhibit nonlinearities such as saturation [3]. These limitations have resulted in the introduction of non-conventional current and voltage transducers. Non-conventional transducers such as the Rogowski coil and capacitive voltage transducers have successfully been used in monitoring current and voltage respectively. Figure 2 shows an example of a primary bar bushing with voltage and current sensing capabilities and various non-sensing bushings being considered for this study. Embedding current and voltage sensors into the non-sensing bushings in Figure 2 have the capability of providing end users with online operational data that can enhance the management of field assets.

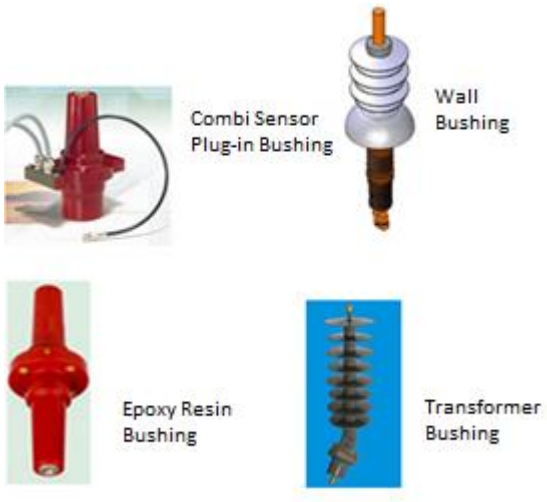

Figure 2: Combined current and voltage sensing and a variety of non-sensing bushings.

3. ROGOWSKI COIL CURRENT TRANSDUCER

Failures of pole-mount transformers due to harmonics, current surges and transients cannot be fully accounted for with existing current monitoring systems within South Africa's distribution network. CT's currently used for monitoring suffer from saturation effects and limited bandwidth. Rogowski current transducers depicted in Figure 3 have however been shown to have the following superior features [3, 4, 6]:

- High bandwidth (suitable for transients)
- Multiple primary current measurement ranges
- Non-intrusive to the primary circuit
- Modular in size

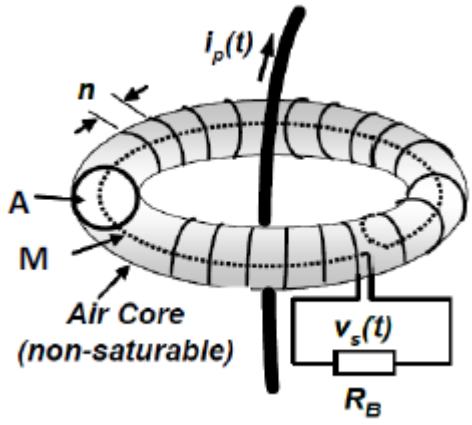

Figure 3 Rogowski coil current transducer [3]

3.1 Rogowski coil design

In this study, focus is on developing a Rogowski coil current transducer that can be embedded in a 24 kV transformer bushing and that has the capability of measuring power frequency currents, harmonic currents and transient currents. The output of the Rogowski current transducer is the induced coil voltage given by [3]:

$$V_c = -M\frac{di}{dt} = -\mu_0 nA\frac{di}{dt} \qquad (1)$$

where:

V_c = Coil output voltage, in V
M = Mutual inductance, in H
A = Coil cross sectional area, in m^2
i = Primary current, in A
n = Number of turns per meter
t = Time, in s

Table 1 below shows the parameters of the Rogowski coil designed for this study. These parameters are determined based on the physical dimensions of the windings and lab measurements.

Table 1: Rogowski coil specification

Parameter	Parameter description	Value
d_w	Wire diameter	0.455 mm
R	Wire resistance	1.08 Ω
d_C	Coil diameter	7 mm
l	Coil length	286 mm
A	Coil area	38.48 mm^2
n	Number of turns per meter	1475/m
u_0	Permeability of air	$4\pi \times 10^{-7}$ H/m
L	Inductance	29.2 μH
C	Coil capacitance	3.3 pF

3.2 Calculation of the primary current from the measured coil voltage

The induced coil voltage V_c is a function of the derivative of the primary current and thus it is necessary to integrate the induced voltage in order to determine the primary current. Based on Equation 1, the primary current is given by:

$$i = \frac{1}{M}\int V_c dt \qquad (2)$$

The integration portion of Equation 2 can be achieved by implementing an electronic integrating circuit capable of wide bandwidth measurements. Passive integration on a correctly terminated Rogowski coil can be used for high frequency measurements; however op-amp integration is required for low frequency measurements [7, 8]. Figure 3 below shows a typical integration circuit suitable for this study. Petting [7], showed that by matching the time constants of the circuit in Figure 4, both low and high frequency integration could be achieved:

$$R_2C_1 = R_3C_2 \qquad \frac{R_1}{R_2} \geq 1000 \qquad \frac{L}{R_C} = R_4C_2$$

In this case R_C represents the characteristic impedance of the cable joining the coil to the integration circuit. By choosing the integrating time constant of $R_1C_1 = 10\text{s}$ with $R_c = 50\ \Omega, R_1 = 1\ M\Omega$, $\frac{R_1}{R_2} = 1000$ and $L = 29.2\ \mu H$(coil inductance) we get:

$$C_1 = 10\ \mu F \qquad C_2 = 1\ \mu F$$

$$R_3 = 805\ k\Omega \qquad R_4 = 47\Omega$$

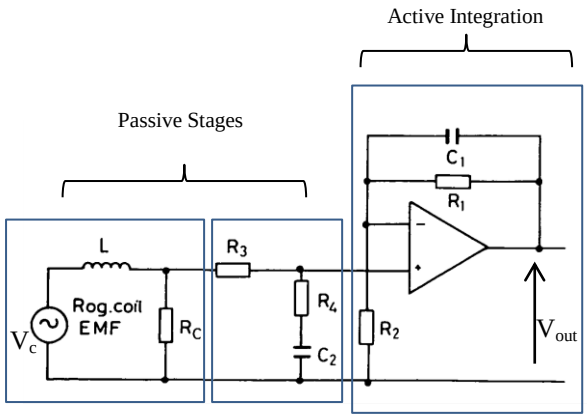

Figure 4: Three-stage integration Rogowski measuring circuit [7]

The circuit designed with the guidelines given above yields simulated results shown in Figure 6. The bandwidth based on the component value selection is of the order of 100 kHz. Other integrators that have higher bandwidth have been developed by Ray [8] and these will also be investigated in this study. Laboratory work still needs to be done to see if the results attained below can be replicated. The integrated voltage is ideally supposed to be in phase with the primary current whilst this voltage is out of phase with the coil output voltage.

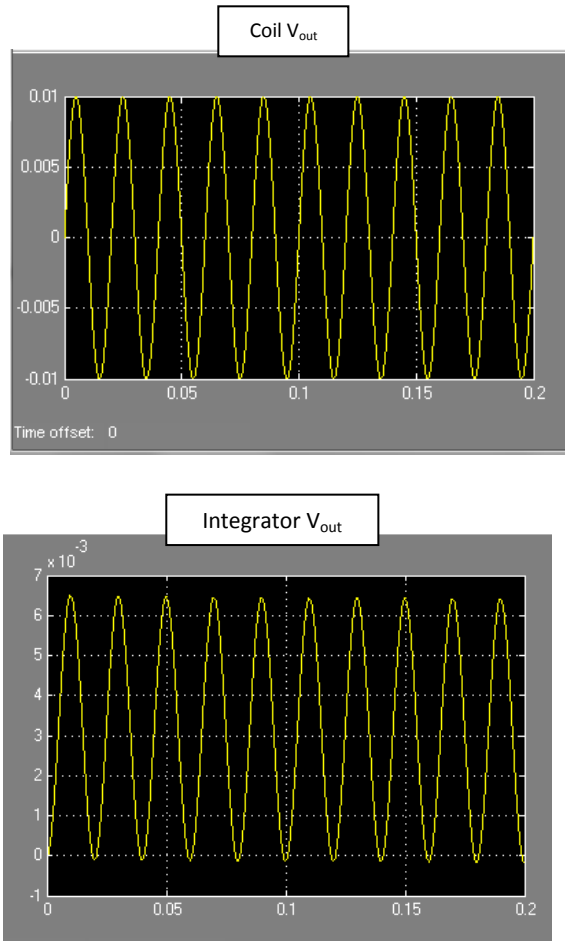

Figure 5: Simulated coil output voltage compared to integrated signal compared

4. CAPACITIVE VOLTAGE TRANSDUCER

High voltage measurements have traditionally been performed using capacitive voltage transformers. Recent developments have resulted in the use of capacitive voltage dividers in medium voltage switchgear and overhead lines [4, 5]. Solid insulation bushings used on transformers can either be ceramic, cycloaliphatic epoxy resin or silicone enclosed epoxy resin bushings for outdoor application. Silicone coated epoxy resin bushings will be considered for this study. Epoxy resin bushings often contain an embedded screen used for electric field control in the area where the bushing passes the earthed transformer tank. The presence of such a screen sets up capacitance between the conductor and the screen. The magnitude of such a capacitance is a function of the dimension of the screen relative to the MV conductor and the dielectric properties of the insulation that separates them.

A 24 kV screened bushing was considered for this research. Figure 6 and Table 3 below show a cutout view and the dimensions of the bushing to be used. The presence of the screen sets up a potential divider

shown in Figure 7 and this relates the conductor voltage V_{in} to the screen voltage V_{out} :

$$V_{out} = \frac{C_1}{C_1 + C_2} V_{in} \qquad (3)$$

where:

C_1 = Capacitance between the conductor and the screen, in F

C_2 = Capacitance between the screen and the transformer tank as well as any external output (load) capacitance, in F

V_{in} = Conductor (input) voltage, in V

V_{out} = Screen (output) voltage, in V

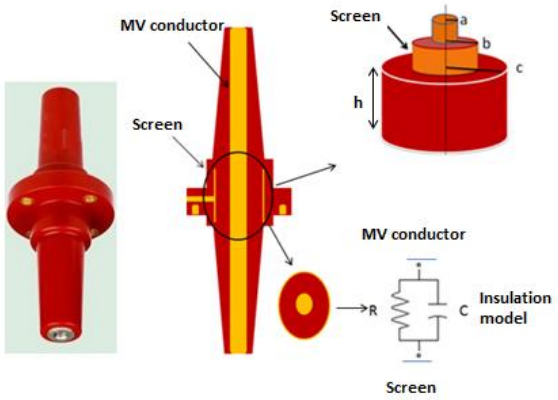

Figure 6: Cross-sectional view of a screened 24 kV epoxy resin bushing with emphasis on the position of the screen relative to the MV conductor.

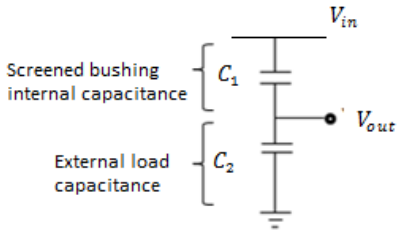

Figure 7: Embedded screen capacitive voltage transducer with the conductor-screen capacitance represented by C_1 and the screen-transformer tank capacitance as well as external load capacitance represented by C_2.

Table 1:24 kV bushing parameters

Parameter	Parameter description	Value
ε_0	Free space permittivity	8.854E-12 F/*m*
ε_r'	Relative permeability(Re)	3.8
ε_r''	Relative permeability (Im)	0.038
tan delta	Epoxy resin tan delta	0.01
a	Conductor radius	0.012 *m*
b	Screen radius	0.03 *m*
h	Screen height	0.06 *m*

The insulation capacitance between the conductor and the screen is given by [10]:

$$C = \frac{2\pi\varepsilon_0\varepsilon_r' h}{ln\frac{b}{a}} \text{ [F/m]} \qquad (1)$$

The corresponding resistance at angular frequency w is given by:

$$R = \frac{h ln\frac{b}{a}}{w 2\pi\varepsilon_0\varepsilon_r''} \text{ [Ω/m]} \qquad (2)$$

Table 3 tabulates the calculated resistance at a frequency of 50 Hz and also compares the calculated capacitance with the simulated capacitance which was obtained by varying the simulated supply voltage. The simulated capacitance in Table 2 was obtained using Finite Element Method Magnetics (FEMM) software and shows an acceptable error of 1.47 % when compared to the calculated value. Figure 7 shows the corresponding voltage equipotential plot with a simulated input of 24 kV. At power frequency, the resistance of the insulation is observed to be very high (GΩ) such that the electrical circuit can be represented by capacitance only. Figure 7 shows how the screen provides both line voltage sensing capabilities and electric field stress control at the interface between the live conductor and the earthed transformer tank.

Table 3: 24 kV bushing parameters

Methodology	Capacitance [pF]	Resistance[Ω], 50Hz
Calculated	13.6 pF	12.8 GΩ
FEMM simulation	13.8 pF	
Error	1.47%	

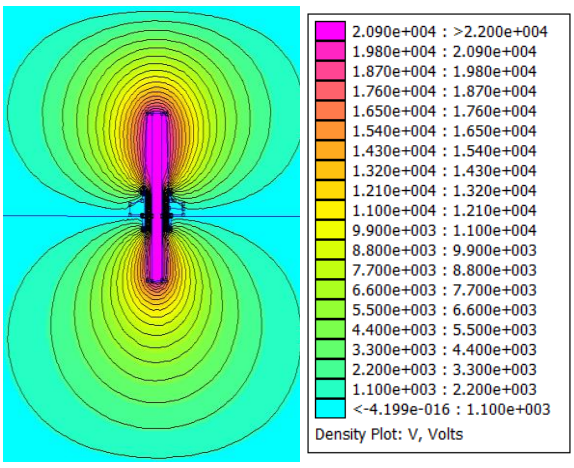

Figure 7: FEMM simulated plot of voltage equipotentials for the screened epoxy resin bushing at a supply voltage of 24 kV (phase to earth).

5. VOLTAGE MEASUREMENT RESULTS

The linearity of the 24 kV bushing capacitive voltage transducer was investigated at the power frequency

of 50 Hz with the supply voltage being varied from 1 kV up to 24 kV. Figure 8 shows the corresponding voltage measurement when an external load capacitance of 57.31 nF was used. One sample of readings with phase to earth voltage ranging from 1kV up to 24 kV was taken and the overall insulation capacitance observed with a fixed load capacitance of 57.13 nF was evaluated. The capacitances observed are shown in Figure 8, and these were then used to reconstruct other phase to earth voltages using measured results and Equation 3.

It should however be noted that the capacitance observed during voltage measurement is three times larger than the simulated and calculated values in Table 3. This variability still needs to be explored. The overall error of the phase to earth voltage reconstruction using the capacitance values obtained in Figure 8 is shown in Figure 9. Voltage measurements at 1 kV have been observed to have the largest error with the maximum error observed being 12.6%. All other voltage measurements were found to be within the 5 % error band. Phase to earth voltages above 13 kV were all reconstructed with the percentage error band being lower that 2%.

A second order polynomial equation was found to be best for relating the input supply voltage to the measured output voltage using the sample data used for the capacitance modeling above. Figure 9 below shows the error obtained whilst the polynomial equation is used to calculate the phase to earth voltage. The maximum error observed whilst calculating the output voltage from the measured voltage was 8.2 %. At phase to earth voltages of 2 kV upwards errors below 5 % were observed. Further analysis also showed that measurements from 12 kV upwards were observed to have a maximum 2% error.

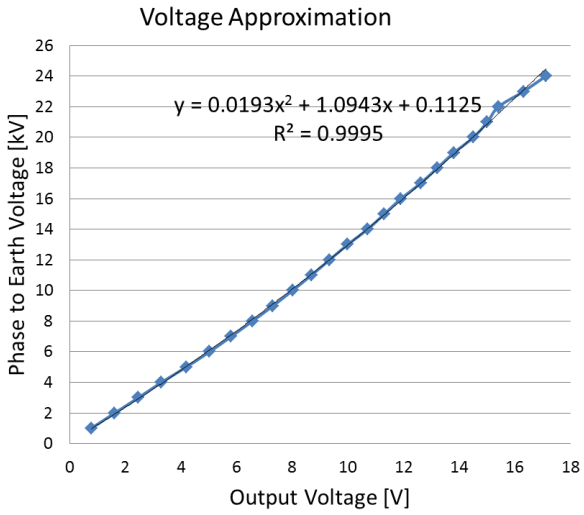

Figure 8: Measured capacitive voltage transducer output at a power frequency of 50 Hz and external load capacitance of 57.13 nF.

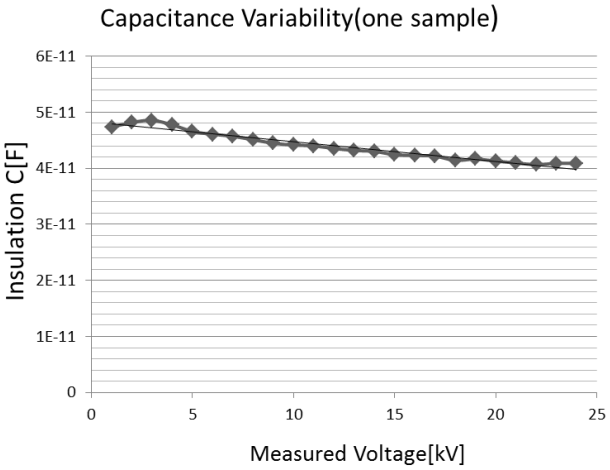

Figure 9: Capacitance variability of one measurement sample with external load capacitance of 57.13 nF.

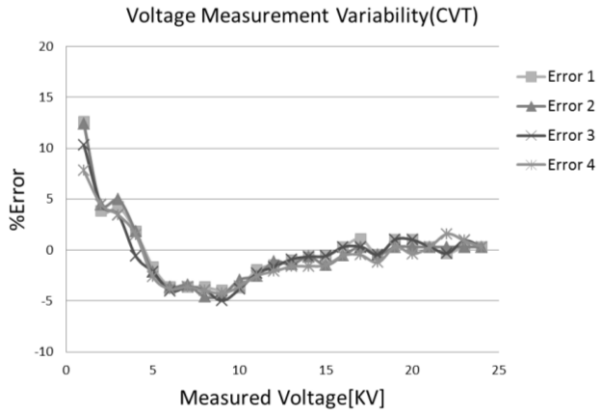

Figure 9: Phase to earth voltage measurement error at power frequency achieved with capacitive voltage division.

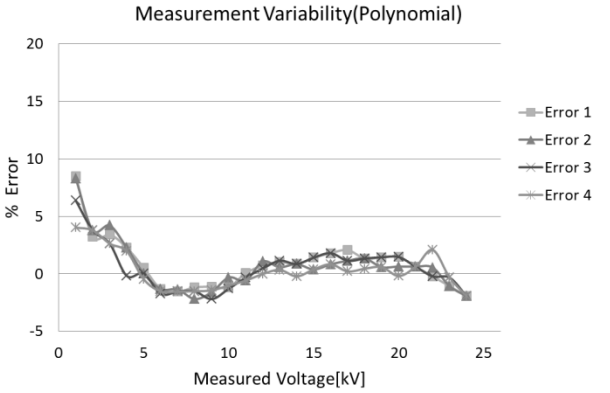

Figure 10: Phase to earth measurement error at power frequency achieved with polynomial curve fitting.

The largest error margin with both polynomial curve fitting and the capacitive voltage division method was seen to be at lower voltage measurements. Other results from 2 kV upwards agree with results observed from an earlier design of the KEVCY_R ABB combi unit sensor which had an error margin of 6% [10]. Further improvement on the error margins are possible, a more recent KEVCY_R ABB combi

sensor unit for indoor application has been optimized to meet error limits of 0.5 % at ±20% rated voltage and a 3% error margin over the full range of measurements.

6. CONCLUSION

The need for better management of distribution transformers has resulted in the need for developing voltage and current sensing transducers that can be embedded in transformer bushings. Both Rogowski coils and screened bushings provide plausible solutions with regard to dimension and overall sensing capabilities. The overall voltage sensitivity of the screened bushing was observed to have an error margin of 5 % for voltages above 1 kV. A polynomial equation approximation of the phase to earth voltage yielded better performance as compared to capacitive voltage division at 1 kV. More work still needs to be done to evaluate the bandwidth limitation of both the designed Rogowski coil transducer and the capacitive voltage transducer. Further work is also required in developing models that result in better accuracy within the rated operational voltage of the bushing (so that error compensation could be performed).

REFERENCES

[1] R. Kleinhans. "Current and Voltage Monitors Combat Theft and Improve Supply Quality". *Energize Transmission and Distribution*, pp. 41-45, September 2011.

[2] A. Khatri. "Evolution of Future Electrical Networks in Eskom". *AMEU 62nd Convention*, pp. 113-118. September 2010.

[3] IEEE Standard C37.235-2007, IEEE Guide for the Application of Rogowski Coils Used for Protective Relaying Purposes.

[4] R. Javora, M. Stefanka, P. Mahonen, T. Niemi, O. Rintamaki, "Protection in MV Networks using Electronic Instrument Transformers", *CIRED 20th International Conference on Electricity Distribution*, Prague, 8-11, June 2009.

[5] R. Behzadi, M. Oskuoee, D. Mohammadi. "Integrated Electronic Metering Insulator for Medium Voltage Overhead Lines". *CIRED 19th International Conference of Electricity Distribution*, pp. 1-4, May 2007.

[6] W.F. Ray and C.R. Hewson. "High Performance Rogowski Current Transducers". *Industry Applications Conference*, Vol.5, pp 3083 – 3090, 2000.

[7] S.J. Petting and J. Siersema. "A Polyphase 500 kA current measurement system with Rogowski coils" *IEE Proc B*. Vol 130, No 5, pp 360-363. Sept 1983.

[8] W.F. Ray and R.M. Davis: "High frequency improvements in wide bandwidth Rogowski transducers", *EPE 99 Conference Proc.*, Lauzanne. Sept 1999.

[9] E. Kuffel, W.S. Zaengle, J. Kuffel. *High Voltage Engineering- Fundamentals*, Butterworth-Heinemann, second edition, chapter 4, pages 201-241, 2000.

[10] ABB Group, Power Indoor Combi Sensor KEVCY_R, Last Accessed 13 Nov 2013. http://www05.abb.com/